1-20-2017

Analytical Flood Risk Models for First Responder Use: Obstruction Detection and Risk Assessment

Brett Edmond Carlock

R·I·T

Analytical Flood Risk Models for First Responder Use: Obstruction Detection and Risk Assessment

by:

Brett Edmond Carlock

A Thesis Submitted in Partial Fulfillment of the Requirements for the Degree of Master of Science in Environmental Science.

College of Science: Thomas H. Gosnell School of Life Sciences
Environmental Science Program

Rochester Institute of Technology
Rochester, NY
January 20, 2017

Committee Approval:

Karl F Korfmacher, Ph.D Date

Chair of Committee

Jan van Aardt, Ph.D Date

Committee Member

Justin G. Cole, GISP Date

Committee Member

Acknowledgements:

I would like to extend my sincerest thanks to my thesis committee advisor, Dr. Karl Korfmacher, for giving me the opportunity to participate in the RIT NSF research grant project that formed the initial basis of what would later become this thesis project. Furthermore, Dr. Korfmacher's continual guidance and support have enabled me to complete this thesis despite many trials and tribulations along the way. To Dr. Jan van Aardt and Justin Cole, GISP., I would like to extend my gratitude for their assistance and guidance throughout the many years this thesis has spanned. I have called upon their expertise and knowledge multiple times to help shape the analyses and processes that have been created herein. To Dr. Christy Tyler, I would like to express my deepest gratitude for her continual support and guidance, from my first days as an undergraduate at RIT, through to my final days as I adventure forth from the graduate program with a Master of Science degree. To Dr. Elizabeth Hane, I would like to express my gratitude for her support at each of my presentations and defenses, as well as her positive influence on my work and study habits. To my wife, family, and friends, I can only say that a lifetime of your support has lead me to where I am now and I owe you a great debt of gratitude.

Abstract:

The objective of this project is to develop and test two qualitative flood risk models for use in first responder and planning roles. The first, the Obstruction Detection Model (ODM), uses Light Detection and Ranging (LiDAR) derived Digital Elevation Models (DEMs) and a slope analysis to detect changes in the free surface of the water that might indicate the presence of a sub-surface obstruction. The product of the ODM can be used as a guide for field inspection, as well as an input scenario for the Risk Assessment Model (RAM). The RAM is the second model developed and serves to create an output product that displays the risk factor of each given parcel in order to help prioritize first responder efforts, as well as planning and mitigation efforts when used as a scenario generation tool. The RAM incorporates various vector data comprised of parcels, Monroe County Critical Infrastructure (CIKR), population, and assessed value in order to generate the Risk Factor. A third model, the Flood Extent Generator (FEG), uses an input scenario from the ODM to generate vector flood extents rapidly. These extents are used with the RAM to create a map that displays the Risk Factor in the flooded parcels.

The ODM appears to pick up riverine obstructions in the various river reaches tested within New York State. The FEG flood extents have 15% spatial agreement when constrained to Monroe County and 32% when constrained upriver of the Ford Street Bridge obstruction. The over-estimated flood extents lead to the RAM over-predicting populations and infrastructure at risk.

Model results, when compared to the more complex Hazus model, suggest that the simplified approach presented needs additional predictor variables or data pre-processing to improve accuracy of each model component.

Table of Contents

List of Figures

List of Tables

Introduction:

Flooding is a natural process wherein a body of water, such as a river, overflows its normal bounds and inundates the surrounding area. Flooding occurs naturally when rainfall exceeds the infiltration rate and/or capacity of the area's soil and landscape depression storage capacity. This process can be exacerbated in many cases by overland flow of water due to development, as developed areas typically have a lower infiltration rate than natural landscapes. When an area becomes highly developed, its Impervious Surface Ratio (ISR) increases, which in turn decreases the rate at which water enters into the water table (Schueler 1994). The effects of a strong rain event, combined with urban development, are demonstrated by the aftermath of the Broome County NY 2011 flood (Matthews and Spector 2012). Though most of Broome County NY is rural, it does contain the relatively large city of Binghamton. The Ithaca Journal estimated the total cost of the state-wide flood damages due to the storm to be $1.6 billion, with $75 million in damages contributed by Broome County alone. Severity of damage varied widely across the counties impacted, and New York State aid provided $61 million for the 25 counties impacted.

As a result of the costs due to flood damage to property and infrastructure, flooding and associated risks are one of the highest environmental management and planning priorities of municipalities in New York State containing major river systems, such as the city of Rochester in Monroe County NY (MonroeCounty.gov 2012), and smaller communities within the Genesee River watershed. In order to strengthen its emergency planning and response efforts, Monroe County has made a strong investment in remote sensing (RS) and geographic information systems (GIS) technologies, two key tools that can be used to help manage the effects of natural disasters such as floods.

Remote sensing can be employed to help manage a natural disaster, such as the 2011 Broome County flood, by providing a county with up to date imagery of the impacted areas. Using an airborne sensing platform enables a county or municipality to have a near real-time view of the situation on the ground. Visual analysis of these data allow decision makers to determine the general location, extent, and severity of the flood damage (Banchini, et al. 2000); (Ramsey, et al. 2009). GIS comes into play when more complex questions need to be answered, such as: what would be the total value of the flooded parcels, how many lives would be impacted within the flood extent, and finally, what critical infrastructure would be at risk? By utilizing the analytical power of GIS, combined with the knowledge source of remotely sensed data, various pre-event scenarios can be generated and tested. Using these data, more informed conclusions can be drawn, enabling decision makers to put into effect Emergency Management/Disaster Response plans.

Emergency management is a process attempting to reduce the severity and occurrence of natural (and sometimes anthropogenic) disasters, pre- and post-event. A four-phase model, proposed by the Commonwealth of Learning (Virtual University for the Small States of the Commonwealth (VUSSC) 2007), breaks the cycle down into *Mitigation*, *Preparedness*, *Response*, and *Recovery*. The mitigation phase of the cycle would encompass the bulk of the administrative efforts to identify, quantify, and manage risk in Monroe County. During this phase, the development of risk management tools is essential, as they will be used during the preparedness stage. In order to properly mitigate damage from disasters, the county needs a reliable means to identify at-risk areas, type of risk, populations at risk, monetary effects of risk, and the collateral effects that risk would have on other parts of the municipality. A qualitative model that examines these factors can be employed to help decision makers focus administrative and mitigation efforts to the areas that will most need them. Similarly, these administrative efforts and plans will impact the effectiveness of the first responders who would have to deploy for a disaster during the response phase, and even into the recovery phase post-event. This project aims to develop models that can be used as risk management tools by first responders in the event of an emergency.

First responders are public service workers like the police, fire department, emergency medical services, or specialized teams like a hazardous materials unit (HazMat), who are trained to deploy and respond to an incident. In order to be effective, they need to know information such as what the incident is, where it occurred, and what impact it has had on the location and its population. For instance, responding to a chemical spill will require different equipment and procedures than responding to a stranded vehicle in a flooded roadway.

If the stranded vehicle case is used as an example, the role of GIS and RS in emergency management and disaster response becomes clearer. Using a network analysis of road layers created with a GIS package, the first responders can create a navigable route from the point of deployment to the emergency site. Any blockages found using crowd-sourced data, RS data, or otherwise reported data, can be put into the network analysis and routed around.

Crowdsourced data are fairly recent technological developments, reliant mainly upon the adoption of always-connected mobile devices, such as modern smartphones. In this context, crowdsourced data would be things such as GeoTweets (Twitter status with GPS metadata) that report a blockage, impassible area, or other hazard. Crowdsourced data have many potential limitations, being subject to intentionally falsified reports, information skewed by the overseeing agency (if there is one), and even just mistaken reports (Hudson-Smith, et al. 2009).

GIS, Remote Sensing and Data Types:

GIS and associated data products, such as satellite imagery, light detection and ranging (LiDAR), digital orthophotos (DOPs), and user-generated products such as parcels, hydrographic features, and census blocks, are powerful tools that can be utilized to investigate and address various environmental problems, such as flooding and emergency management (Gunes and Kovel 2000). Each data type and source has different limitations and benefits that must be considered when leveraging them in an analysis. Products like LiDAR offer high degrees of spatial resolution with similarly high precision, but also produce massive datasets that can be cumbersome to work with. Likewise, DOPs can be expensive to fly, process, and work with, as they are taken at high resolutions, which results in very large file sizes. DOPs, like LiDAR, provide high spatial resolution data (typically sub-meter pixels), are flown on demand (temporal resolution control), and can be taken at various angles to better image the built environment or tall natural structures, as seen in imagery produced by Pictometry (Figure 1).

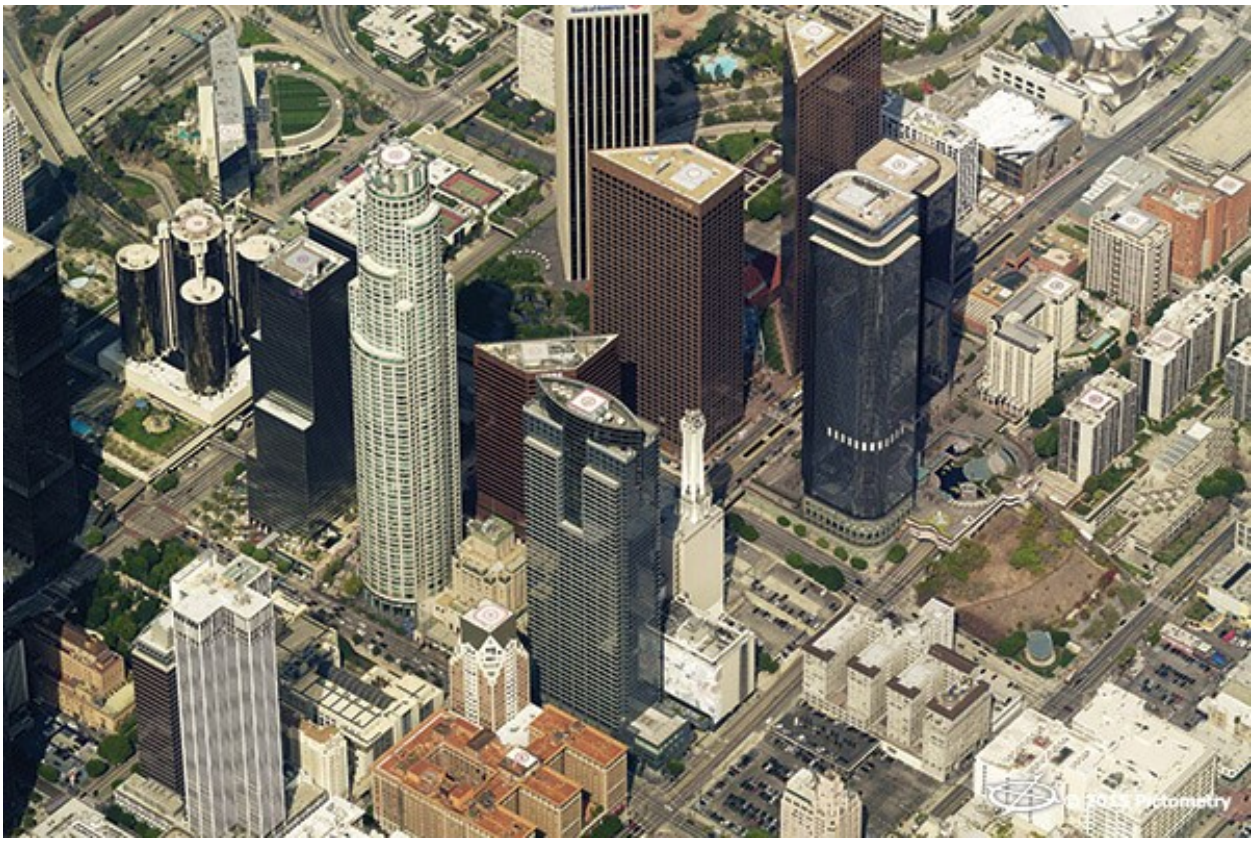

Figure 1 - Pictometry Oblique Image of Downtown Los Angeles, California (03/05/14). Courtesy of Pictometry International, Inc.

LiDAR imagery is distinct from photographic imagery in that it is a three dimensional representation of the space that is being imaged, as opposed to a planar, or two dimensional, representation. In order for a LiDAR image, or point cloud, to be formed, there must be a sensor which

knows its exact location on the Earth as well as its exact nature of movement. The LiDAR sensor operates by pulsing a laser at a specified light frequency and rate of pulse. The scanner may be static, may oscillate, or may articulate. The articulated scanners serve to increase the ground coverage by moving the laser pattern across the surface being imaged, as opposed to having to move the sensor and its platform across the surface to be sensed, as is the case with a fixed, or static system. The LiDAR sensor, knowing its exact location, speed, and orientation, calculates how long it takes for the returns of an outbound pulse to reflect off the sensed surface and back into the sensor. The time it takes for each return determines its exact distance from the sensor, and that information is used to create the three-dimensional representation of the sensed scene. The positioning information enables the locations to be incredibly accurate and precise, typically to 15cm of accuracy or better. The sensor also records a myriad of other properties that describe the data in greater detail (Nayegandhi 2007). One potentially interesting property is the intensity of the return. This value represents the "brightness" of the return as it reached the sensor. Unfortunately, this value is not calibrated to take into account incident scene radiation, and therefore, is not valid for analytical use. However, it can be used when visualizing the data to render a scene that can be interpreted in the same manner as a photograph.

Digital Orthophotos, referred to simply as DOPs, are high-resolution digital photographs taken from an airborne sensing platform, similar to how aerial LiDAR is acquired (National Mapping Division 1996). The height that the sensor is flown determines the resolution of the DOP, also called its Ground Sample Distance (GSD) (Federal Geographic Data Committee 2008). A typical DOP is comprised of at least three bands, covering the Red, Green, and Blue parts of the spectrum used in digital images. Many sensors will have an additional band, typically in the infrared part of the spectrum. In the case of the imagery used in this analysis, sourced from the Rochester Institute of Technology Digital Imaging and Remote Sensing (DIRS) Wildfire Airborne Sensing Platform (WASP) sensor, there are the three color bands (Red/Green/Blue [RGB]) as well as a Short-Wave Infrared (SWIR) channel (LIAS - RIT 2008). The Medium and Long-Wave (MWIR and LWIR, respectively) bands of the WASP sensor are not used for this analysis.

A limitation that DOPs share with LiDAR is their large file-size. This means that in order for DOPs to be used in the field, a device would need many gigabytes of storage. If local storage was not feasible, the device would have to employ a wireless data connection to stream the DOPs. This type of streaming requires an always-on connection and high bandwidth, two properties that may not be present in emergency response situations. Many field-deployed GIS stations will bring with them redundant data storage drives, containing copies of the needed DOPs and other imagery in order to be self-sufficient when deployed (Cole July 25, 2012). As was seen in the aftermath of the Hurricane Katrina disaster,

critical infrastructure elements such as power, internet, and wireless radios can be down during the response phase. Hurricane Katrina was one of the largest and most powerful storms to make landfall in the US during the 20th and early 21st centuries. The storm had displaced more than 250,000 people and caused more than $125B in damages (Graumann 2005). It is not unimaginable that such a powerful storm event would wreak havoc upon the infrastructure in Louisiana and as a result, cripple the area. The National Wetlands Research Center (NWRC) handled this outage by hand-delivering the needed data to the satellite field stations on a daily basis (Wilson and Cretini 2007). This manual dissemination of data is time consuming, introduces further age into the data (not real-time nor near real-time), and can put the couriers at risk as they have to deliver the data manually.

In light of the constraints LiDAR and DOPs put on devices, it is more common to see LiDAR data used on the back-end to create products such as Digital Elevation Models (DEMs) and Digital Surface Models (DSMs) for pre-disaster planning purposes. It has been found that LiDAR-derived DEMs and DSMs have far superior accuracy when compared to DEMs created by differential global positioning system (DGPS) and the existing 9 arc-second (roughly 250m) DEMs in the tested area (Rayburg, Thoms and Neave 2009). It is necessary to note here that most places on Earth have at least 30m coverage for DEMs, with 10m and higher resolution coverages becoming more common. For large map scale analyses, the full-coverage 1 arc-second (30m terrain data) can be too general and may negatively influence the accuracy of the results (Vaze and Teng 2007). Currently, the USGS offers partial coverage in 1/3 arc-second (10m) and 1/9 arc-second (3m) (USGS 2012). Since availability varies and releases are done as the data are collected and processed, they are not being considered for this analysis. In these situations, the spatial resolution of LiDAR (1.62 points per meter^2 in our case), combined with its high precision, allows for the creation of more accurate products like DEMs or DSMs when compared to those derived from the Shuttle Radio Tomography Mission (SRTM) data or other terrain datasets. For context and visualization purposes, compressed versions of the DOPs can be used for visual analysis, as having an up-to-date and comprehensible view of the area is critical throughout the Emergency Response phases (Banchini, et al. 2000), (Ramsey, et al. 2009). When DOPs are neither available nor feasible, satellite image products can be used in their stead to provide the needed context.

Satellite imagery is available through many providers with varying spectral, spatial, temporal, and radiometric resolutions (Table 1). Some datasets, such as government provided Landsat images, are of intermediate spatial, temporal, and radiometric resolution, and as such, are not typically sufficient for small-scale projects and analysis. In these situations, products such as DOPs are more appropriate as they provide a much higher spatial resolution and can be flown on-demand, ensuring the user has the temporal representation they want. There are some commercial satellites that provide high temporal and spatial

resolution, such as WorldView 2's 1.1 – 2 day revisit (Satellite Imaging Corporation n.d.), compared to the 16 day revisit of satellites like Landsat. Other satellite products such as the SRTM focus on mapping the surface contours of the Earth and freely disseminating this information. SRTM accuracy and resolution differs between the various releases and locales for distribution (NASA 2005). Typically, SRTM1 USA data are 30m in resolution, matching the Landsat images perfectly.

Table 1 - Overview of Satellite Sensor Specifications.
Abbreviations: VNIR – Very Near Infrared SWIR – Short Wave Infrared TIR – Thermal Infrared FIR – Far Infrared B/W – Black and White BPP – Bits per pixel m – meter

Name	# Bands	Resolution (GSD)	Bit depth	Revisit Time
ASTER	3	15m VNIR, 30m SWIR, 90m TIR	8, 12 bpp	16 Days
GeoEye-1	5	.41m B/W, 1.65m color	11 bpp	2.1 – 8.3 Days
IKONOS	5	.82m B/W, 3.2m color	11 bpp	3 Days
Landsat 7 ETM+	7	15m B/W, 30m color, 120m FIR	8 bpp	16 Days
QuickBird	5	.61m B/W, 2.44m color	11 bpp	1 – 3.5 Days
RapidEye	5	6.5m Color, 5m rectified	12 bpp	1 – 5.5 Days
WorldView 2	8	.46m B/W, 1.8m color	11 bpp	1.1 – 3.7 Days

Flood Risk Models:

Monroe County Emergency Operations Center (MCEOC), in cooperation with the National Science Foundation (NSF) and the Rochester Institute of Technology (RIT), requested a general framework for a project that would help them predict, manage, and quantify flood risk. The reason for this request was that the lack of a quantitative risk model for flooding leaves Monroe County ineligible for Federal Emergency Management Agency (FEMA) funds in the case of a flood event. In response to this, two preliminary models were developed by RIT's Science Master's Program (RIT SMP) for possible use by Monroe County. The two models were an **Obstruction Detection Model** and a **Risk Assessment Model**. Both employ LiDAR and Orthophoto data in order to ensure very high spatial resolution and concurrent coverage of the image and terrain data. The Obstruction Detection Model relies upon LiDAR for analysis, using the DOPs only for visual inspection, clipping feature creation, and providing context for recognizing features and better understanding of the generated imagery. In the case of the Risk Assessment Model, various vector data (comprised of social and infrastructure information) from Monroe County and New York State are used in conjunction with LiDAR and DOPs, with the potential to use the areas identified by the Obstruction Detection Model. The resolution of the LiDAR-derived DEMs were also varied in order to determine the sensitivity of the RAM to the DEM resolution. Finding the optimal

resolution would reduce the computation time needed to generate the DEMs and would have potentially significant impacts on file size. Out of the project implementation of the ODM and the RAM, the Flood Extent Generator (FEG) was created in order to better test and develop a means to create flood extents for usage in the RAM based upon risk points identified by the ODM. Following upon having the methodology for creating flood extents split off from the ODM, the Truth Assessment Model (TAM) was created as a simple means of comparing the FEG extents against extents from other, more tested and trusted models, such as Hazus (Department of Homeland Security FEMA 2016).

Hazus is a standardized methodology and toolset that has been applied to many different disaster scenarios across the US, which has the ability to help determine and visualize risk to infrastructure and populations. As an accepted standard for risk analysis and quantification, Hazus serves as the benchmark against which this project's models will be compared. If this project can produce results substantially similar to Hazus more rapidly and more simply, then the models and methodologies proposed herein have been successful. If the results do not demonstrate significant agreement with the results of Hazus, the various models will need to be improved in order to increase their predictive accuracy.

The goal of the Obstruction Detection Model is not to completely negate the need for human involvement, but to help assess potential problem areas that can be evaluated ahead of time; the Risk Assessment Model can be used when a problem has been identified to ascertain, in near real-time, the extent of possible damages. The Risk Assessment Model can also be used to run predictive scenarios based upon data from the Obstruction Detection Model and extents from the Flood Extent Generator, enabling decision makers to see what a potential flood and its damage could look like given an obstruction as identified by the Obstruction Detection Model and the flood extent created by the Flood Extent Generator.

An example that illustrates how the models are envisioned to function is as follows: A possible flood point is identified using the Obstruction Detection Model. This flood point is used to generate variable resolution flood plains using the LiDAR-derived DEMs of the Flood Extent Generator. There will be multiple flood plains of varying spatial resolution so that the sensitivity of the Risk Assessment model results to FEG resolution can be analyzed using the TAM to compare the newly generated extents against extents from more proven models, like Hazus. Using the flood level values, a series of maps are generated that show the possible monetary and human impacts a given flood could have upon the study area. These maps can be consulted to help guide decision makers in determining sites for investigation of potential flood hazards, improvement of flood protection measures, and finally, routes that are critical for First Responders in emergencies. See Figure 2 below for a visual representation.

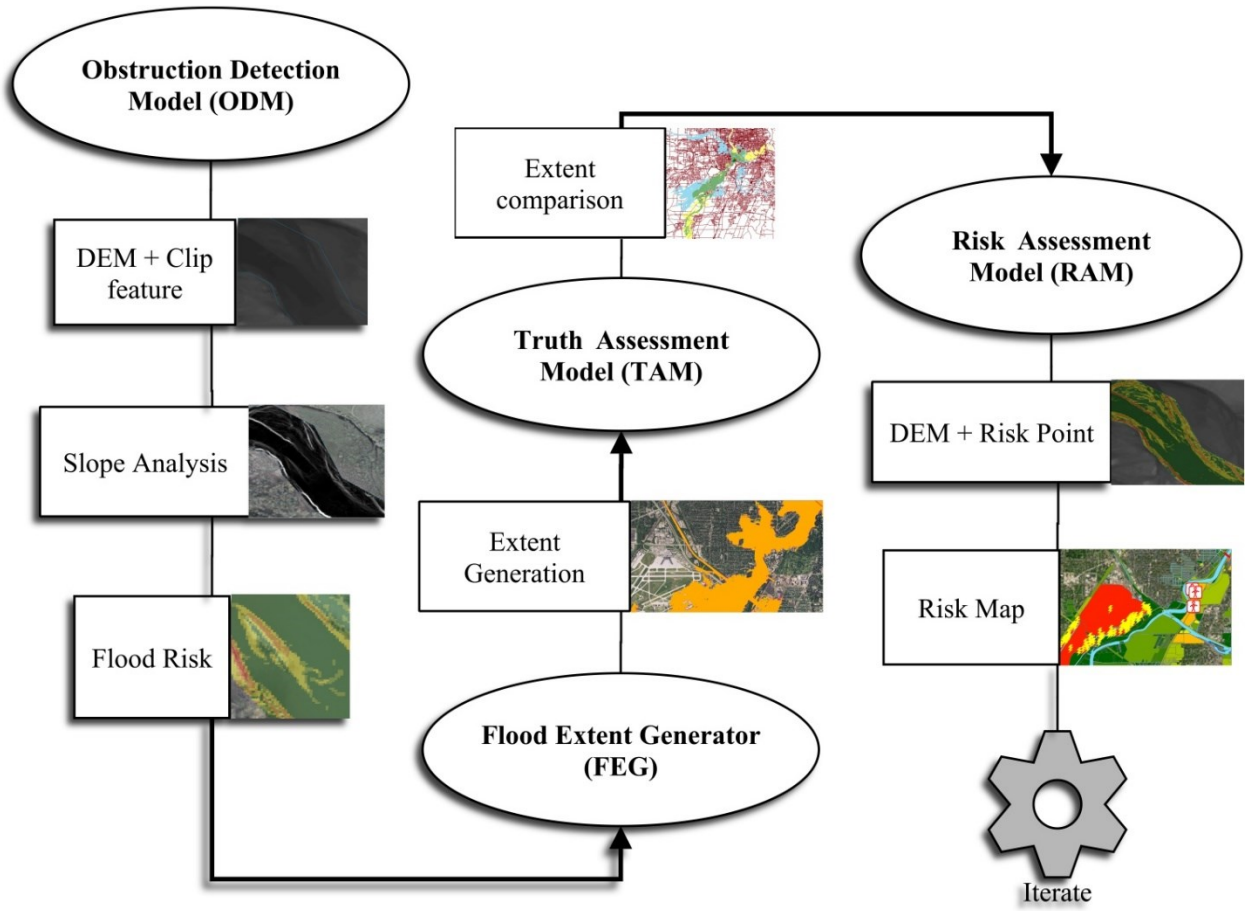

Figure 2 - Model Interaction Overview. This illustrates the proposed interaction between the ODM, FEG, TAM, and the RAM, using the ODM to generate scenarios for the RAM to evaluate for Risk.

Obstruction Detection Model (ODM):

The Obstruction Detection Model is a five-class predictive slope-analysis model that, when given a DEM or DSM of a river, will output a map that highlights the areas that may contain sub-surface obstructions in the waterway. Currently, the DOPs serve only to enable a user to do a visual analysis on the results of the ODM by providing context that is easy to interpret. The high spatial resolution of the LiDAR derived DEM allows the Obstruction Detection Model to analyze the slope deviations of the water surface, and as such, limits the model to being a computer processing-intensive analysis that is ill suited for in-field or real-time use. However, when used as a predictive tool where processing time is not a constraint, it can generate obstruction maps that can be used to investigate risk in-situ. Figure 3 illustrates how the ODM is structured.

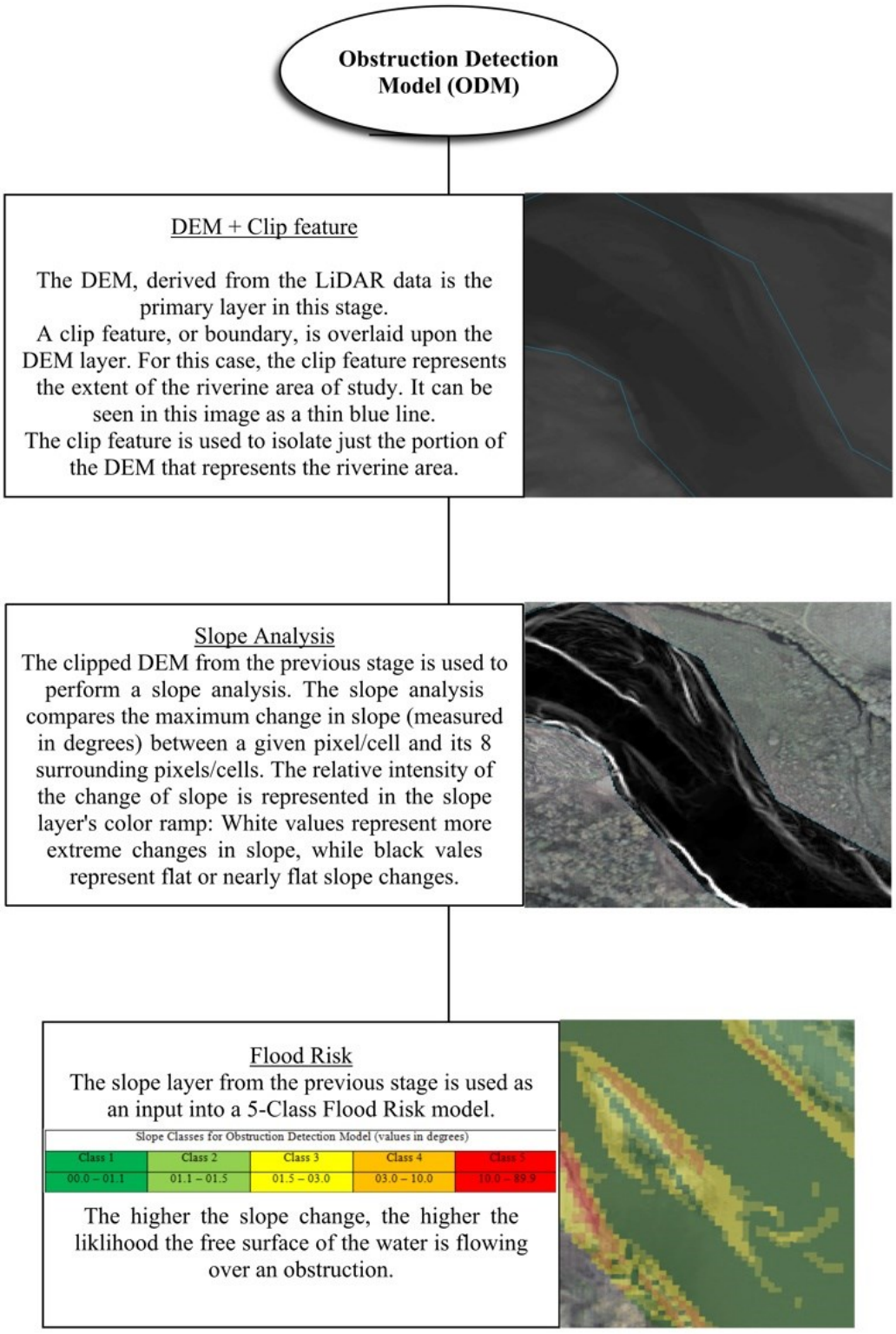

Figure 3 - ODM Overview and Explanation. This overview serves to explain the major components of the ODM, and to explain the steps of the ODM process.

Another consideration in the production of the various LiDAR-derived DEMs is the interpolation method. Each interpolation method uses a different algorithm to determine how to fill gaps in the data, and as such, will produce different results when applied to the imagery. The different algorithms also have different computational requirements, with some algorithms being very simple and fast to run, such as Nearest Neighbor, whereas interpolation methods like Kriging are highly complex computations that take many times longer to run. Since the point of both proposed models is to be fast and easy to run, the computational load of the different interpolation methods will be taken into account. Ultimately, the interpolation method chosen should be the most accurate approximation (given other constraints) of the water surface slope contained in the point cloud. There are many interpolation methods that can be employed, but methods such as Original Kriging, Regression Kriging, and Gradient plus Inverse Distance Squared (GIDS) have been found to be the most accurate and least sensitive to noise in the dataset (Li and Heap 2011). However, these methods tend to be very computationally intensive. IDW was found to be one of the most recommended methods of interpolation, and is relatively light on computing resources (Li and Heap 2011).

The five slope classes currently used in the model were derived by visual inspection of the river areas in the DOPs. The first class roughly corresponded to flat water and flat ground. The second class roughly corresponded to slightly rolling water. The third class corresponded mostly to water immediately surrounding the banks of the river or other large objects mid-stream. The fourth class was comprised mostly of in-river sandbars and other obstructions that were not clipped out beforehand as being "land" returns. The fifth class mostly corresponds to areas where trees run up directly to the water's edge, representing a very large change in slope. Testing of the five slope classes against various locations throughout NY, including Broome, Erie, Genesee, Jefferson, and Livingston Counties, indicate that the classes may be appropriate for usage in other locations and river reaches.

The goal of the synergy between the ODM and the RAM is to create a map that decision makers and first responders can look at in order to evaluate how and where to respond. The ODM, run prior to the event, will provide the RAM with the locations of possible obstructions, as well as the DEMs the RAM needs for flood modeling. The RAM will yield Risk Factor values that can be mapped and visually interpreted easily. Figure 3 illustrates how the various components of the ODM create a product that can be used to generate scenarios in the RAM.

Flood Extent Generator (FEG):

The Flood Extent Generator (FEG) is a simplistic model that creates flood extents by using a manually placed obstruction (identified by the ODM), a filled DEM, and a reclass of the heights contained in the filled DEM. The goal of the FEG follows the goals of the entire Flood Risk Model

project: simple to run, quick, and computationally light. The FEG was created by looking at the difference in height between the water surface and the maximum height of an obstruction or other object. For a preliminary test scenario, the Ford Street Bridge in Rochester, NY, within the Genesee River was used. Using the elevation difference between the two, a flood height was created creating a scenario where the Ford Street Bridge is completely blocked from the Genesee River up until the bridge surface. The range of height values represent the flood boundaries that the FEG will create by "flooding" those heights, making areas in the DEM matching those height ranges count as flooded. Once the FEG raster has been created, it is converted to a vector to ease display and analysis. The actual test scenario used was a ≈4.7m flood height that matches a Hazus modeled 46300cfs historic flood on the Genesee River.

The FEG was run against 3, 5, 10, and 30 meter data to evaluate if the resolution of the input DEM would appreciably influence the resultant flood extents. These values were chosen as the Hazus data was 3m cells and 5, 10, and 30 meter data match up with the spatial resolutions of other data products employed in the Flood Risk Model project, as well as data resolutions of popular products that could be used in the Flood Risk Model project such as SRTM 1 arc-second (30m) and NED 1/3 arc-second (10m) data.

The FEG data are used as input data for both the TAM and the RAM. Ideally, the coarsest possible resolution would be used further along in the model to maintain manageable dataset file size and processing times.

Truth Assessment Model (TAM):

The Truth Assessment model (TAM) is a qualitative model that compares the results generated by the FEG against the results of various Hazus models run by Justin Cole, in Monroe County, NY (Justin Cole 2013). The scenarios provided encompass the Black Creek, Irondequoit River, and Genesee River at various flood stages in each location. For the purposes of this analysis, the greatest flood stage for each location was chosen by selecting the provided data with the largest flow in cubic feet per second (cfs). The provided data are rasters that show the flood height above the normal terrain, giving a means to determine the depth of a flood at a given location. These data were converted to vector extents using raster to polygon in order that they can be used in the RAM and have their areas compared numerically with the results of the FEG.

The TAM compares the results of the FEG-generated data to the Hazus-generated data by comparing both the total flood extent area (as calculated by the Area field in the shapefile) and the total area of overlapping flood extent coverage. This geographic agreement is determined by using the Union analysis on the vector flood extents from the FEG and Hazus data. The output of the Union command

shows the areas flooded only under the FEG model and the Hazus model, as well as the areas flooded under both models. Using the results of the TAM, the relative agreement between the models can easily be visualized and computed by comparing the area of agreement against the total area of the Union analysis.

Risk Assessment Model (RAM):

The Risk Assessment model is a qualitative numerical model that provides numerical values for a few key factors that have been identified as important in risk management scenarios, as determined in several discussions with Fred Rion, Monroe County Emergency Operations Center spanning 2011 to 2015. For this model, these factors are: priority rating (rated importance of structure/parcel as defined by Fred Rion of Monroe County), cost (monetary, derived from parcel information), human impact (lives lost/impacted, derived from census and/or parcel information), and flood percentile (height above mean river flow, measured or modeled value derived from USGS information). The purpose of the resultant calculated Risk Factor value is to provide a scalar value (based on a coded numbering system) that can be used to assess relative risk across a given area for a given flood event, thus facilitating planning and emergency response efforts. This approach was inspired by the Social Vulnerability Index (SOVI). The SOVI is a linear averaging model designed by Susan Cutter (Hazards and Vulnerability Research Institute (HVRI) 2011) which incorporates various social data such as age, gender, race, and income to help quantify the risk level of a given population in a given area. The general framework of the SOVI has been adapted to develop the Risk Assessment Model, though it is not planned to incorporate the full 31-variable set as defined in the SOVI 2009 formulation.

Use of Pre-Existing Tools:

An important part of the RAM is the integration and use of pre-existing tools from the GIS industry. Table 2 below explains how these tools will be used to process and analyze the various data ingested by the RAM. The table establishes the basic dataflow of the RAM, from the LiDAR data necessary to generate the DEMs to using ArcGIS to input the DEMs and integrate the social data, to one of various potential hydrological modeling tools to create flood extents.

Table 2 - Tools for RAM. This table explains and summarizes the tools proposed for use in the RAM and how they will benefit the analysis.

Tools for use in RAM	
LASTools	LasTools is a suite of command-line and/or graphical user interface (GUI) tools, developed by Martin Isenburg, aimed at processing and developing LiDAR data and products (rapidlasso GmbH n.d.). LasTools was used to process the LiDAR files into first-return values only. LasTools was also used to visualize the data in 3D.
ArcGIS	ArcGIS is a popular GIS suite commonly employed by academic institutions, government agencies, and private firms (ESRI n.d.). ArcGIS is where all of the model functions will be built, and where the bulk of the analysis and processing will take place. It is proposed that ArcGIS will also be used in order to build the two models into GUI tools that can be run from within ArcGIS, packaged as an Arc Toolbox.
Arc Hydro **ArcGIS Hydro Tools** **Fema Hazus**	These are all hydrological modeling tools that are commonly used by planners and decision makers, and have been cited by Justin Cole as acceptable for use in the RAM. FEMA's Hazus model is used to generate the Flood Insurance Risk Maps (FIRMs), and as such, would be accepted by FEMA as an analytical tool (U.S. Department of Homeland Security FEMA 2016). However, Hazus has noted compatibility issues with some recent ArcGIS builds, and is currently not the prime candidate. ArcHydro (ESRI n.d.), or Hydrological tools in Spatial Analyst (ESRI n.d.), will be the primary focus for use with the RAM because ArcGIS 10.x ships with these tools, and they will be present/available for all who run the ODM and RAM.

Data Inputs:

The data inputs below are the general types of data needed to successfully run the RAM and generate results. Generally speaking, the RAM needs a DEM or TIN (preferably created using LiDAR data for extra precision), vector data containing the needed social data for the model, and user inputs for where the obstruction is and how much the area has flooded. The section below gives an overview of the types of inputs, what is done with them, and what they create as a general framework for application of the model.

LIDAR

Process LIDAR (subset data)

- Processed LIDAR → LIDAR derived DEM or TIN
- DEM/TIN → Overlay orthophoto (or other imagery)

DEM/TIN + Vector

Add in census/parcels data, priority areas, tax maps (property values)

- DEM/TIN + Vector → Hydrology maps (river beds, etc)

User Inputs

- River Height: The user can define a river height and "flood" the area of concern
- Obstruction: The user can define/detect the location and severity of the obstruction
    - (Obstructions from Obstruction Detection Model can also be used)

The social data inputs required for the Risk Assessment Model can loosely be classified as parcel data and census data. The infrastructure data are the location of key structures in Monroe County, and are tied to parcel feature data. The parcel data provide the assessed value of the parcel (both the plot and the structures) and Land Use/Land Cover, while the census data provide the population of the census unit (census blocks for this analysis). The infrastructure data, taken from Monroe County, are used to create a prioritized list of critical infrastructure are used in the Risk Assessment Model formula. Areas of inundation are derived from the LiDAR and DEM data.

The near real-time data inputs would have been water level data and potential integration of field-reported data concerning flood extents for model verification purposes. However, community sourced real-time data regarding flood damage and other obstructions can be inaccurate and may not add much value to the model (Hudson-Smith, et al. 2009). With water-level inputs, the flood extent layer could be updated to match the in-field conditions. This would then cause the parcels impacted to change and would result in a new risk map as the water level changes. This re-running of the model, based upon new data, could help the model to maintain a closer relationship to the in-field conditions, as opposed to simply being a static representation. The model should be computationally simple enough to be run in the field and would benefit from the close communication between responders and the field station, but could also be run back in the Emergency Operations Center, independent of the field in order to ease the responder's task load. See Figure 4 for an overview of the RAM and how each variable contributes to the model.

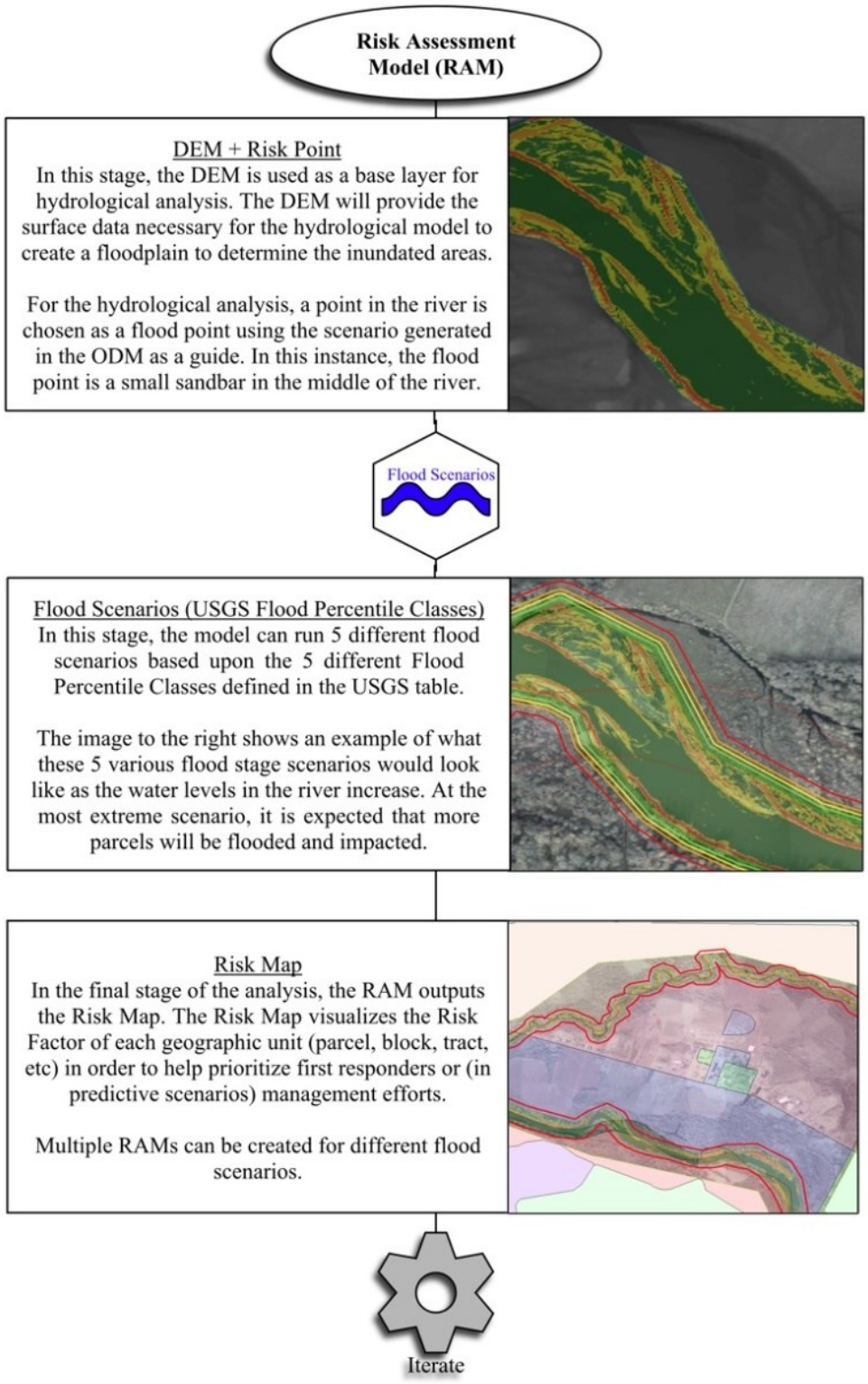

Figure 4 - RAM Overview and Explanation. This image shows what the major steps in the RAM could look like.

It is essential to the functioning of the model that various, often disparate, inputs are ingested into the model and potentially weighted to produce a value that the end user can then use to form a decision. For this reason, it is critical that the inputs used in the model be analyzed for their sensitivity and interactions between variables. The goal is to reduce the model to only the variables that contribute the most to the model's predictive ability (Gouldby, et al. 2010). It is hypothesized that the variables of risk factor, cost, human impact, and flood percentile will most simply describe the impact of a flood on a given parcel of land.

As a hypothetical, based on the Monroe County rankings list, an open field that contains no infrastructure would rank as a priority 1/10 (low priority) item. An area of land that contains a critical piece of power, defense, health, or other civil infrastructure would rank much higher on the scale. The size of the scale depends upon how many classes of infrastructure Monroe County has already defined in their internal Critical Infrastructure and Key Resources (CIKR) rating system (Monroe County Emergency Operations Center 2012). This Priority Rating value would contribute a high rating to a structure like the Ginna Nuclear Power Plant, whereas an open field would contribute a low Risk Factor value to the model. Table 3 demonstrates how this Priority Ranking could be defined.

Table 3 - Priority Rating (Based upon Anderson Level 1).

1	Undeveloped		6	School and Care
2	Rural Unoccupied		7	Hospital and Med.
3	Rural Developed		8	Electrical Infrastructure
4	Suburban		9	Fossil Fuel Power
5	Urban/Populated		10	Nuclear Power

As the Risk Assessment model stands currently, it is a strictly linear model with no weighting of the input variables. There are two potential approaches to weighting input variables: objective and subjective weighting. Subjective weighting would assign a higher weight to variables that are more important to Monroe County, whereas objective weighting would give more or less weight to a given variable dependent upon its sensitivity (Maggino and Ruviglioni 2009). The sensitivity of a variable determines its strength and relevance in determining the output of the model. A more sensitive variable contributes more to the model's computation than a less sensitive variable does. An advantage of a weighted subjective model would be that the model would potentially predict risk more accurately for parcels in a manner that Monroe County cares about (i.e.: weighting human impact more than cost or priority rating) (Maggino and Ruviglioni 2009). An objectively weighted model will likely achieve greater predictive accuracy than the subjectively weighted model, but may underestimate risk for certain parcels and in so doing commit a Type II error. A Type II error is a failure to reject the null hypothesis,

here being that the parcels are not at risk. However, in this instance, the error would not necessarily be that the parcel is not at risk at all, but rather that the parcel's risk is under-estimated. Despite the potential predictive advantages of the subjective and objective weighted models, a liner model was created for this project for the sake of simplicity. Over the course of discussions with the Monroe County Emergency Operations Center, the linear model was favored as the Emergency Operations Center felt that all contributing model variables were equally important.

Project Objectives:

As stated prior, the objectives of the project were to produce easy to use, quick to run, and computationally light, flood risk and flood modeling tools for usage in disaster management and emergency response situations, being the Obstruction Detection Model (ODM), Flood Extent Generator (FEG), Truth Assessment Model (TAM), and Risk Assessment Model (RAM).

The ODM contributes to the project goals by identifying potential subsurface or within-river obstructions using a slope reclassification analysis on LiDAR-derived DEMs (or other fine spatial resolution data). The FEG takes the risk points identified by the ODM and rapidly creates flood extents using a reclassification analysis of sink-filled DEM data.

Following the ODM, the TAM can be used to validate the FEG data against other truth data by using a union analysis to determine the areas of overlap. The greater the area of spatial agreement, the better the utility of the FEG data for the given site and dataset.

After the TAM has determined whether or not the FEG data are usable for the given site, the RAM generates an output map with the risk factor values to help visualize and prioritize first responder efforts. The RAM output is created by using the reclass tool, and as such, is quick to run and generate results.

Methodology (Obstruction Detection Model):

Objective:

The Obstruction Detection Model has been designed to be a DEM-based analysis that will help identify possible flood obstructions in river areas. This model is intended to be easy to run and general enough that it can be used in any study area, using data that most municipalities have access to. In order to identify possible flood obstructions, the ODM uses a slope analysis on the water's surface and then reclassifies the degree slope into five Slope Classes. The most computationally intensive part of this analysis is interpolating the DEMs from the LiDAR data.

Model Overview (Obstruction Detection Model):

There are five flood-risk classes in the model, corresponding to different slope values (Table 4). It is hypothesized that the higher the slope value, the greater the risk that object is an obstruction that could cause a flood. Computer modeling of free surface deformation in cases of fluid flowing over a semi-circular obstruction indicates that there will be turbulence on the leading edge of the obstruction (Lu, et al. 2008). I believe that this turbulence and displacement of the free surface of the flowing water will be proportional to the speed of the flow and the proximity of the obstruction to the free surface of the water. DOPs used for visualization and context are processed photo data from the WASP sensor. In the event of a need for newer data than the county's DOP library, other high resolution (sub-meter) image products should be able to be used in the place of DOPs for visual analysis with minimal negative effects upon interpretability.

The slope analysis relies upon the minute spatial resolution of the LiDAR terrain to detect changes in elevation over the surface of the water reliably (Vaze and Teng 2007). A series of LiDAR derived DEMs was produced at varying resolutions in order to determine whether the original resolution is required (Vaze and Teng 2007), or if more generalized products could be used. The DEMs were generated at the original LiDAR resolution ($1.62m^2$) as well as at $3m^2$, $5m^2$, $10m^2$, and $30m^2$. DEMs below the original resolution were investigated ($0.25m^2$, $0.50m^2$, $0.75m^2$, $1m^2$), but nearly all failed to complete interpolation and as such, were discarded from this analysis. It is not certain why the super-sampling failed to process properly in ArcGIS, but it may have to do with the size in memory of the dataset while it is being super-sampled and interpolated. ArcGIS is not natively 64-bit for most of the analysis tools, so the maximum memory space for a given tool is roughly 2GB, with 4GB only for the large-address-aware tools (ESRI 2016). The simpler NN and IDW analyses would complete super-sampling, but SPLB and Kriging failed. The multipoint dataset being interpolated contains 5,121,450 records, though no documentation within ArcGIS was found to support the possibility that there are any

limits on the number of entries contained in a Multipoint dataset, nor on the filesize that can be processed by the Kriging and Spline with Barriers tools, it is possible a tool or analysis is exceeding its memory space, causing a buffer overflow and subsequently crashing. Furthermore, ArcGIS applies a Nearest Neighbor interpolation on all data being super-sampled before doing the requested interpolation (ESRI 2014), compounding the distortion from interpolation and making the super-sampled DEMs of questionable utility.

The slope classes were determined using a combination of visual analysis and histogram analysis. The riverine area was inspected for flat looking water (Class 1 – 2 [dark green – light green]), water with some turbulence (Class 3 – 4 [yellow – orange]), and river banks (Class 5 [red]). Using the Identify tool against the slope rasters, the slope values of various areas could be determined. Now that the slope classes have been determined, future uses of the model need only use the classes by importing them into the reclass tool. It is unlikely that another person completing the same inspection using the above methodology would arrive at exactly the same class bounds, so it may be beneficial for future runs of the model to implement the provided classes as starting points, and then using visual analysis and site-specific known obstruction locations, check for agreement. Based upon the findings in the user's study site, the class boundaries can be adjusted to improve the detection of riverine obstructions. Averaging or another method, such as supervised or unsupervised training, could be used to account for variability of class boundary creation, eventually leading to a more robust classification. By using a method such as supervised training against verified obstructions in a riverine area as training data, the supervised classification algorithm could systematically determine what slope values would represent obstructions. A potential limitation of the slope-based classification is that changes in river stage will result in variability of surface deflection as the river stage rises and falls, making choosing appropriate training data and verification data difficult. Site variability will also play a large role in determining what class boundaries are most suitable, but the current class boundaries have produced consistent results by identifying objects within riverine areas across various river reaches in New York State including Broome, Erie, Genesee, Jefferson, and Livingston Counties, as outlined later in this report (see Results & Discussion (Obstruction Detection Model):).

Table 4 - Slope Reclassification Values for ODM.

Slope Classes for Obstruction Detection Model (values in degrees)				
Class 1	Class 2	Class 3	Class 4	Class 5
00.0° – 01.1°	01.1° – 01.5°	01.5° – 03.0°	03.0° – 10.0°	10.0° – 89.9°

The Obstruction Detection Model is run against clipped DEMs that represent the river area. The clipped layers were hand-digitized to the river edges, though county provided hydrological shapefiles can also be used when they exist in the area of study. A buffer can be applied to the shapefiles to compensate for any areas that are not encompassed by the shapefile, though no buffer was applied against the digitized river extents.

The Obstruction Detection Model focuses on attempting to find sub-surface obstructions in riverine areas, and as such, requires detailed height information such as LiDAR DEMs, as well as high spatial resolution imagery for visual analysis. The LiDAR being used is pre-processed and consists of the ground (final) returns (see Figure 5 below). The two DOPs being used are Short Wave Infrared (SWIR) and Visible Spectrum (RGB) images. They are sourced from the WASP sensor. Since the DOPs are used solely for visualization purposes, they can be sourced from anywhere that provides imagery with sufficient spatial resolution for visual analysis.

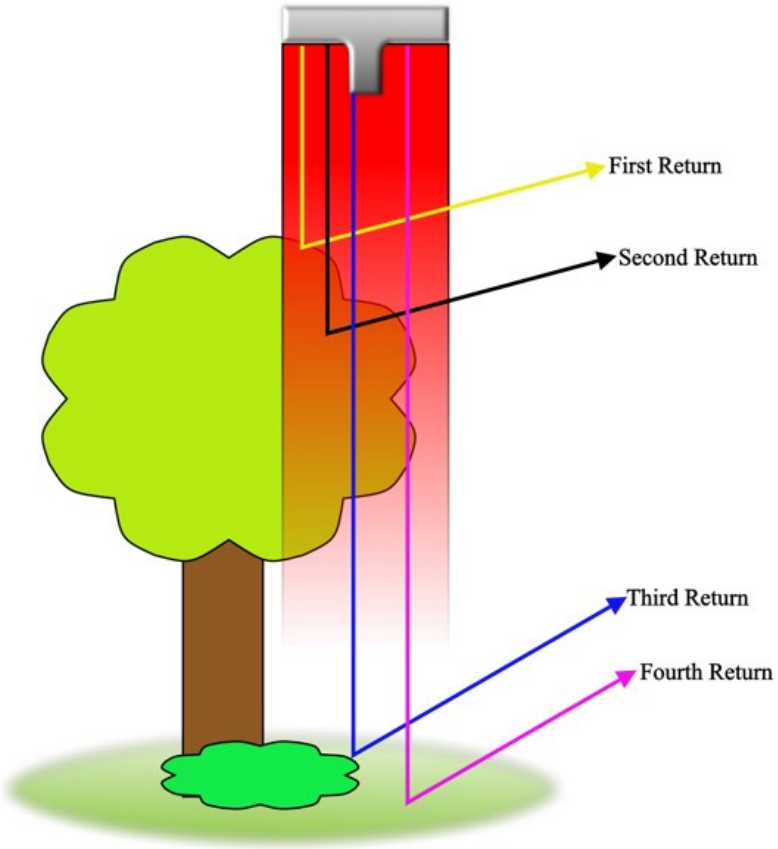

Figure 5 - Multiple Return LiDAR Overview. This figure illustrates how a single LiDAR pulse can be comprised of multiple returns, and what the Return Number and Number of Returns variables can represent in a typical scene.

LiDAR Imagery:

The LiDAR data were processed by Dr. Jan van Aardt in Merrick MARS® Explorer (Merrick & Company 2017) into first, ground, and all/classified sets. Only the first return LAS file was imported into ArcGIS, in order to detect the top-most surfaces of the features in the site, including vegetation, built features, and the water surface. The ground return set was classified to only show the ground returns, removing the vegetation, built features, and the water returns, proving unsuitable for usage in this analysis. Using the LAS to Multipoint tool in ArcGIS, the LiDAR data were converted into a multipoint file. The data were checked to make sure the import process functioned properly and were then used in the Point to Raster tool with default values of Cell Assignment: MOST_FREQUENT, Priority Field: None, Cellsize: 1.619524, and Z (return height) specified for the "Value Field", creating the layer "ground_new".

The resultant raster generated from the Point to Raster conversion covered the whole extent of the study site (Seneca Nation of Indians, Cattaraugus Indian Reservation, Irving, NY) beyond the immediate riverine areas of interest. To focus the analysis, the raster was clipped to be a more manageable size that encompassed only the riverine areas. A shapefile was hand-digitized and used to clip the raster. The shapefile was created by visually inspecting the river extents and digitizing the water's border as shown by the high resolution imagery. In order to create the slope classes, visual inspection of non-water features only at the immediate border to the river and the area encompassing the entirety of the water's surface and any features that were present within the bounds of the river were observed. The riverine areas were determined using visual inspection and delineated using hand digitizing. Going forward, usage of pre-existing hydrography boundaries is preferred to reduce time to create the data needed for the ODM. The borders were made general on purpose to include the vegetation and structures at the edge of the river, as these features would be used to help determine the slope classes. In this manner, the riverine borders encompass all of the features that are concerned with the slope classes: the river's surface, earth/dirt/sand/rock, and vegetation.

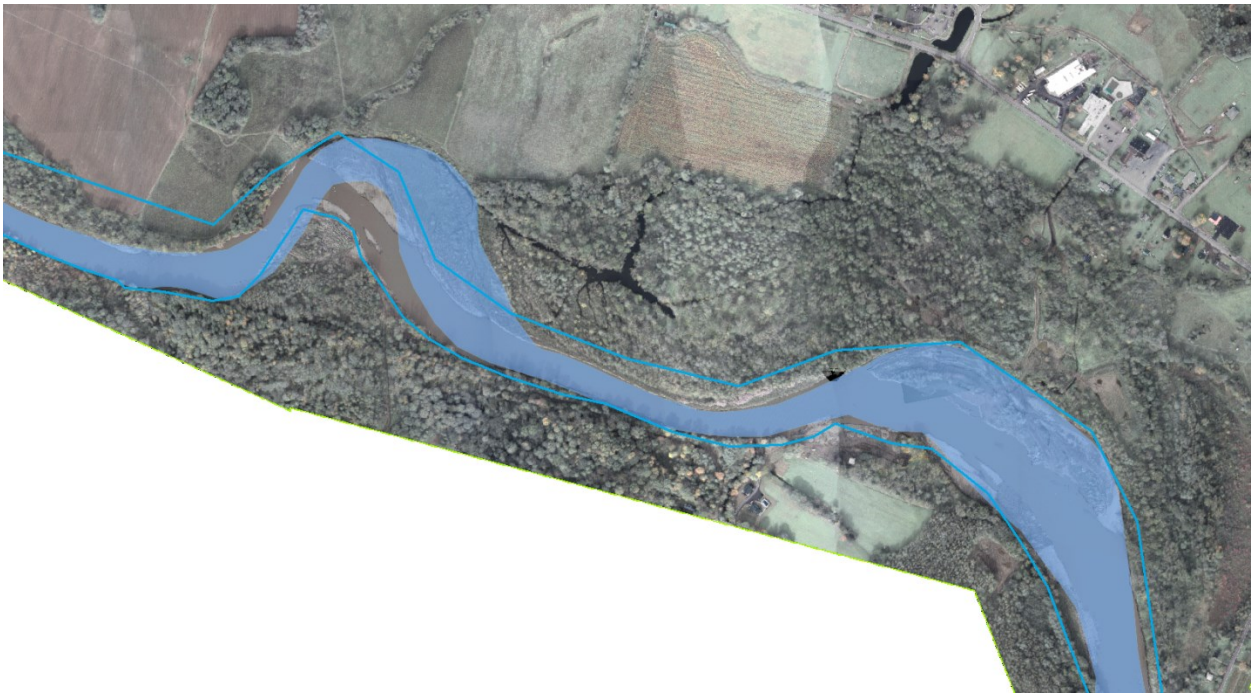

Figure 6 - Riverine extent (Hydrological Features) vs USGS NHD (National Hydrography Dataset). This figure illustrates the differences in extent of the Cattaraugus Creek between the hand-digitized Hydrological Features layer (blue line) and the USGS NHD provided layer (solid blue polygon).

In Figure 6, the differences between the hand-digitized layer (thin blue line) and the USGS NHD layer (solid blue polygon) can be examined. A confounding factor is the fact that the water level is variable in rivers, leading to variable river extents based upon the stage height and flow. This is one of the many reasons why it is ideal for the LiDAR to be flown coincident with the imagery to be used for analysis, though it isn't explicitly necessary. The USGS boundaries are in some areas more general than the hand-digitized boundaries and also appear to be shifted or translated over the ground, possibly as a result of projection differences, scale differences, or shifts in the river bounds over time. However, these boundaries encompass the riverine areas in the target site nearly completely, and would do so easily with an added 30m buffer. It is likely that going forward, county provided vector files (with a recommended buffer of 30m) could be used for the river extents now that the slope classes have been developed.

The clipped raster, being derived from a point file, had many no-data pixels that needed to be smoothed and interpolated. It was found that Kriging (with defaults of a variable search window and 12 sample points) and other computationally complex interpolation analyses would silently fail under ArcGIS 10, 10.1, 10.2, 10.3, and 10.4, outputting a flat image up until the point where it stopped. As discussed previously, it is possible that the more complex interpolation analyses failed due to a buffer overflow or an using improper search window (too small or too large). Too small a search window can lead to the interpolation failing to identify variation in the raw surface, potentially leading to an

interpolated surface that under-represents surface changes. Too large a search window can lead to the analysis taking exponentially longer or failing to produce a predicted value (ESRI n.d.). For this reason, the three interpolation methods used were Inverse Distance Weighted (IDW), Natural Neighbor (NN), and Spline with Barriers (SPLB), as they would consistently produce a viable raster. The interpolation tools were run with defaults, except for cell size, which was set to match the point file (1.619524). A possible analytical method would be to use a cross-tabulation or a raster subtraction process to see how each cell differed between the two images.

Interpolation Algorithms:

As part of the optimization of the ODM, three different interpolation methods built into ArcGIS were employed to interpolate the raw multipoint data from the converted LAS files. Interpolation serves to predict missing values in a raster file by sampling other data points within the raster and performing various mathematical transformations on the missing data (ESRI 2016). Figure 7 below shows the distribution of height values in the raw dataset (Seneca Nation of Indians, Cattaraugus Indian Reservation, Irving, NY), as well as key statistical summary data for the dataset as a whole. The distribution of the Z-data as well as any changes in the statistical summary data were used as a means to evaluate the impact of the various interpolation methods on the data, and to better understand how they would impact the LiDAR-derived DEMs that had been generated.

Inverse Distance Weighted (IDW) is an interpolation method that uses a search window to look at neighboring data points to the target location, taking an average of those points' values. IDW assumes that data points closest to the target location will have more influence than data points further way, or more simply, that objects nearer one another are more similar than objects further from one another. The statistical summary values of the IDW data did not change significantly from the raw data, however the distribution of heights was altered, resulting in a slight left (lower height) skew, with overall fewer data points in each height value (Figure 7). The standard deviation of the dataset was reduced from 4.13 to 4.03, which is expected given that the interpolated data would be similar to other data near it, and local variance would be reduced.

Natural Neighbor is another interpolation method that was investigated for this project. The NN interpolation works by finding the closest subset of data points to sample around the point of interest, creating a Voronoi diagram of the sampled points, and then overlaying another Voronoi polygon over the point of interest. Weights for the sampled Voronoi polygons are determined by the amount of overlap of the point of interest polygon with the sampled polygons (ESRI 2016). An interesting featured of the NN interpolation is that it the interpolated values will be within the range of the values sampled for that point,

preventing the interpolation from creating erroneous features in the interpolated surface like pits and peaks. The statistical summary values of the NN data were nearly indistinguishable from the values from IDW, and similarly to IDW, the distribution of Z-values were skewed slightly left when compared to the raw data (Figure 7). The min and max values were slightly reduced from both the raw and IDW data, resulting in a slight reduction of the mean Z-value, aligning with the expected behavior of NN in making sure all values are within the range of sampled test values.

Spline with Barriers is the final interpolation method that was investigated for this project. SPLB works by using a mathematical transform that seeks to reduce the total variance of the surface, resulting in smooth surfaces. SPLB accomplishes this by making sure that the surface passes through each point in the dataset, and that the variance in height between the points is as small as possible (ESRI 2016). According to the ESRI documentation, SPLB is most appropriate for interpolating datasets such as ground surfaces, water tables, and plume concentrations. As with the previous two interpolations, SPLB results in a slight leftward skew of the data, and more constrained min and max values (Figure 7). The standard deviation of the dataset is greater than in IDW and NN, though it is still reduced when compared to the raw dataset. The mean value is the lowest of the three interpolations, likely due to the constrained min and max values.

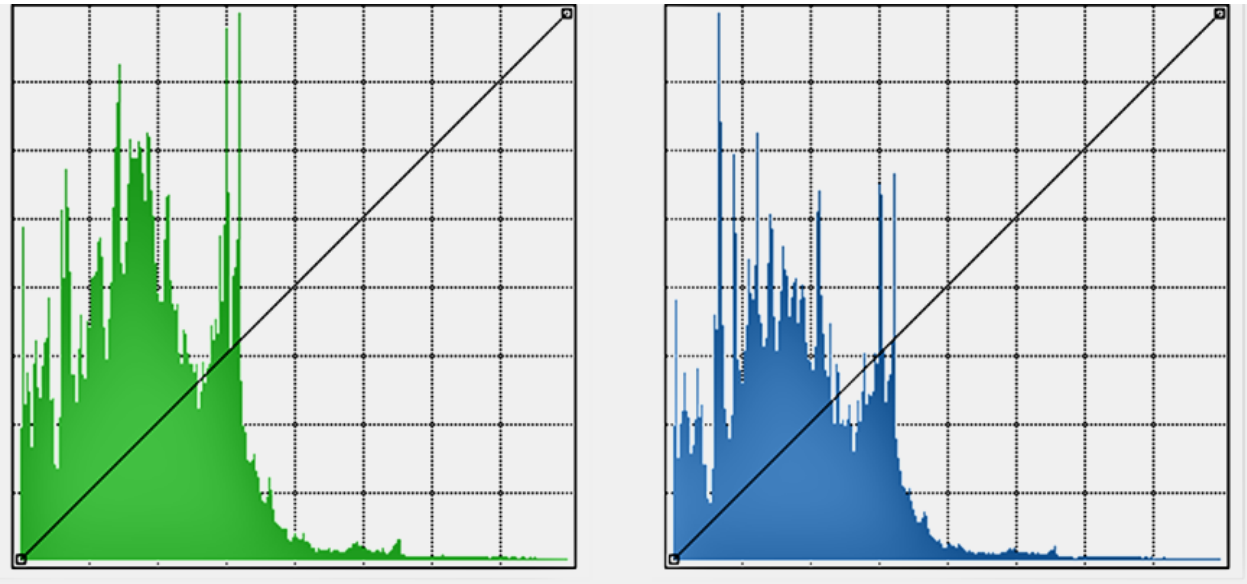

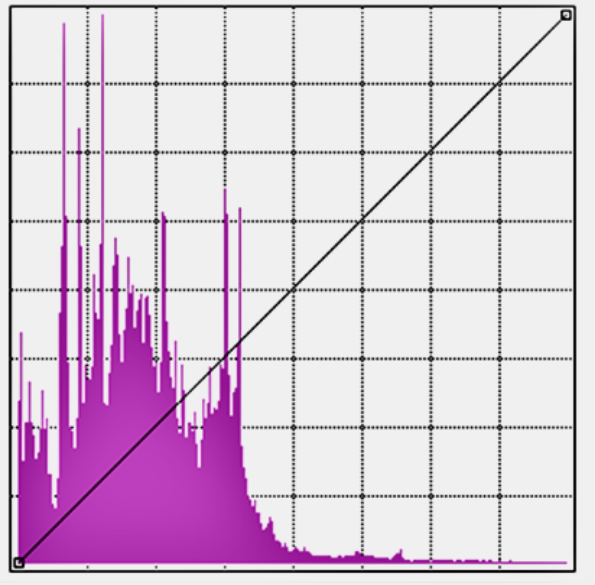

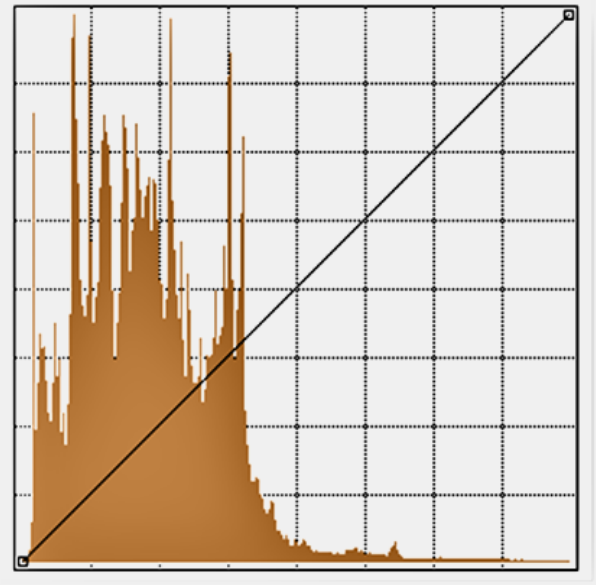

	RAW	IDW	NN	SPLB
Min	151.70	151.71	151.72	151.13
Max	182.75	182.51	182.50	183.43
Mean	158.98	158.67	158.65	158.63
Std. Deviation	4.13	4.03	4.03	4.07

Figure 7 - RAW, IDW, NN, & SPLB Statistical Summaries. This figure shows the distribution of values in the Value field (Z data, or height) for the original/raw data, the Inverse Distance Weighting interpolation, the Natural Neighbors interpolation, and the Spline with Barriers interpolation.

The final means of comparing the various interpolation methods tested in this project is illustrated in Figure 8 below, and that is how long the interpolation methods take to interpolate the same data layer, resampled to 1.62m, 3m, 5m, 10m, and 30m. IDW and NN both have a similar trend resulting in an exponential increase in processing time as the resolution of the data increases. SPLB's processing time did not closely follow either a linear or an exponential trend, instead most closely following a fourth-order polynomial. It is unclear why SPLB does not follow the same (and expected) trend of an exponential increase in processing time as the data become more dense, though SPLB remained consistently the most lengthy interpolation analysis run, with minimal variance in completion time when comparing 1.62m and 30m data (1.2X), whereas IDW and NN both took multiple times longer to complete the 1.62m data than they did the 30m data (2.2X and 10X, respectively).

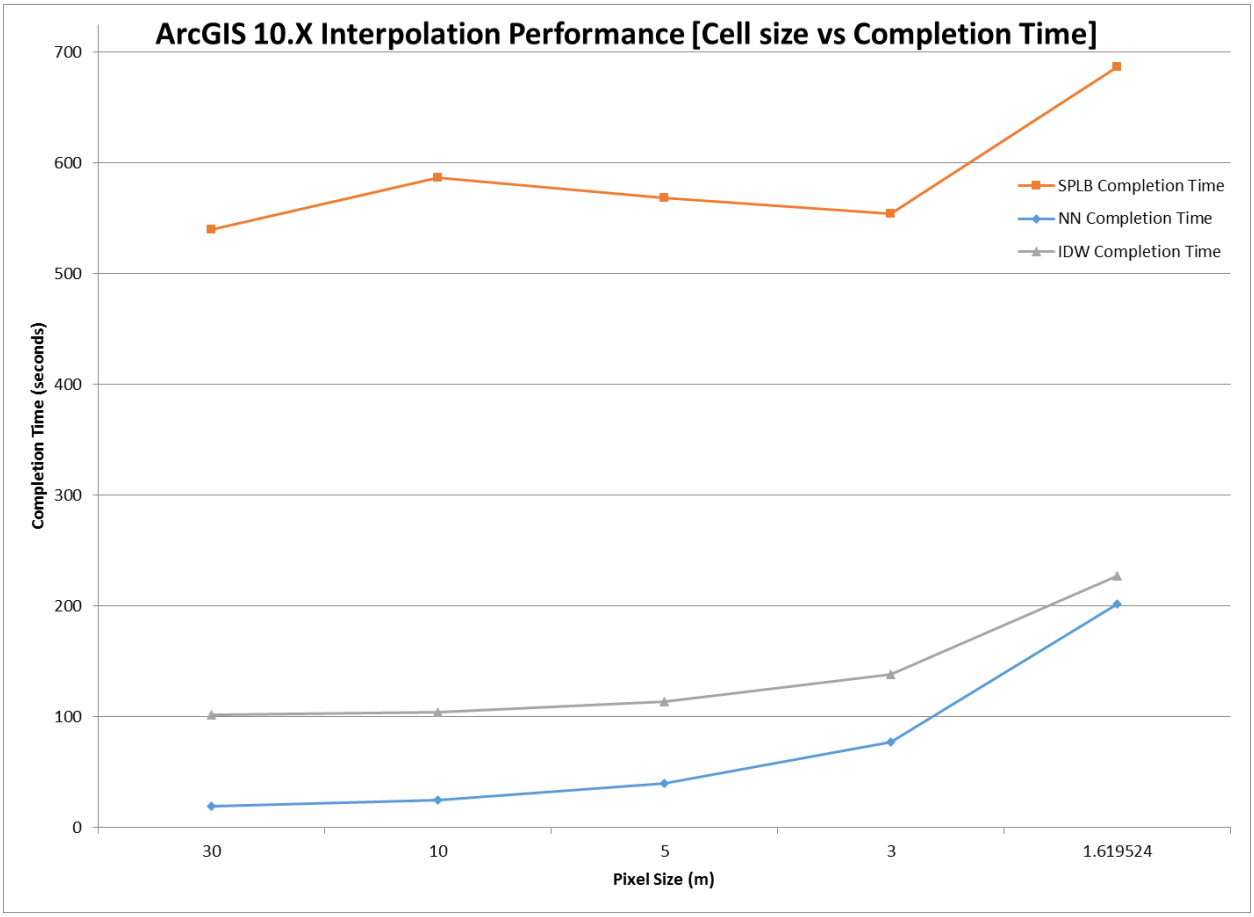

Figure 8 - Comparison of interpolation method performance. This figure shows the differences in interpolation performance between the three interpolation methods (IDW, NN, SPLB) across the various cell sizes in the dataset, with NN being the fastest and SPLB being the slowest.

Digital Orthophotos:

The two DOPs, RGB and SWIR, are used solely for context and visualization purposes in this analysis. Initially, it had been hoped that spectral classification could be used to help remove extraneous hits from edges, sand bars, and the like. This aspect of the Obstruction Detection Model has been shelved for the time being. The decision to simplify the Obstruction Detection Model was based upon the constraint of keeping the model simple, light, and fast to run. In terms of model simplicity, having more data sources and more calculations makes the model more complex. The extra data necessary for the spectral analysis would increase the file size of the dataset and the model's operating environment. Finally, algorithms for spectral analysis such as feature extraction can be very computationally intense, requiring longer processing times than the ODM's current slope-based analysis. These three mitigating factors had to be addressed in order to meet the goal of keeping the models simple, fast, and light.

The RGB and SWIR DOPs are clipped to the same extent as the LiDAR coverage rasters using the clip shapefile. This step is solely to reduce the size of the dataset as the RGB and SWIR images consume about 15GB for this study site when not clipped. For visualization purposes, the SWIR image was overlaid upon the RGB image with a transparency of 50%. This arrangement highlights the water areas, while still allowing some color information, making visual distinction easier.

Data Layer Overview (Obstruction Detection Model):

A number of intermediate image products have been created as a result of the analysis. IDW refers to rasters interpolated with Inverse Distance Weighted, NN refers to rasters interpolated using Natural Neighbor, and SPLB refers to rasters interpolated using Spline with Barriers. Full refers to products that encompass the entire site extent, while Hydro refers to products that have been clipped to only include the hydrological areas as defined by the Hydrological Features clip layer. The images can be broken down as in Table 5.

Table 5 - ODM Image Products. This table lists the intermediate products used to create the final classified obstruction map.

ODM Image Products		
Base Rasters	*SWIR Clip* *RGB Clip*	This set is comprised of two rasters taken from the RIT DIRS WASP sensor. The two rasters are overlaid upon one another with a 50% transparency in the SWIR layer to help with visual inspection.
Multipoint Data	*Ground (Full Site)* *Hydrography (Clipped)*	This set is comprised of two multipoint datasets that were created by importing the LAS file data.
Clip Features	*Hydrological Features Site Extent* *LiDAR Extent*	This set is comprised of vector files used to clip the source LiDAR/DOPs and/or other products.
Ground Rasters	*Ground (Raw)* *Ground (IDW)* *Ground (NN)* *Ground (SPLB)*	This set is comprised of rasters that cover the whole site extent as well as clipped versions (clipped to the LiDAR Extent layer's bounds). The "Raw" file is not interpolated, and the others have been interpolated as indicated. Each interpolation method contains a set of rasters at each of the five different output resolutions (1.62m, 3.00m, 5.00m, 10.00m, 30.00m).
Hydrography Rasters	*IDW Clip* *NN Clip* *SPLB Clip*	This set is comprised of raster files that were created by clipping the Ground Rasters with the Hydrological Rasters clip layer.
Slopes	*IDW Full/Hydro* *NN Full/Hydro* *SPLB Full/Hydro*	This set is comprised of rasters that cover the full site extent as well as just the hydrological features. They were generated by running a Slope analysis against the IDW, NN, and SPLB Ground Rasters and Hydrography Rasters.
Reclassed	*IDW Reclass Full/Hydro* *NN Reclass Full/Hydro* *SPLB Reclass Full/Hydro*	This set is comprised of rasters that have had a Reclass analysis run on them with the input being the Slope rasters (Table 4).
Interpolation Differences	*IDW – NN Hydro* *IDW – NN Slope* *IDW – SPLB Hydro* *IDW – SPLB Slope* *NN – SPLB Hydro* *NN – SPLB Slope*	This set is comprised of rasters that have been subtracted to illustrate the magnitude of the differences between the interpolation methods. There are two sets, Hydro (interpolated DEM clipped to hydrography features) and Slope, which illustrates the differences in resultant slope analyses.
Hydrological Buffers	*Buffer (00ft)* *Buffer (20ft)* *Buffer (40ft)* *Buffer (60ft)* *Buffer (100ft)*	This set is comprised of vectors that represent different buffer widths around the Hydrological Features layers. These buffer widths are used to visualize the extent of the river's flooding.
Point Spacing Summary	*LAS: Ground (New)* *LAS: Classified* *LAS: First* *LAS: Ground*	These layers show the different point spacing of the various LiDAR datasets using ArcGIS' Point Spacing Estimation technique.
Random Point Samples	*Random Sample* *R.S. NN Slope Hydro* *R.S. IDW Slope Hydro* *R.S. SPLB Slope Hydro*	These layers illustrate the points generated by Random Sample with the extracted slope values from the slope rasters (IDW, NN, SPLB).

Deriving Flood Risk Classes:

In order to develop the flood risk classes for the ODM, extensive visual inspection of the riverine areas was performed with manual random sampling using the *Identify* tool. Values for sampled locations for each of the five classes were recorded and then averaged to arrive at the preliminary manual class boundaries. At this stage, the boundaries still produced results that were too noisy, so the symbolization of the layer was adjusted manually until it was determined that the maximum number of features were being identified with the minimum number of false positive pixels. This method of establishing the flood risk classes is subject to scrutiny, as exact replication is not likely between users and there is the potential for any number of cognitive biases to influence the distribution, frequency, and criteria for the randomized sampling that was performed manually. In order to determine a more statistically robust and scientifically sound flood risk classification, random sampling and statistical reclassification were performed and the results evaluated.

In order to obtain the values needed for the statistical reclassification, *Random Sample* was run with 1,528,334 points and a minimum allowed distance of 1.62m to estimate approximately 50% coverage of the Slope (Hydro) layers and their native LiDAR point spacing (Figure 9). Even at 50% coverage, the sample density proved to be too high as ArcGIS printed an error stating that "the specified number of points could not be created in all cases due to restrictions from the minimum allowed distance."

Once the RSample layer was created, *Extract Values To Points* was run against the different Slope (Hydro) layers, being NN, IDW, and SPLB. *Extract Values To Points* samples the values for a raster at the location of a given point in a dataset, effectively assigning those values to the multipoint data. In this manner, the different multipoint layers now had randomly sampled slope values against which to run the different statistical classification methods to determine the flood risk classes.

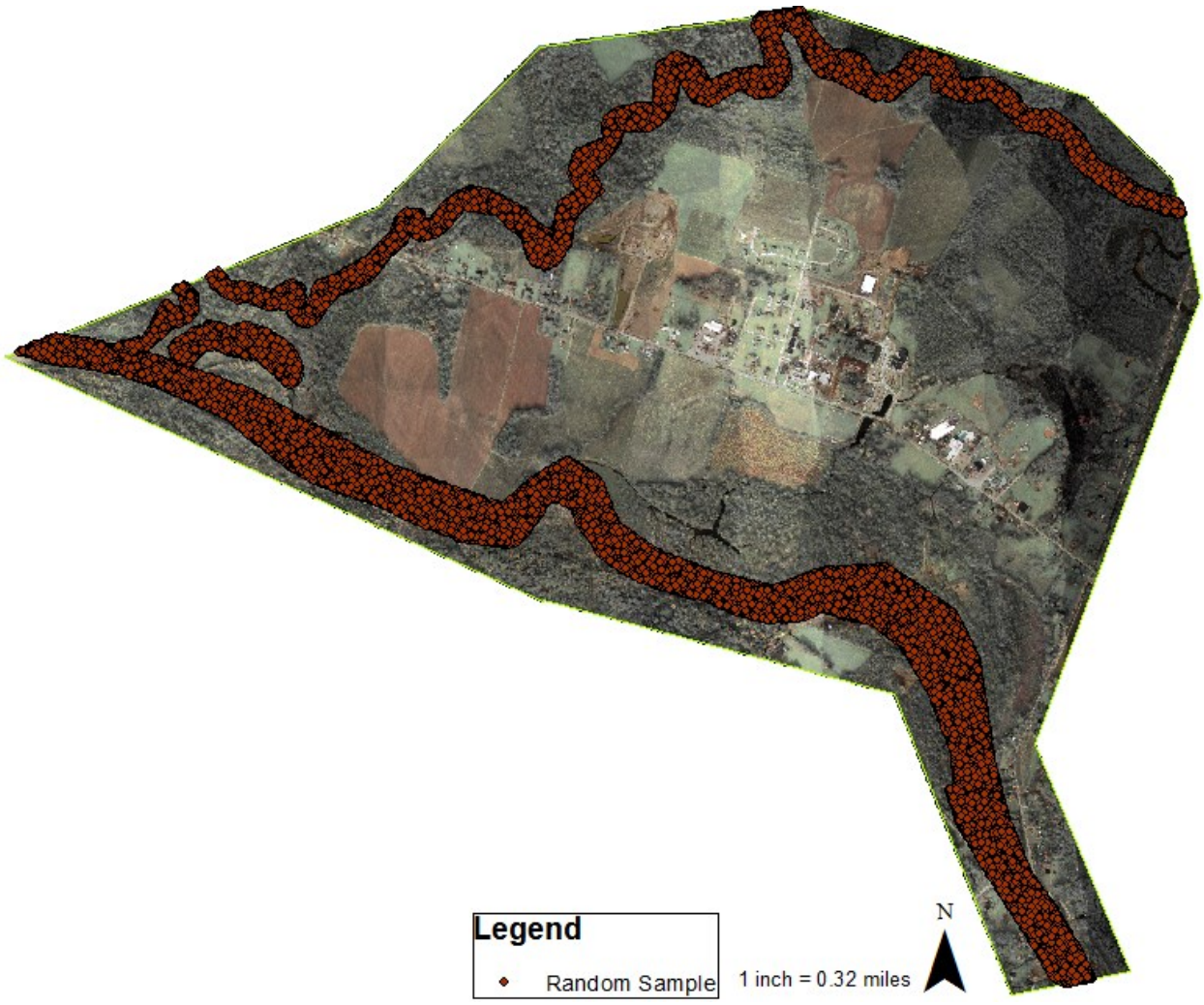

Figure 9 - Random Sample locations for NN Slope (Hydro). This figure demonstrates the random sample point density on the NN Slope (Hydro) data layer.

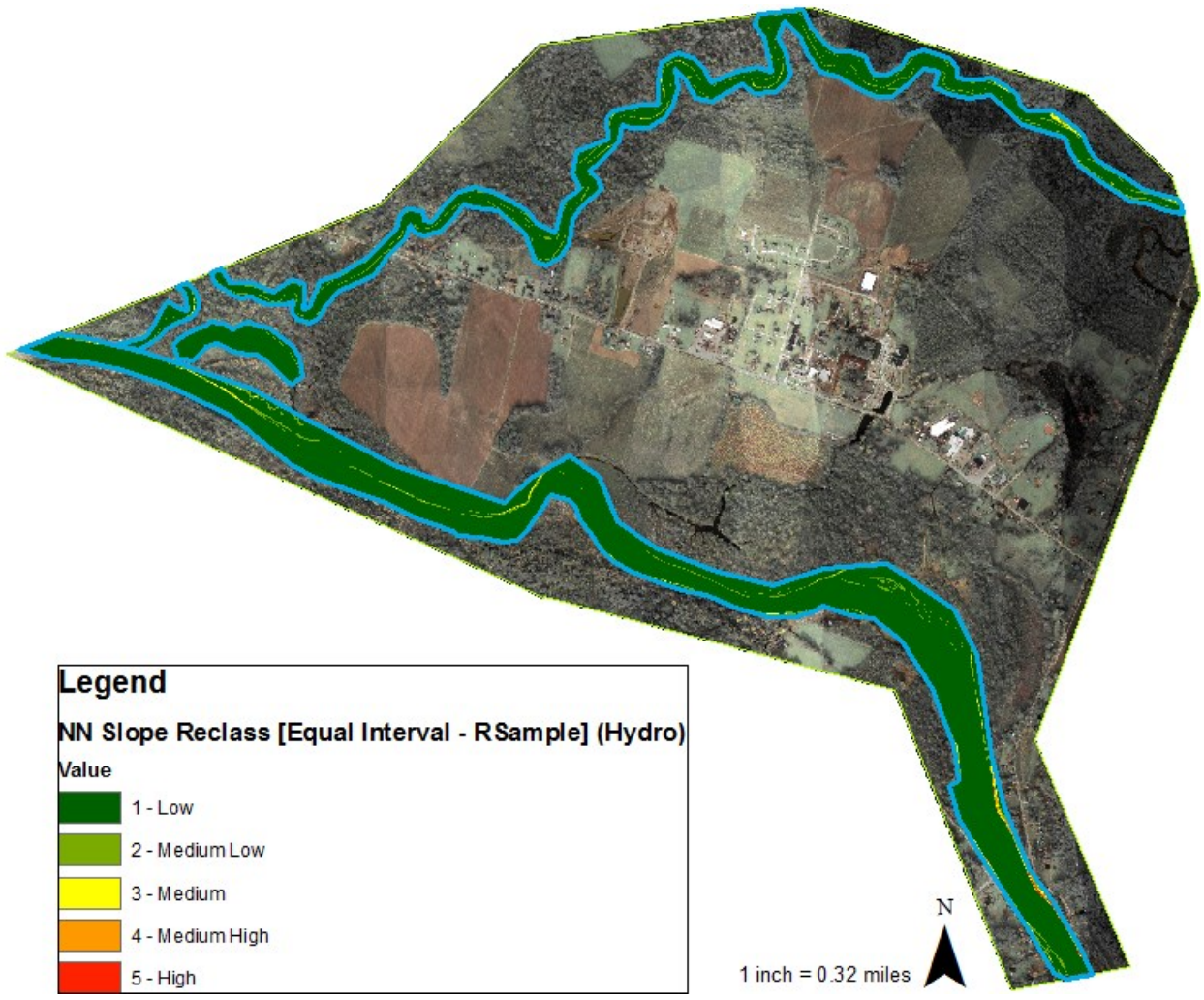

Figure 10 – Flood risk detection for NN Slope Reclass [Equal Interval – RSample] (Hydro). This figure demonstrates the flood risk detection capability of the Equal Interval classification method against the NN Slope (Hydro) dataset. Few detections are evident using the Equal Interval classification.

As evidenced in Figure 10, the Equal Interval classification yields a nearly entirely flat image with minimal detections. Given how the Equal Interval classification works by equally dividing the minimum value and the maximum value by the desired number of classes, it is not surprising that the classes would not accurately define the various features within the riverine areas.

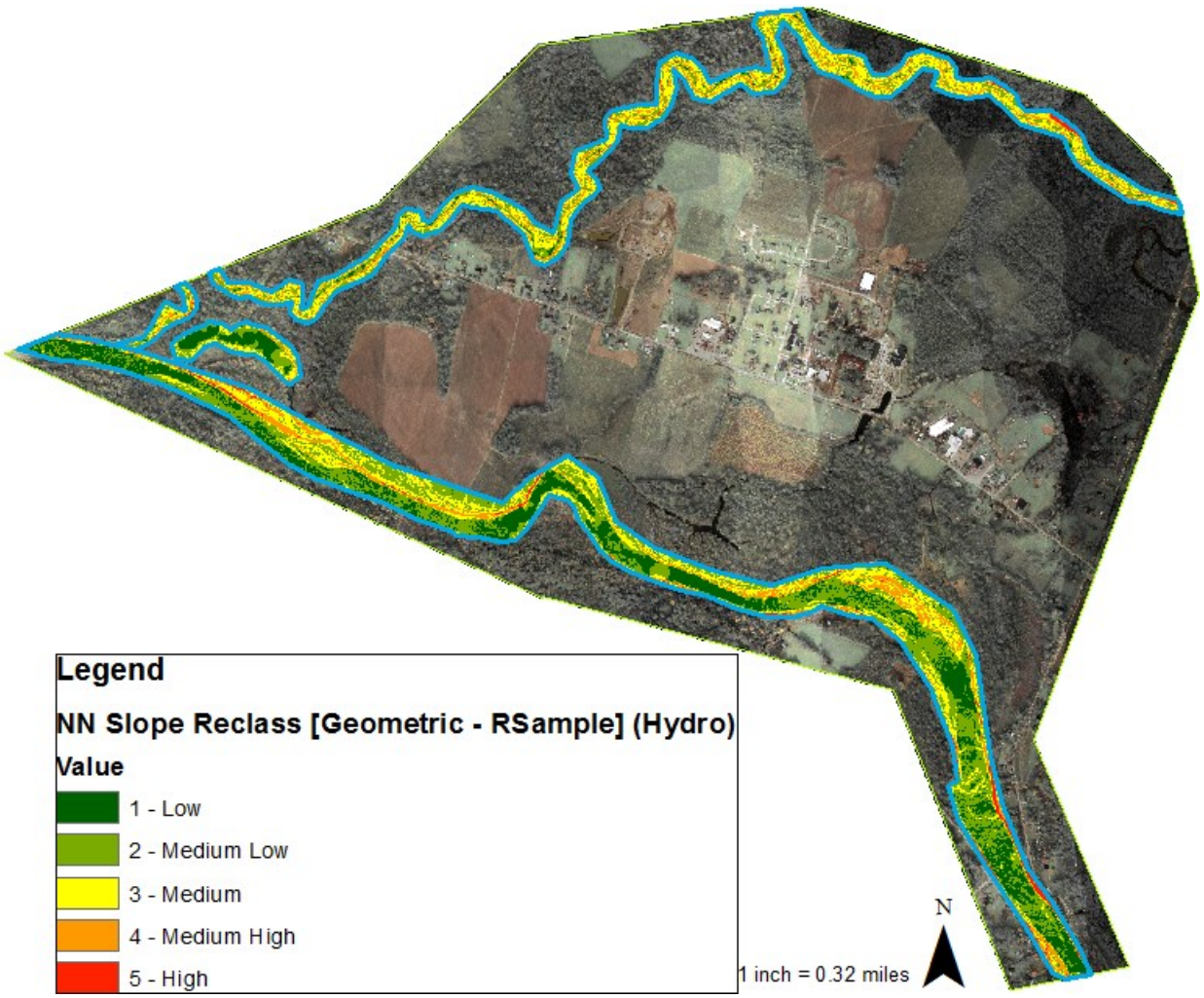

Figure 11 - Flood risk detection for NN Slope Reclass [Geometric – RSample] (Hydro). This figure demonstrates the flood risk detection capability of the Geometric classification method against the NN Slope (Hydro) dataset. The Geometric classification yielded noisy results which did not visually match the riverine surface as presented by the RGB Clip and SWIR Clip layers.

Figure 11 demonstrates how the Geometric classification is able to detect riverine obstructions, as well as marking many non-critical returns Class 2 – 3 [Medium Low – Medium]. The Geometric classification works by ensuring that each class has similar numbers of data points, as well as that the change in the classes is fairly linear (ESRI 2016). Due to the way this classification works, the layer's roughly equal proportions of Classes 1-3 data seem consistent with the classification's balanced intent, but does not seem to produce clean hydrologic features.

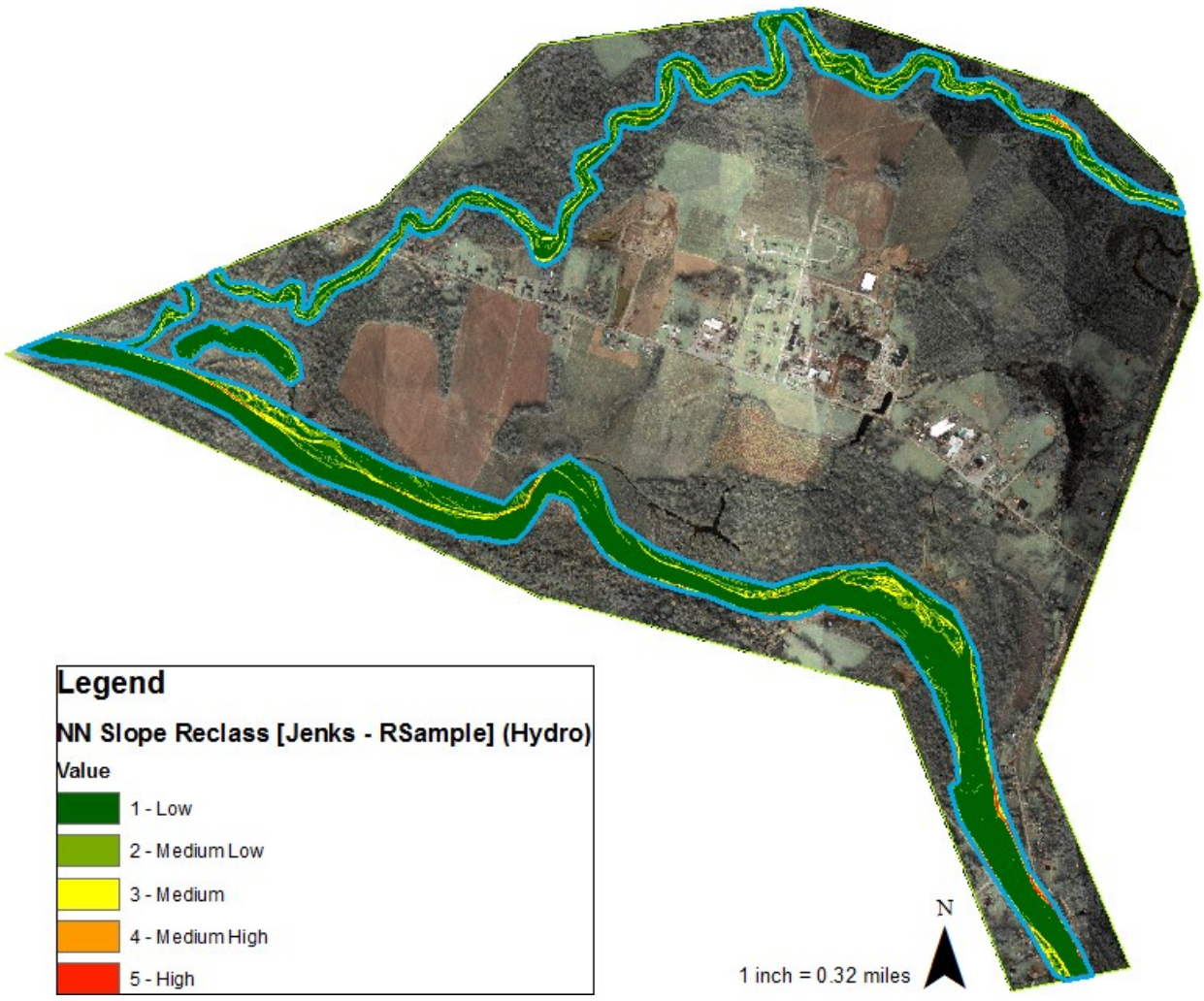

Figure 12 - Flood risk detection for NN Slope Reclass [Jenks – RSample] (Hydro). This figure demonstrates the flood risk detection capability of the Jenks Natural Breaks classification method against the NN Slope (Hydro) dataset. The Jenks classification struck a reasonable middle ground between under-representing and over-representing potential riverine flood obstructions.

The Jenks classification seeks to reduce intra-class variance while maximizing inter-class variance, meaning that data points most similar to each other fall into a class together, while the classes themselves represent significant changes in the data. The output of the Jenks classification, as seen in Figure 12 above, demonstrates a reasonable effectiveness in picking up riverine obstructions while not having as much noise as the Quantile and Geometric classifications.

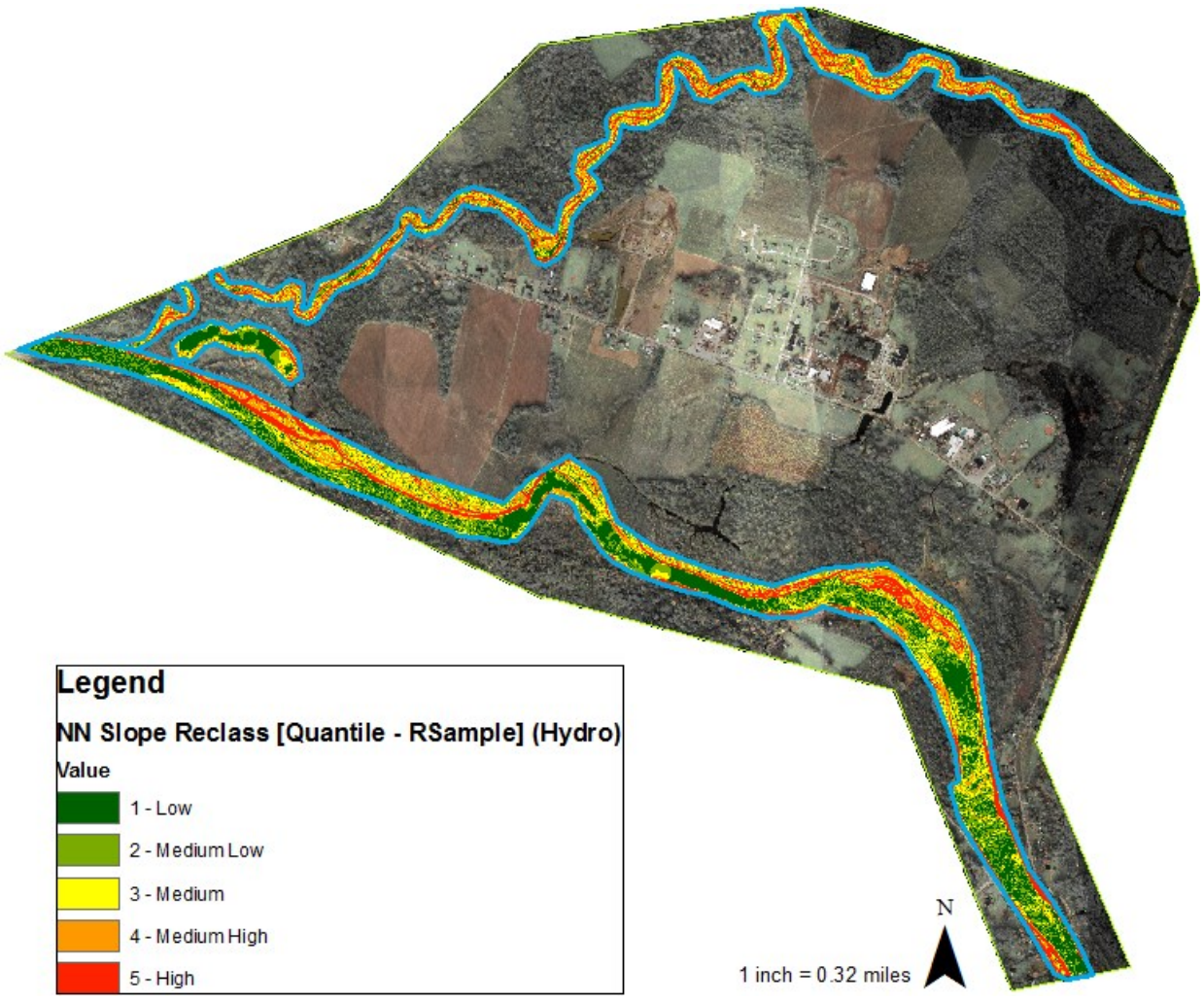

Figure 13 - Flood risk detection for NN Slope Reclass [Quantile – RSample] (Hydro). This figure demonstrates the flood risk detection capability of the Quantile classification method against the NN Slope (Hydro) dataset. Similar to the Geometric classification, the Quantile classification produced noisy results that did not represent the scene as depicted by the Orthophoto data, though the Quantile seems to have moved many of the detections into higher classes by skewing the classification right.

The Quantile classification works by dividing the number of data points into unequal range classes to ensure that every class has exactly the same number of data points. This classification method did not accurately capture the riverine obstructions, and similar to the Geometric classification, there is strong noise in its representation. However, the results seem to have been skewed right in the Quantile as there are more Class 4 – 5 results than the other analyses.

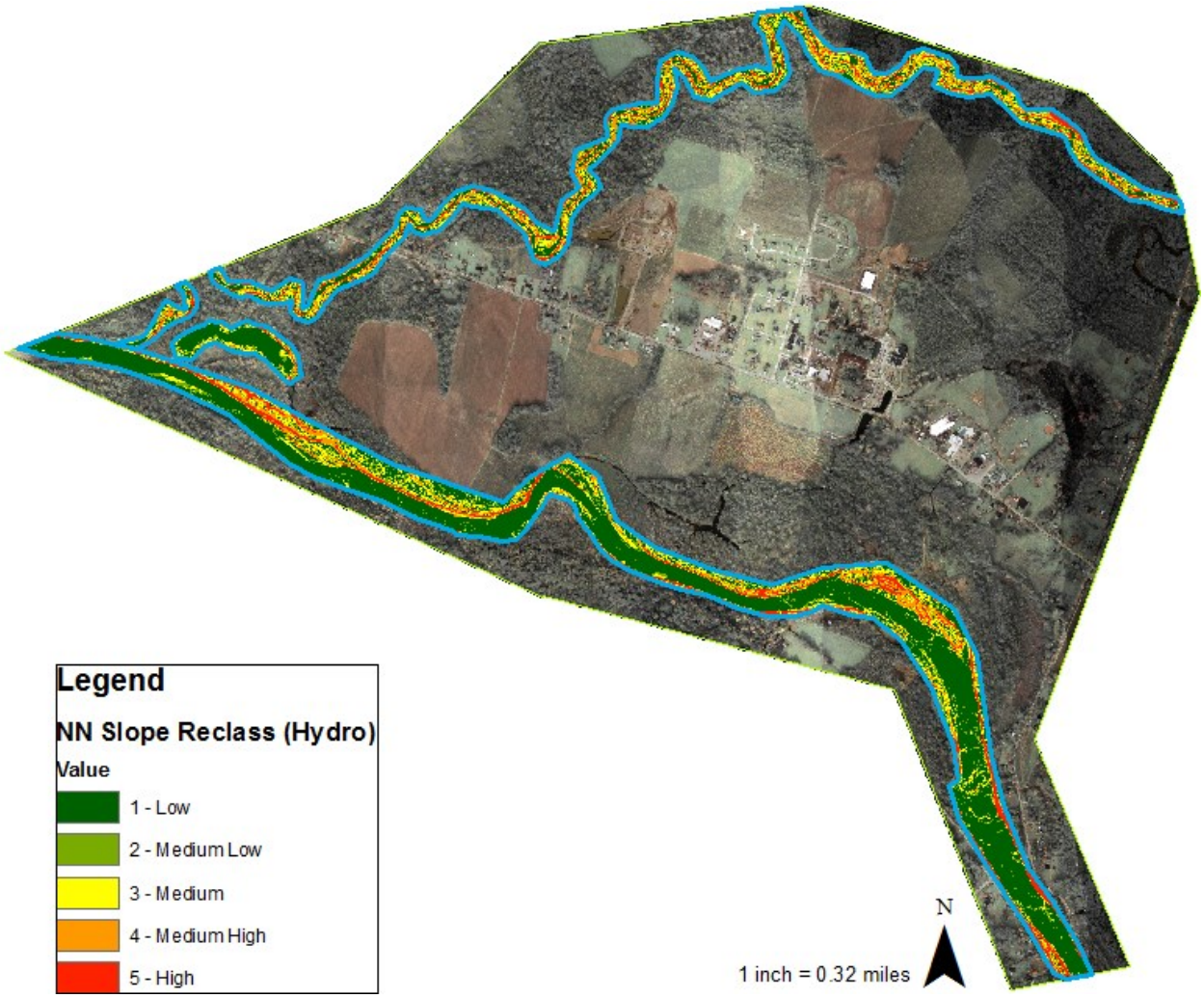

Figure 14 - Flood risk detection for NN Slope Reclass (Hydro). This figure demonstrates the flood risk detection capability of the manual classification method against the NN Slope (Hydro) dataset. This classification system presented riverine obstructions clearly, while not having too much noise.

Figure 14 demonstrates the manually derived flood risk classes and how those class boundaries detect possible flood risk obstructions in the riverine areas. The manual class boundaries are most visually similar to the Jenks classification, yielding results with less noise than Equal Interval, Geometric, and Quantile, while still demonstrating the ability to have positive detections for riverine obstructions.

Each classification varied greatly from the Manual classification in metrics such as pixel count per class, percent composition by class, and class boundaries (Table 6). Due to the limited utility of the Equal Interval, Geometric, and Quantile classifications in properly classifying the NN Slope (Hydro) data, the manual classification was used for the ODM.

Table 6 - Statistical Comparison of Manual, Equal, Geometric, Jenks, and Quantile classifications. This table demonstrates the differences in pixel count, percentage by class, and the class boundaries (in degrees slope) between the various classification methods.

		Class 1 - Low	Class 2 - Medium Low	Class 3 - Medium	Class 4 - Medium High	Class 5 - High
Manual	Pixels	171736	39257	56295	49537	41215
	Percent	48	11	15.7	13.8	11.5
	Boundary	0.0 - 1.1	1.1 - 1.5	1.5 - 3.0	3.0 - 10.0	10.0 - 90.0
Equal	Pixels	332388	19541	4186	1330	595
	Percent	92.8	5.5	1.2	0.4	0.2
	Boundary	0.0 - 14.63	14.63 - 29.26	29.26 - 43.89	43.89 - 58.52	58.52 - 90.0
Geometric	Pixels	74572	124464	95684	50968	12352
	Percent	20.8	34.8	26.7	14.2	3.4
	Boundary	0.0 - 0.40	0.40 - 1.75	1.75 - 6.30	6.30 - 21.60	21.60 - 90.0
Jenks	Pixels	261274	57836	26122	9997	2811
	Percent	73	16.2	7.3	2.8	0.8
	Boundary	0.0 - 3.67	3.67 - 10.56	10.56 - 21.24	21.24 - 38.61	38.61 - 90.0
Quantile	Pixels	72141	71493	71923	71702	70781
	Percent	20.1	20	20.1	20	19.8
	Boundary	0.0 - 0.39	0.39 - 0.94	0.94 - 2.1	2.1 - 5.5	5.5 - 90.0

Methodology (Flood Extent Generator):

Objective:

The Flood Extent Generator aims to quickly and easily create flood extents for a given scenario as a step between the ODM and the RAM when there is no extant flood condition. The FEG is meant to be easy to run as it works off of DEMs and ArcGIS' standard/built-in tools and extensions, not requiring any third-party libraries or extensions. Depending upon the area of interest and the resolution of the data, the FEG can generate an extent very rapidly, having taken less than an hour to generate flood extents for all of Monroe County, NY in this analysis.

Model Overview (Flood Extent Generator):

The Flood Extent Generator works by taking a DEM with obstructions added to the DEM with *Raster Calculator*, filling the resultant DEM, and then classifying the new raster based upon the obstruction location's original and augmented height. The difference between the original and augmented height represents the flood depth and blockage one is expecting. Once the rasters have been created, they are converted into vectors using Raster to Vector in order to calculate the flood extent area, and so that Union, Intersect, and other spatial analyses can be rapidly performed on the vector to both analyze the output within the TAM, as well as to provide the flood extent needed for the RAM. Table 7 illustrates the general workflow for creating the various image products needed to generate the final flood extent, with Table 8 outlining the reclassification values used in the ≈4.7m flood depth tests for the Genesee River.

Data Layer Overview (Flood Extent Generator):

Table 7 - FEG Image Products. This table lists the intermediate image products created and used in order to run the FEG analysis.

LiDAR Base Layers	LiDAR (Monroe County) [02,03,05,10,30m]	This set is comprised of DEMs mosaicked into 2m sets and then resampled to lower spatial resolutions for testing.
Ford Street Obstruction	Ford Street Bridge (4.7m Depth Test) Ford Street Obstruction (Raster) [02,03,05,10,30m]	The Ford Street Bridge (4.7m Depth Test) vector layer was hand-digitized to represent a flood obstruction. The raster versions were created and resampled to be added to the LiDAR Base Layers.
Ford Street Road Dam [Raw]	Dam [02,03,05,10,30m]	This set was created by running *Raster Calculator* against the LiDAR Base Layers and the Ford Street Obstruction (Raster) layers to create products that contained the desired obstruction.
Ford Street Dam [Fill]	Dam (Fill) [02,03,05,10,30m]	This set was created by running *Fill* with no Z-Limit against the data from the Dam set to create DEMs without sinks so contiguous drainage areas would be created.
Ford Street Dam [Flood Depth]	Flood Depth [02,03,05,10,30m]	This set was created by subtracting the Dam layers from their related LiDAR Base Layers using *Raster Calculator*, resulting in rasters that represented the depth of inundation.
Flood Extent	Flood Extent (4.7m Depth) [02,03,05,10,30m Cell)	This set was created by running *Reclassify* against the Dam (Fill) layers using the classification values in Table 8, resulting in layers that represent the flood extents.

Table 8 - Flood Level Reclassification Values (≈4.7m scenarios) for the Ford Street Bridge.
This table represents the specific value ranges used to create the reclassification of the DEM to represent the flood extents, with the Value columns representing meters above mean sea level, or elevation.

≈4.7m Flood Depth Test	
Old Values	New Values
-9999 - 155.1	NoData
155.1 - 159.76	1
159.76 – 283.00	NoData
NoData	NoData

Methodology (Truth Assessment):

Objective:

The Truth Assessment aims to compare the flood extent generated by the RAM against flood extents modeled by Justin Cole, using Hazus, as well as against field-collected ground truth points which were collected during the Black Creek Flood event in May, 2011. Black Creek is hydrologically connected to the Genesee and was the location of the most relevant field verification data against which Justin Cole had run Hazus scenarios. The FEG scenario's flood extents overlap the Black Creek scenario boundaries created by Justin Cole, and so ground truth data collected in that reach of Black Creek can be used to further verify the FEG extents. Since the FEG is a simplified way of generating flood extents, it needs to be tested against more established and popular tools and methods to see if the data it produces makes sense and are viable for use.

Model Overview (Truth Assessment):

The Truth Assessment model is very simple and consists of a visual and spatial comparison of the Hazus-generated flood extents versus the FEG flood extents for the Ford Street Dam ≈4.7m flood event that most closely matched the Hazus data. The FEG layers are overlaid on the Flood Scenario Rasters that were generated by Justin Cole, in order to visually compare the distribution and size of the flooded areas. In order to determine the consistency of the FEG when compared to the Hazuz-generated extents, the areas of both were calculated, as well as the area that intersected. The percentage area that is common between the two models is used to show the areas of complete spatial agreement of the FEG with Hazus for a similar flood condition.

Data Layer Overview (Truth Assessment Model):

Table 9 - FEG Image Products. This table lists the intermediate image products derived from the FEG and Hazus data used in order to run the TAM.

Points Of Interest	USGS 04231600 Ford Street Dam	This set is comprised of vector files that give context to the TAM, such as the location of the Ford Street gauging station and the Ford Street Dam obstruction.
Flood Scenario Rasters (Hazus)	GENESEEMAJORFLD55000CFS GENESEEMAX4630CFS HAZUS_BLACK_CREEK_MAX4880CFS IRONDEQUOITCREEK3300CFS	This set is comprised of raster files created by Justin Cole, using Hazus and various flood scenarios. These data are what the FEG extents are compared against.
Flood Scenario Rasters (FEG)	Dam (Fill) [02,03,05,10,30m]	This set is comprised of rasters created by running *Fill* against the Dam layers to remove sinks and prepare them for reclassification.
Binary Flood Scenario Rasters	Dam Fill Vector (4.7m scenario) [03m]	This set was created by running *Reclassify* against the Dam layers using the values in Table 8.
Flood Scenario Vectors	Dam Fill Vector (4.7m scenario) [03m] Genesee Major 55000cfs Vector Genesee Max 46300cfs Vector Black Creek Max 4880cfs Vector Irondequoit 3300cfs Vector HAZUS Flood Extents Merge Dam Fill [03m] Union Hazus Flood Extents Dam Fill [03m] Union Genesee Max 46300cfs	This set was created by running *Raster to Polygon* and *Dissolve* against the raster data to generate vector extents that could be easily analyzed for spatial agreement with the Hazus data. The Union layers were created by running *Union* against the FEG and Hazus data for the ≈4.7m scenarios to investigate spatial agreement between the flood extents.
Parcel Data	Road Centerlines (Monroe County)	This set was comprised of TIGER/Line data that was used to give location context when looking at flood extents.

Methodology (Risk Assessment Model):

Objective:

The Risk Assessment Model focuses on attempting to quantify risk of flood damage, due to an event generated flood-plain using LiDAR derived DEMs, flood stage height (from USGS gauging stations), and overlaying social/infrastructure data such as parcels, critical infrastructure, and census data. Attributes such as assessed value (parcels), population density (census), and the CIKR will be reclassed to a 10-class scale. The breaks in the scale for cost and human impact will be determined using histogram analysis, and the resultant ranks from all the variables will be summed to produce a vulnerability score, or risk factor. A risk factor is calculated and assigned to each parcel in order to help prioritize areas that should be responded to first in an emergency event.

Model Overview (Risk Assessment Model):

The RAM is an analysis that does a spatial selection on the data layer containing the RAM social data, using the FEG data for the select by feature, thus creating an output layer that contains the impacted parcels. By running the analysis using spatial selection with intersect, the output data are created with the assumption that the entire unit is impacted even though only a small fraction of it may intersect the flood extent. However, using centroid with spatial select leads to parcels being selected that are likely mostly encompassed within the flood extent, more closely representing what would be impacted by the flood. The primary method of symbolization uses the risk factor field to view the risk factor generated for each impacted unit (parcel data provide the boundaries of the units, with Census Blocks providing population data for the units). The risk factor is visualized using an ArcGIS color ramp running from green to red (low risk factor to high risk factor). Having this risk factor map may help someone to make a judgement call about which parcels are actually critical to respond to.

LiDAR Derived DEMs:

Varying spatial resolutions (1m, 3m, 5m, 10m, 30m) of the DEMs were tested to determine the sensitivity of the flood model to the spatial resolution of the DEMs. For this test, the Black Creek flood site, provided by Justin Cole of Monroe County, was used to assess the model results, as in-situ truth points were taken by the Monroe County team. For this test, the flood model was run against the LiDAR derived DEMs at the varying spatial resolutions and the resultant extents compared for total area of coverage, as well as a visual comparison of flood boundaries. The target of the LiDAR derived DEM is coarsest spatial resolution possible while still maintaining boundaries that still appear to respect the topography of the site. Any further spatial resolution will add processing time and increase data volume for an uncertain gain in model accuracy.

Model Variables:

The priority rating term is a value ascribed to various infrastructure features based upon their importance to Monroe County (Table 10). Monroe County keeps a prioritized list of infrastructure elements (Brooks and Rion n.d.) and this can be developed into a simple numerical rank or class system, while cooperating with the Monroe County Office of Emergency Management (Table 11). Currently a 10-class Priority Rating system is used, though the number of classes and their composition could be changed in follow-up discussions with Monroe County in order to replicate the Monroe County CIKR (Table 12). This vector dataset comprises various infrastructure elements (points, lines, polygons), including health and energy production facilities, power lines, bridges, roadways, and railways.

Table 10 - Priority Ratings; Created in collaboration with Frederick Rion, Jr., Monroe County Office of Emergency Management. This table shows the Priority Ratings as of August, 2013.

0	Business		5	Agriculture & Food
1	Telecommunications		6	Care Facilities
2	Schools		7	Government
3	Chemicals & Haz-Mat		8	Transportation Infrastructure
4	First Responders		9	Power

Table 11 - Monroe County CIKR Classes. This table shows the CIKR classes as defined in the Monroe County CIKR dataset.

OID	CIKR_TYPE	OID	CIKR_TYPE	OID	CIKR_TYPE
0	Agriculture and Food	9	Govt	18	School
1	Airport	10	Govt/EMG Services	19	School/Police/EMS
2	Chem and Haz Mat	11	Information Tech	20	Telecommunications
3	Commercial Facility	12	Mall/Police	21*	Hospitals
4	EMS	13	Nursing Home	22*	Power
5	Fire	14	Police	23*	Rail Transportation
6	Fire/EMS	15	Police/Govt	24*	Bridges
7	Fire/Govt	16	Police/School		
8	Fire/Police	17	Postal and Shipping		
Items marked with "" indicate proposed additions to CIKR_TYPE field*					

Table 12 - Grouping CIKR types into Priority Rating Classes. This table shows the 25 CIKR classes that were grouped into the 10 Priority Rating classes.

Input: CIKR OIDs	Output: Priority Rating Class	Priority Rating (P_r)
3, 11	Business	0
20	Telecommunications	1
16, 18, 19	Schools	2
2	Chemicals & Haz-Mat	3
4, 5, 6, 8, 12, 14	First Responders	4
0	Agriculture & Food	5
13, 21	Care Facilities	6
7, 9, 10, 15	Government	7
1, 17, 23, 24	Transportation Infrastructure	8
22	Power	9

The cost value of the model is derived from the parcel data layers. These layers are able to estimate the value of a given plot of land in millions of dollars. These evaluations typically are based upon number and size of buildings, quality of the built structures, adjacent structures, developments, as well as other data. The cost variable helps the model assign a priority to parcels of land that contain very expensive infrastructure, dense infrastructure, or singular elements of high monetary value. If a parcel of land is largely undeveloped, not only will it have a low priority rating, as defined above (Table 10), but it will also likely be of less monetary value than a higher rated parcel, and thus will contribute a small cost factor to the model. If the parcel happens to be of high monetary value, for example a recently built bridge or dam, that parcel of land will contribute a high cost value to the model and will, as a result, increase the calculated risk factor for that parcel.

The final social variable for the risk factor model is the human impact variable. This variable, unlike the cost variable, is derived almost exclusively from census block (or best available census data unit) datasets. Population values of a given polygon determine its human impact value. This unfortunately presents a difficulty in cases such as schools, business parks, hospitals, or other high-occupation buildings that have variable levels of occupation. For the purposes of this model, it is assumed that the areas that are not permanently occupied are being occupied at the time of the flood as it is not currently possible to model variable occupation within the RAM. Furthermore, the US Census Bureau does not give population data at the parcel level, meaning that the model variables are based upon different geographic scales, with the population variable being based upon the census block, which can oftentimes contain many parcels. Due to this difference in geographic scale in the data, the human impact variable's population data was kept as-is for every parcel that was contained within a given census block since the population value is reclassified into a ranking of relative population versus the rest of the blocks. In future

analyses, a geographic normalization of the human impact variable should be investigated to help mitigate the issues of scaling the resolution of the data down from the census block to the parcel level. Unfortunately, human dwellings are not normally distributed across the planet's surface, and a simple population per area normalization will likely not well represent the potential impacted persons per parcel.

For both the cost and human impact variables, the 10-class classification was performed by using the Jenks Natural Breaks analysis on the dataset. The Jenks classification seeks to minimize intra-class variance and maximize intra-class variance by performing an iterative clustering analysis on the datapoints until the sum of the intra-class variances approaches zero. In other words, the Jenks classification seeks to best sort the data into like groups, with the goal of evenly distributing the "blanket of error" across the mapped surface (ESRI 2016).

The flood percentile variable is derived from the USGS Flood Percentile classes. Using historical data, oftentimes more than 30 years long in the case of New York State (USGS 2012), the flow of each river is broken down into percentile classes, as can be seen below in Table 13. The flood percentile will be used as another term in the RAM, increasing the risk factor value when the river's flow is much above the historical norm for that time of year, and decreasing the risk factor value when the flow is well below the historical norm. In this way, the severity of the flood event can be taken into account in the risk factor, replacing the impact the "recurrence interval" variable would have had as a divisor. Flood years, or the recurrence interval, represent the statistical likelihood that a flood of a given magnitude will happen in a given time period, typically 100 years or less (Robinson, Hazell and Young 1998). This value is only the chance that a flood of that magnitude will happen in any given year, and floods with large recurrence intervals have happened one after another, making the term difficult to use as a predictor (USGS 2012). For these reasons, the flood percentile values were chosen to normalize the risk factor value.

Table 13 - USGS Flood Percentile Classes. This table illustrates the 7-Class system the USGS employs to categorize a given gauge station's measurements based upon historical data for the same river.

●1	●2	●3	●4	●5	●6	●7
Low	<10	10 – 24	25 – 75	76 – 90	>90	High
Historic	Much below normal	Below normal	Normal	Above normal	Much above normal	Historic

The risk factor value, as mentioned above, is a four digit coded number created by summing the values of each of the variables, as outlined in Table 14 below. Each of the variables represents a 10-class range of values, with the exception of the flood percentile variable, comprised of 7-classes.

Defining a Risk Factor:

The risk factor is a coded sum of the following values: flood percentile (river stage/water height), priority rating, human impact (census), and cost (parcels), with each variable representing one significant digit in the 4-digit value (Table 14, Equation 1). The priority rating was derived from the Monroe County Emergency Operations Center (MCEOC) CIKR, as these databases contain a list of high risk/priority areas.

Table 14 - Risk Assessment Model variables.

Variable Name	Variable Symbol	Variable Range	Variable Classes
Risk Factor	R_f	1-111 – 5-999	Sum of below
Flood Percentile	F_p	**1**-000 – 7-000	USGS Flood Percentile Classes
Priority Rating	P_r	0-**1**00 – 0-**9**00	0-9 (MCEOC CIKR)
Human Impact	H_i	0-0**1**0 – 0-0**9**0	Undefined
Cost	$C_\$$	0-00**1** – 0-00**9**	Undefined

$$R_f = F_p \mid \sum P_r + H_i + C_\$ \qquad Equation\ 1$$

Equation 1 - Risk Factor Equation. This equation shows the process used to create the Risk Factor from the component variables.

Example: Using Equation 1 above, a 76th percentile flood that would impact 500 people, cost 1.2M in damages, and threaten Level 1 sites would yield a Risk Factor of **41XX** given that

$$\mathbf{R_f = 4000+0100+00X0+000X}$$

Data Layer Overview (Risk Assessment Model):

Table 15 - RAM Image Products. This table demonstrates the various data layers and intermediate products created to create the final RAM data.

Monroe County Vectors	Road Centerlines (Monroe County) Parcels (Monroe County)	This set is comprised of vector layers that contain the roadways for Monroe County, as well as the parcels with the associated cost and infrastructure data.
CIKR (Critical Infrastructure & Key Resources)	CIKR Points (Monroe County) CIKR Parcels (Monroe County)	This set is comprised of CIKR points and parcels which represent locations in Monroe County of high importance or value.
Block Data (Monroe County)	Census 2010 Block (Monroe County)	This set is comprised of the US Census Bureau TIGER/Line block data, which contain population.
Parcel & CIKR Spatial Join	Parcel, Block, & CIKR Spatial Join	This set is comprised of a spatial join of the CIKR and parcel data against the census block data, creating a layer that has all the attributes needed to calculate the risk factor.
RAM Variables	RAM Parcels	This set was created by creating fields to calculate FloodStage, Priorityrating, HumanImpact, Cost, and RiskFactor. FloodState was set to 7000 for all records, PriorityRating respected CIKR_TYPE from Table 12, HumanImpact was set using Jenks with 10 classes in accordance with Table 16, and Cost was set using Geometric with 10 classes in accordance with Table 17. The RiskFactor field was calculated using Equation 2.
RAM Impact Visualized	Risk Factor Priority Rating Human Impact Cost	This set is comprised of copies of the RAM Parcels layer symbolized differently to highlight the highest class of each variable. Risk Factor is visualized by Graduated Colors to provide the “risk surface” on which to overlay the highlight points from the other layers.

Table 16 - Population (Sum) & Human Impact.
This table shows the 10 Human Impact classes that were derived from the Population Sum data.

Sum_POP10	Human Impact (H_I)
0 – 46	00
47 – 97	10
98 – 155	20
156 – 222	30
223 – 312	40
313 – 433	50
434 – 586	60
587 – 754	70
755 – 2001	80
2002 - 5940	90

Table 17 - Total Assessed Value & Cost.
This table shows the 10 Cost classes that were derived from the Total Assessed Value data.

TOTAL_AV	Cost ($C_\$$)
0 – 47668	0
47669 – 61473	1
61474 – 109141	2
109142 – 273739	3
273740 – 842091	4
842092 – 2804600	5
2804601 – 9581113	6
9581114 – 32980297	7
32980298 – 113777282	8
113777283 – 392767900	9

$$RiskFactor = [FloodStage] + [PriorityRating] + [HumanImpact] + [Cost] \qquad Equation\ 2$$

Equation 2 - RiskFactor SQL Query in ArcGIS. This equation shows the query written to calculate the RiskFactor using the Field Calculator tool within ArcGIS.

Results & Discussion (Obstruction Detection Model):

The ODM appeared to be effective at finding obstructions in riverine areas with sufficiently high-resolution LiDAR data (sub-5m), although visual analysis is limited to low river stage conditions due to available imagery (Figure 15 - Figure 20). In the case of the 1.62 points/m^2 data in the Cattaragus Indian Reserve, the ODM was able to pick up the deflection in the water as it flowed around sandbars and other obstructions within the river, easily highlighting the obstructions, whether or not they broke the surface of the water. Elsewhere in New York State where 1m LiDAR data were available (Broome, Erie, Genesee, Jefferson, and Livingston Counties), the ODM picked up rocky riverbeds, small waterfalls, dams, and other features within the river reliably when the data were finer than 10m pixels. Super-sampling of the data proved ineffective as it nearly always failed and was simply compounding interpolation errors by performing two rounds of interpolation upon the data. If the ODM is being run in an environment where processing time and data storage are not a constraint, it is recommended that the ODM is run against the finest resolution DEMs available. If time and/or storage are constraints, the ODM demonstrated that 10m resolution data provides reasonably good detection with a marked decrease in processing time and file size over finer resolution data.

The ODM is a computationally intense analysis that requires high-quality data and a large amount of storage. For these reasons, the ODM is ill-suited to being run from mobile platforms, most in-field portable devices, or on-demand. It is best suited to be used as a planning and risk mitigation tool so that processing time, data availability, and data storage constraints aren't as important. As can be seen in the previous results, the ODM picks up obstructions that are potentially visible above or at the surface of the river, which are observable with the naked eye. The benefit of the ODM in these situations lies in its ability to classify the riverine area and highlight these features so that possible areas of concern can be more readily noticed and investigated when looking at the imagery.

Some limitations of the ODM that became apparent through testing and implementation were that subsurface obstructions themselves will likely not be detectable in the LiDAR data. Therefore, it may be necessary to combine spectral classification along with the slope-based analysis of the ODM to help determine what riverine hits are actually of importance. As demonstrated by the LiDAR and Orthophoto data that were not flown concurrent, water heights within the riverine areas are highly changeable, making some obstructions visible in the Orthophoto data not visible in the LiDAR data and vice-versa. Furthermore, riverbed size and location can, and oftentimes do, change over time, making non-concurrent LiDAR and Orthophoto data more difficult to analyze.

If the ODM were run with the riverine areas being clipped out of the surroundings using preexisting river extents, the ODM would help to quickly identify possible flood risk points that could then be used to generate scenarios with the FEG to create the extents, and the RAM to evaluate the populations and infrastructure that would be at risk.

Obstruction Detection Examples:

Table 18 - Obstruction Detection Model Slope Class Values. This table shows the slopes in degrees that determines what class the detected pixels are classified into.

Slope Classes for Obstruction Detection Model (values in degrees)				
Class 1	Class 2	Class 3	Class 4	Class 5
00.0° – 01.1°	01.1° – 01.5°	01.5° – 03.0°	03.0° – 10.0°	10.0° – 89.9°

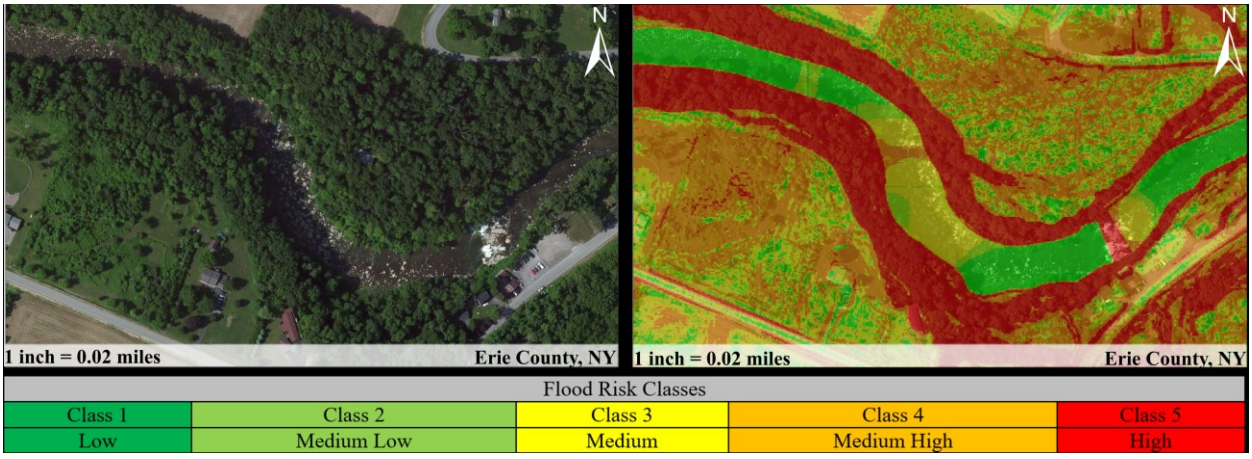

Figure 15 - Waterfall and Rocky Riverbed. This figure demonstrates the ODM detecting the waterfall, the rocky riverbed, and the other riverine obstructions in the center of the image.

In Figure 15 above, the ODM is demonstrated to be able to find possible flood obstructions, with the slope ranges as displayed in Table 18, which apply for all subsequent figures in the ODM analysis. It highlights the waterfall feature as being a very high risk (Class 5) flood obstruction, and it picks up the exposed rocky riverbed as a Medium/Medium-High flood obstruction risk (Class 3 – 4). The "clear" water parts of the river are shown as Class 1, which is a Low Risk. As designed, the trees bordering the riverine area are marked as Class 5, making the results in this location consistent with the original test site.

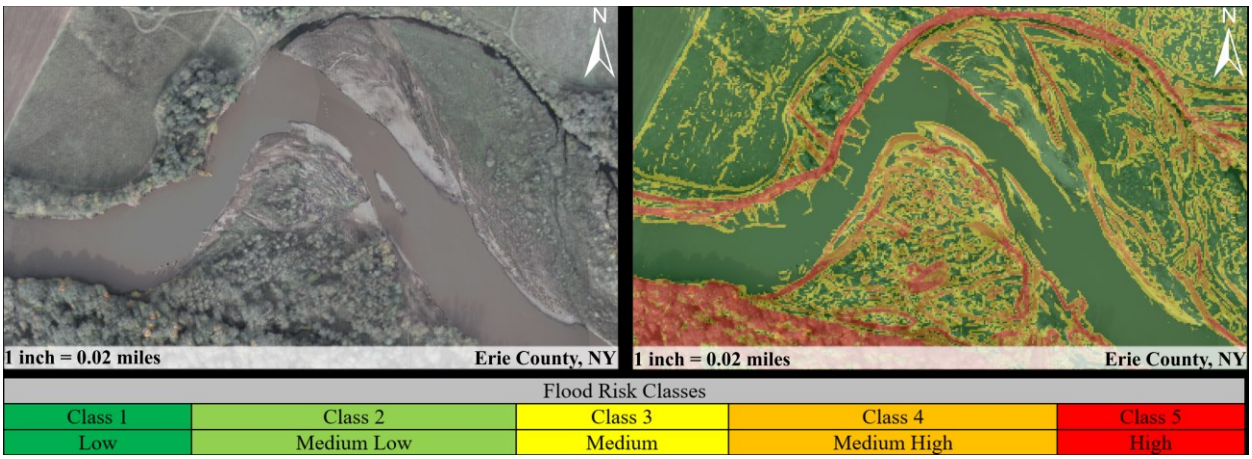

Figure 16 - Sandbars and Current Flow. This figure demonstrates the ODM detecting a sandbar in the upper center of the image, as well as the eddy currents caused by the water flowing around the sandbar.

In Figure 16 above, the ODM demonstrates that, given sufficiently small Ground Sample Distance with LiDAR data, the analysis is able to detect eddy currents caused by a sandbar within the river. The sandbar is completely encompassed within the Class 3-4 risk category, along with the eddy currents coming off the sandbar. Along the top edge of the river there can be seen interpolation artifacts, likely due to the low density of LiDAR returns in that particular area. This location is within the original test site and was used to help derive the ODM Flood Risk Classes.

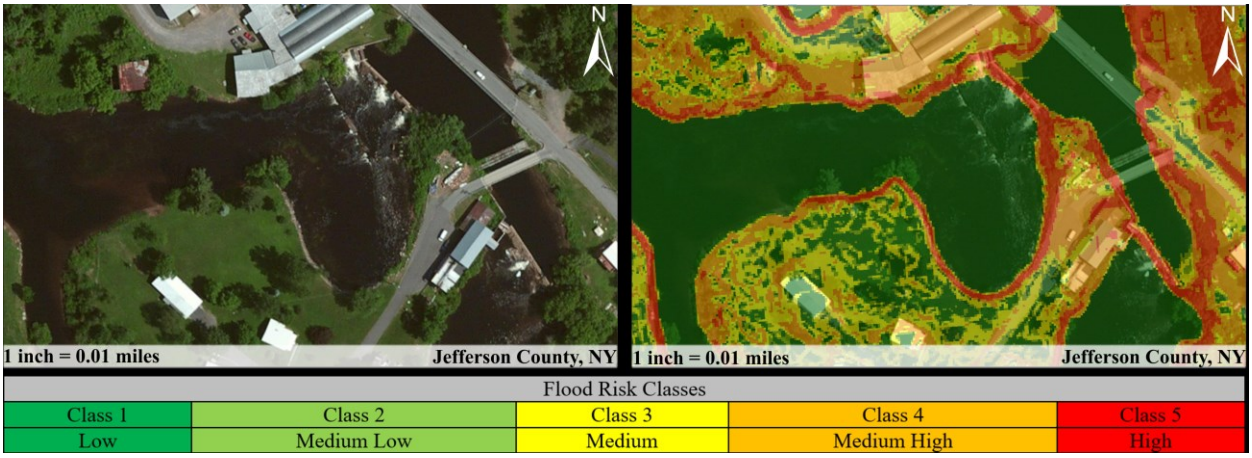

Figure 17 - Man-Made Obstructions (dams). This figure demonstrates the ODM detecting a dam in the upper right, while ignoring the riverine area below it.

In Figure 17 above, the ODM demonstrates its ability to detect man-made obstructions, such as dams, provided that they have not been post-processed out of the LiDAR data as the roadway in this section has. The dam is a very likely cause of flood obstructions and the ODM classifies it successfully as high risk (Class 5). Much like in other locations, the immediate riverine borders are being detected as

Class 5, which makes sense as there is normally a fairly drastic change in slope from a flat surface like water to a highly varied and oftentimes steep surface such as a tree's canopy or other vegetation.

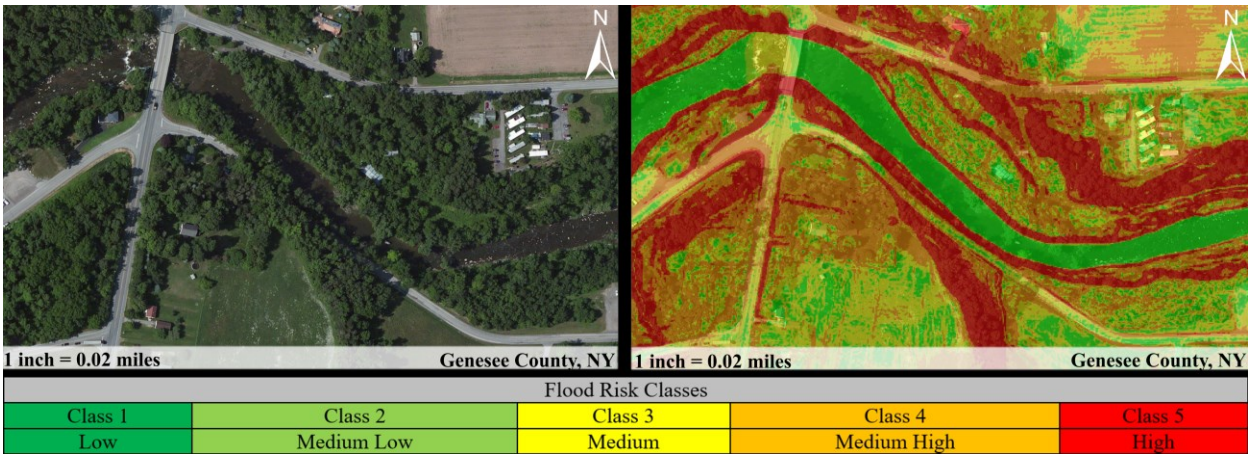

Figure 18 - Rocky Riverbed. This figure demonstrates the ODM detecting a rocky riverbed just after a bridge in the upper left corner.

In Figure 18 above, the ODM demonstrates its ability to detect a shallow and rocky area of the riverbed near a bridge that passes over the water as a Class 3 flood risk. Much like in Figure 17, the bridge itself has been removed from the LiDAR dataset in processing. The In addition to the rocks potentially accumulating debris and causing a flood, the bridge supports could potentially also dam up with debris, leading to the identification of this site as promising for ODM.

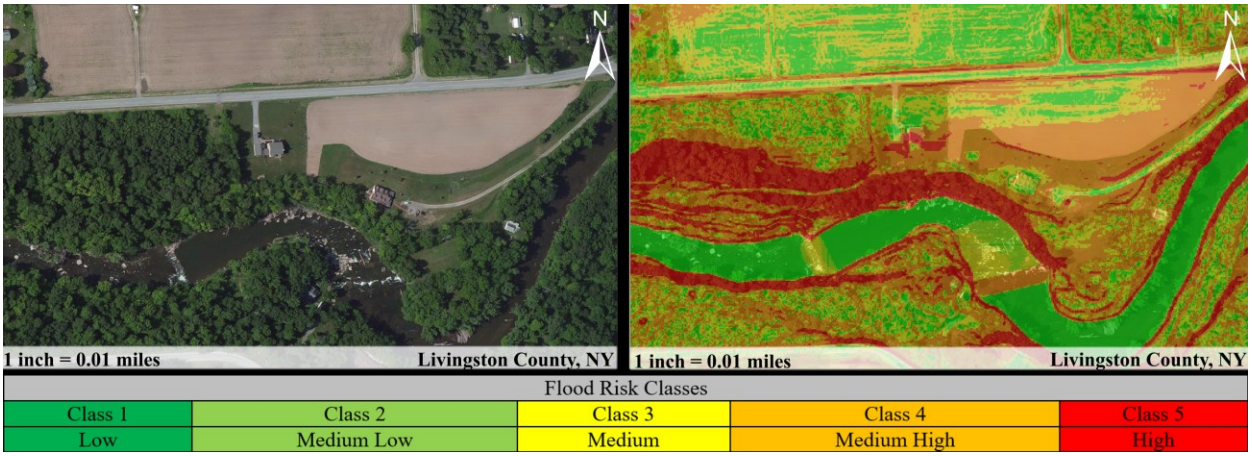

Figure 19 - Waterfalls and Rocky Riverbed. This figure demonstrates the ODM detecting two small waterfalls and the rocky riverbed around them.

In Figure 19 above, the ODM successfully detects two small waterfalls (Class 3 and Class 4, respectively) and the rocky riverbed around both of them. The calm water between both waterfalls is

classified correctly as low risk, highlighting the trouble area clearly. In this particular instance, it can be seen that the ODM failed to detect rocks in the river that are visible in the western portion of the Orthophoto data. Since the Orthophoto data and LiDAR data were not flown concurrent, it is likely that those obstructions were concealed by the river's depth at the time of LiDAR sampling, not creating enough of a deflection to be detected by the ODM.

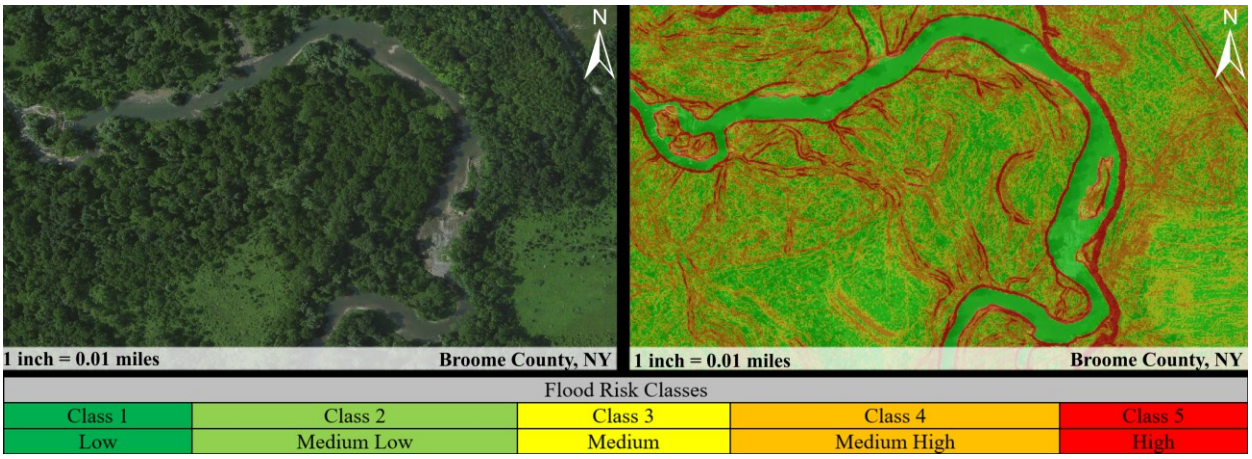

Figure 20 - Sandbars and Islands. This figure demonstrates the ODM detecting small sandbars and islands within the body of water.

In Figure 20 above, the ODM highlights small sandbars as possible flood obstructions, as well as islands contained within the body of water. These islands could very easily have debris deposited upon them, blocking the flow of water around them where the river constricts. Similar to the results in Figure 19, the rocky area visible in the Orthophoto data was not detected by the ODM in this instance. It is probable that this is due to the Orthophoto and LiDAR data not having been flown concurrently.

Results & Discussion (Flood Extent Generator):

The FEG succeeded in generating flood extents rapidly using both coarse and fine data, with reasonable similarity between the two extremes. The FEG generated extents seemed reasonable, given the shape of the terrain in the area (Figure 21, Figure 28). The FEG extents tracked along natural and built features in the environment, approximating what one would expect of water flowing in such a location, flowing to areas of lower elevation while tracking along the boundaries of channels made by higher elevation areas.

FEG data at 2-5m resolution are most suitable for analysis at the parcel level, as those resolutions closely approximate smaller features in the natural and built environment, such as roadways and changes in terrain within a residential parcel (Figure 29 - Figure 34). FEG data at 10-30m resolution are suitable when results are being analyzed at the block, block group, or census tract level, as the differences in extent are far less important at that scale as the area being investigated when using data of that scale will be large enough that the small variation in the extent's periphery will not meaningfully impact the selection of the impacted geographic units (Figure 22 - Figure 27). In the case of the RAM, the Census block data were the finest common unit, so 10-30m data were optimal.

Figure 21 demonstrates the underlying topography in the University of Rochester area near the Ford Street Bridge. The Genesee River and the Erie Canal were some of the lowest elevation areas in this figure, and as such, they're flooded during the FEG analysis. Just north of the University of Rochester campus gets flooded as well, being sufficiently low in elevation to be flooded during the FEG analysis.

In Figure 22, the flood extent is highly detailed and very granular, being generated at the same 2m cell size as the LiDAR coverage. When viewed at a small scale, the 2m flood extent is capable of detecting streets, parking lots, driveways, and other small areas of sufficient elevation to avoid flooding. The 3m cell size data of Figure 23 proves to be nearly indistinguishable from the 2m data cell size data. Small features are generally well-preserved, and the outline of the flood extent remains largely consistent with the 2m data. With the 5m cell size data of Figure 24, it is now more plainly apparent that the data are becoming increasingly generalized, though it still closely approximates the coverage of the 3m and 2m data. The flood extent is nearly indistinguishable from the higher resolution data and small features are still generally well preserved. The 10m cell size data of Figure 25 demonstrates that the changes from the 5m cell size data still apply. The flood extent is still very similar to the original 2m data, but it is visibly more coarse and generalized. Smaller features in the high-density urban areas are being aggregated into the larger pixel size, though the outline remains mostly consistent with the 2m data. At the 30m cell size data of Figure 26, the generalization of the data is plainly visible. The 30m cell size data are visibly very

coarse and loss of smaller features can be seen. Finer details and “islands” are filled in, resulting in a likely over-approximation of impact. The overall extent is still very similar, though obviously less detailed. Figure 27 demonstrates that the variations in the flood extent can be observed between the different resolutions. The resolutions are stacked from smallest cell size to largest, top to bottom. The general outline of the coverage is fairly consistent when taken as a whole, with some minimal increase in flood extent due mostly to the increased cell size, though some extraneous flooded cells are introduced during the resampling as similar areas are aggregated and averaged together, forming pixels that meet the criteria for being considered flooded. Given the scale of this analysis, 10m pixels were sufficiently detailed and representative of the underlying terrain to be the recommended resolution for parcel-scale generation of flood extents. If the analysis were targeted toward building footprints, then 3m would likely have been most appropriate.

Figure 21 - Dam (Fill) Elevation (Small Scale). This figure emphasizes the topography behind the FEG’s generation of Figure 22 - Figure 27, giving context for the flood extent boundaries.

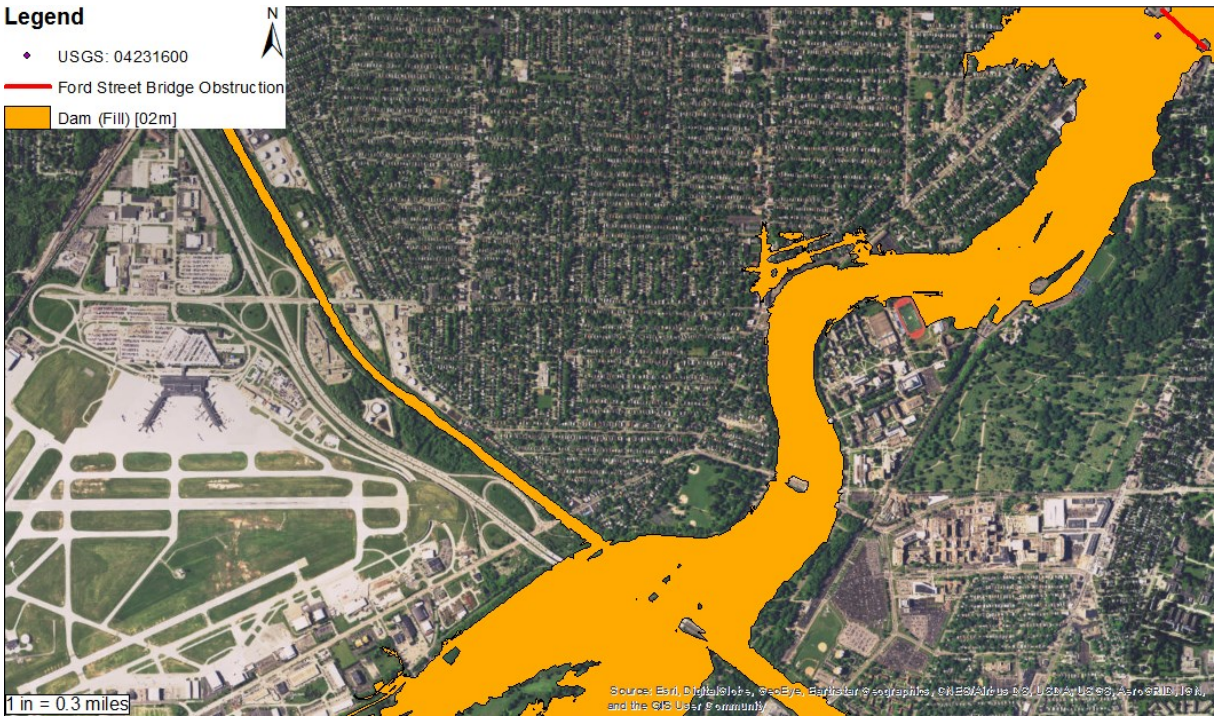

Figure 22 - Dam (Fill) [02m]. This figure demonstrates the fine granularity of the 2m cell size flood extent generated by the FEG.

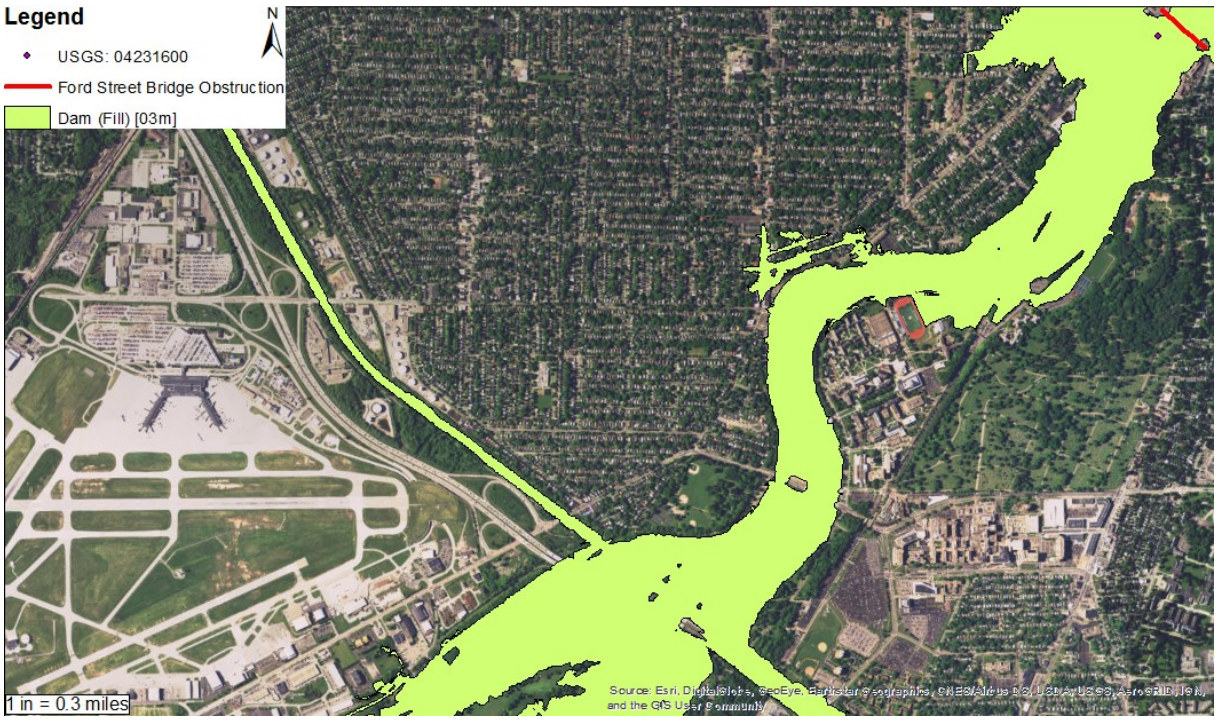

Figure 23 - Dam (Fill) [03m]. This figure demonstrates the fine granularity of the 3m cell size flood extent generated by the FEG.

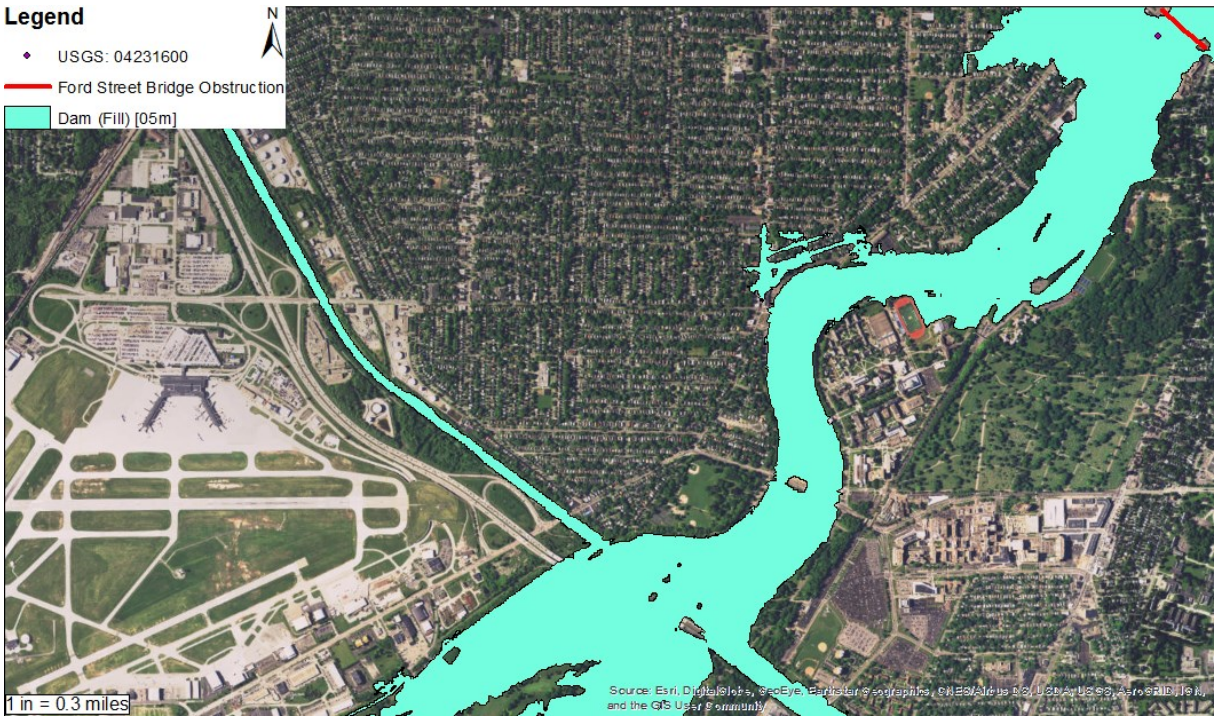

Figure 24 - Dam (Fill) [05m]. This figure demonstrates the semi-fine granularity of the 5m cell size flood extent generated by the FEG, with some perceptible loss of smoothness on the extent boundaries.

Figure 25 - Dam (Fill) [10m]. This figure illustrates how coarse the data become over Figure 24, as many finer details are lost and some extraneous data appear (especially near the running track on the University of Rochester Campus) as gaps in the extent become filled in, and the extent boundaries grow slightly.

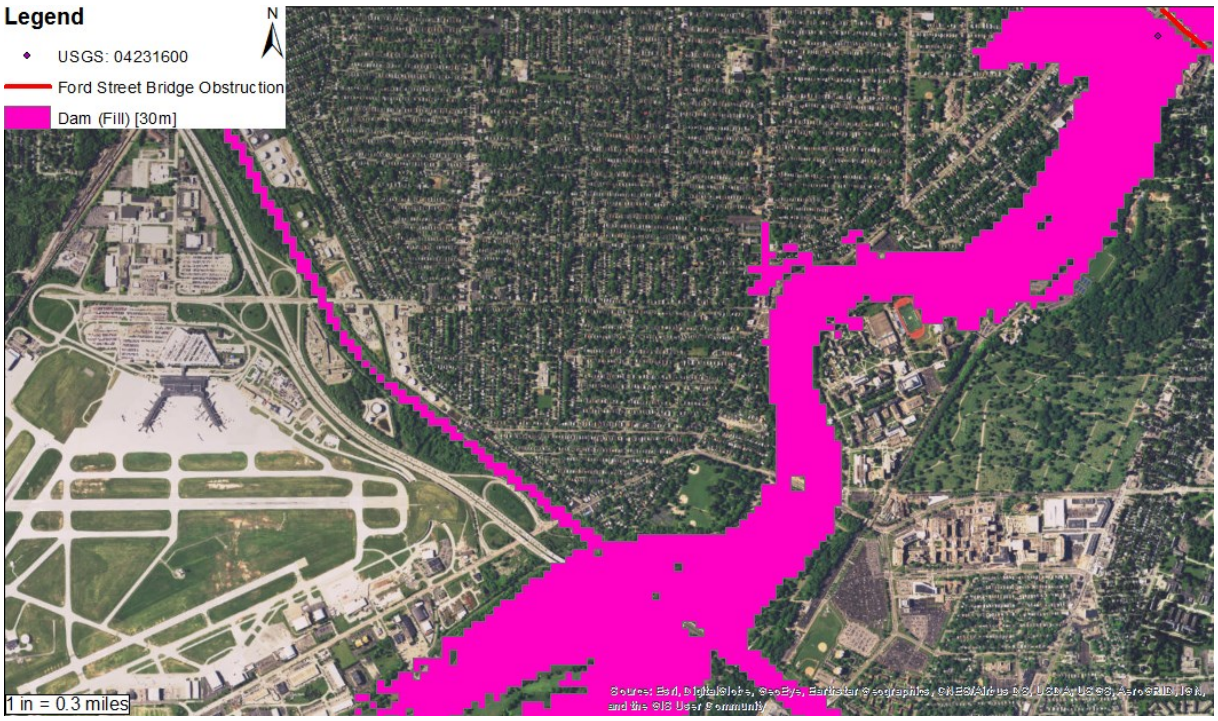

Figure 26 - Dam (Fill) [30m]. This figure illustrates how at 30m cell size almost all of the smaller rivulets of flooding near the Ford Street Bridge Obstruction have disappeared, along with many small gaps.

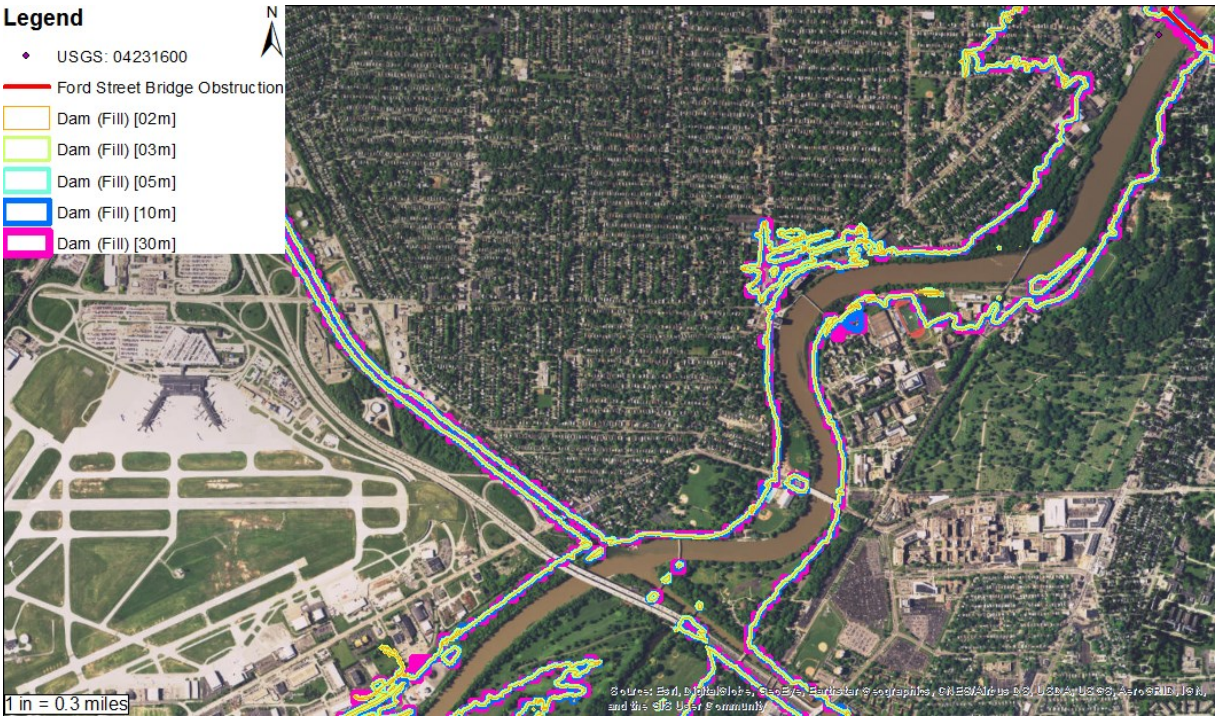

Figure 27 - Dam Small (Fill) [02m, 03m, 05m, 10m, 30m]. This figure demonstrates the differences in coverage between the various resolutions of the flood extent at once so that changes in coverage are easier to visualize.

Figure 28 demonstrates the underlying topography of the Rochester Institute of Technology campus, highlighting areas of relatively high elevation with a white color, with lower values fading to darker shades of gray. The buildings on the left side of the campus are at a higher elevation than the dormitories on the right side of the campus, with both the central north and south parts of the campus being at lower elevations.

In Figure 29, the fine cell size of 2m allows for flood extents that follow very closely around man-made and natural features in the map, such as a slightly elevated playing field, roadways, and even the drainage features surrounding a parking lot. Fingers of the flood extent can be seen following roadways, building footprints, and other features. The 3m cell size data of Figure 30 are nearly indistinguishable from the 2m cell size data of Figure 29, with features being preserved well at 3m and the extent matching almost exactly. Figure 31 represents a turning point in the flood extents, as it can be seen that smaller "island" features are now being absorbed along with finer details along the flood extent boundary becoming visibly generalized. However, at this resolution the boundaries still appear to follow features in the landscape with reasonable detail. In Figure 32, the boundaries of the flood extent are getting increasingly less natural and are following features in the environment much less than in the prior finer resolution extents. Curves and subtle details of the built environment are being replaced with long distances of straight lines as the locations along the edge become averaged together, marking the point where the relationship between the flood boundary and the environment become noticeably abstracted. In Figure 33, the flood boundaries have become highly abstracted from the minor features in the built environment. Due to the aggregation of elevation data at 30m pixels, some features have been filled in that were previous not flooded by the FEG, such as RIT's entranceway on Jefferson Road. At this resolution, the data are usable for coarser datasets like Census Blocks, Block Groups, or Tracts whereas its utility on fine units like Parcels is questionable. In Figure 34, the differences in flood extent coverage can more clearly be seen and compared, since the layers have been stacked from coarsest to fine. As expected, the 30m data do not follow curved features nor preserve small "island" features as well as even the 10m data.

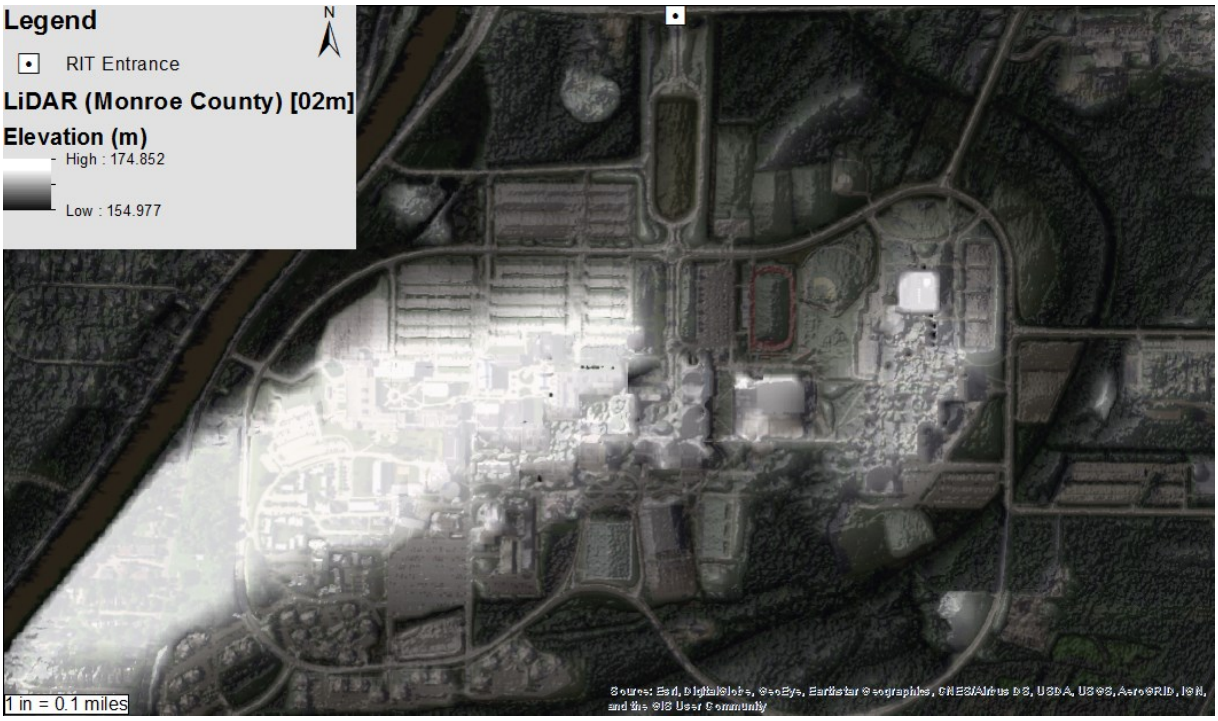

Figure 28 - Dam (Fill) Elevation (Large Scale). This figure illustrates the topography local to the RIT campus, giving insight into the FEG extents in Figure 29 - Figure 34.

Figure 29 - Dam (Fill) [02m]. This figure demonstrates the ability of the 2m data to follow closely features in the built environment.

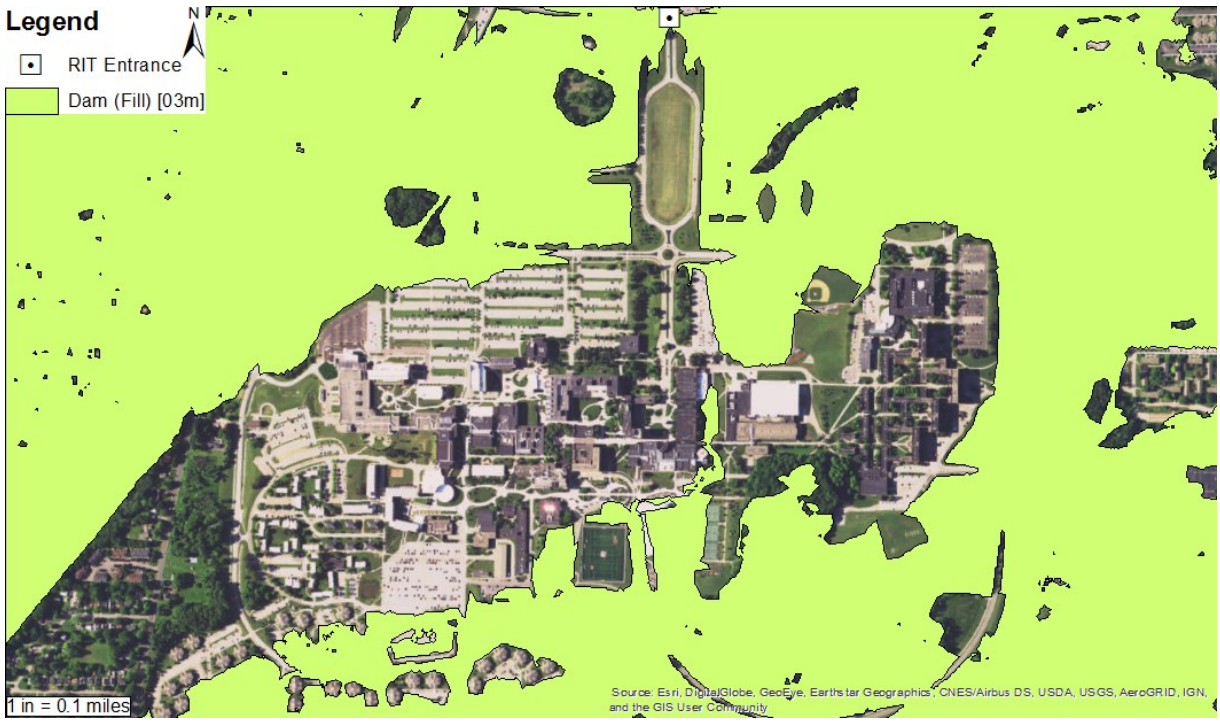

Figure 30 - Dam (Fill) [03m]. This figure demonstrates the 3m cell size data's ability to closely follow features in the built environment nearly as well as the 2m cell size data, preserving fine details such as property boundaries.

Figure 31 - Dam (Fill) [05m]. This figure demonstrates the 5m cell size data beginning to generalize features in the built environment.

Figure 32 - Dam (Fill) [10m]. This figure demonstrates the 10m cell size data becoming noticeably abstracted from the built environment, featuring clean straight lines where they're not present.

Figure 33 - Dam (Fill) [30m]. This figure demonstrates how the 30m cell size data have become highly abstracted from the smaller features in the built environment.

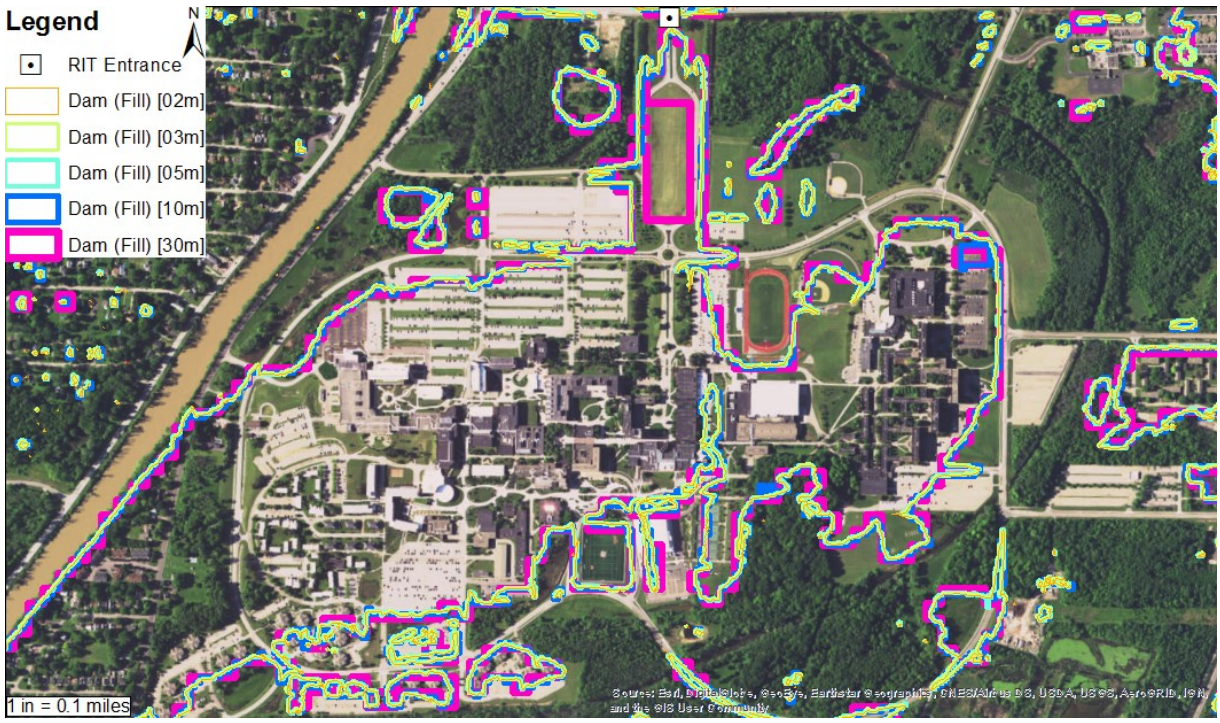

Figure 34 - Dam Large (Fill) [02m, 03m, 05m, 10m, 30m]. This figure demonstrates the differences in flood boundary prediction between the various resolutions by stacking them from coarsest to fine.

In Table 19 below, the difference in file size between the various cell sizes of the dataset can be observed. When considering deploying uncompressed raster layers in the field, the 10m data becomes much more realistic as its 99mb file size can be downloaded relatively quickly over modern 4G/LTE datalinks, and its 99mb is less than most short HD video clips, meaning storage is less of a concern. The processing time decreases nearly linearly with respect to cell size, compared to file size which decreases in an exponential fashion. Since processing of the FEG data would likely be done in an operations center on computer or server hardware, there would likely be more processing power and storage to generate and process the FEG data layers at the smaller cell sizes, with the possibility to resample and compress the FEG layers for distribution to field-deployed devices (mobile phones, laptops, etc). When investigating the change in area from the smallest area of FEG extents under the 2m cell size to the largest area under the 30m cell size, there is a difference of just 1.9% in areal coverage between the finest and coarsest resolution FEG extents. The change in areal coverage is consistent with the slight increase in FEG boundaries as a result of the coarse 30m pixels. The change in perimeter from least to most (30m to 10m) is a roughly 21% change and does not follow a linear decrease as expected. With smaller pixel sizes, there will be more pixels used to define a given shape or curve, resulting in more perimeter used to cover a

given area as the perimeter will be more detailed and will consist of more cells. The linear decrease holds only from 2m to 3m cell size, with an increase from 5m to 10m. A decrease in perimeter when cell size increases is expected as there will be fewer cells used to represent the flood extents, leading to reduced perimeter length. A possible explanation for the increase in perimeter for the 5m and 10m cells is that, at these cell sizes, many of the holes in the surface had not been filled in yet, like they are at the 30m cell size, as well as the fact that at 5m and 10m cell size, many features of the environment can still be outlined, whereas at 30m cell size, the more complex shapes in the environment tend to be aggregated into lager, simpler forms on the exterior as well as within the extent which results in reduced perimeter, as expected.

Table 19 - Processing times, file size, and extent dimensions for variable-resolution Dam Fill layer. This table demonstrates the differences in file size and processing time as cell size changes in a dataset, as well as the change in area and perimeter of the extents as the resolution changes.

Data Layer: Dam Fill [02m, 03m, 05m, 10m, 30m]					
Cell Size	02m	03m	05m	10m	30m
File Size (MB)	2410	1070	394	99	11
Processing Time (m:s)	28:21	23:46	22:17	20:30	14:27
Perimeter (km)	1593.2	1540.9	1604.9	1690.4	1335.1
Area (km^2)	90260.2	90562.9	90557.8	91126.3	92007.4

Results & Discussion (Truth Assessment Model):

When comparing the FEG data with the Hazus-generated extents visually, there is a lot of commonality in terms of flood location and extent. However, when the data are compared using a *Union* analysis, it becomes clear that the agreement between the FEG (71,320km^2) and Hazus (43,737km^2) data is low when constrained to the entirety of Monroe County, at around 15% (19,717km^2) for the Genesee River scenario. When the analysis is constrained to the areas upriver (south and west) of the Ford Street Bridge obstruction, the spatial agreement between the FEG (19,011km^2) and Hazus (17,754km^2) rises to 32% (16,947km^2). The areas of greatest agreement were in the areas of highest development, likely indicating that the FEG works best with high local spatial contrast, such as variations in elevation due to building footprints, crested roadways, etc. Possibly contributing to the change in behavior of the FEG across the different geographic areas would be in influence of other terrain variables not taken into account in the FEG such as soil type, impervious surface ratio, and the flow of the water itself or other data pre-processing done through the Hazus model. Though these variables were not included in this iteration of the model, future iterations of the model could attempt to integrate more variables in an attempt to improve accuracy and agreement with Hazus data, while still keeping the model simple and quick to run. As the flood extent goes towards the less developed and more flat south-west portion of Monroe County, the agreement between the FEG and Hazus drops off significantly.

Another possible compounding factor contributing to the low agreement of the FEG and Hazus is that the FEG appears to have allowed for the flood extent to overflow into the canal and other waterways, flooding along and past these routes. It is uncertain if this result is desirable or not in terms of modeling the flood extent, though this is certainly a possibility in the event of a real flood, especially if the locks are unable to deal with the volume of floodwater that could present itself in such scenarios as modeled in this analysis.

Finally, the Hazus analysis constrains the flood extent analysis to the river reach, whereas the FEG is allowed to search globally at the given elevation range for the impacted elevations causing the FEG to over-estimate the flood extents and create extents beyond the riverine area, which could either be realistic due to terrain changes, or over-estimates where impediments to surface water flow exist and are not accurately capture by the FEG. This unconstrained search leads to the FEG creating extents that can surpass the probable flood boundaries, as well as creating non-contiguous flood extent pixels, which end up greatly reducing the spatial agreement of the FEG with the Hazus data. Post-processing the FEG data to remove small clusters or non-contiguous data, along with clipping the FEG results to the given river reach might serve to help improve the accuracy and agreement of the FEG with Hazus and other flood risk models.

The FEG extent matches the Hazus extent for the Genesee River closely near to the city of Rochester and slightly southwards. The FEG's extent flows west into Black Creek, east into Irondequoit Creek, and has boundaries scattered across other portions of Monroe County well outside the bounds of the Genesee River reach (Figure 35). Constraining the FEG analysis to the river reach being investigated would likely mitigate the over-estimation of impacted areas by the FEG, while increasing spatial agreement with models like Hazus

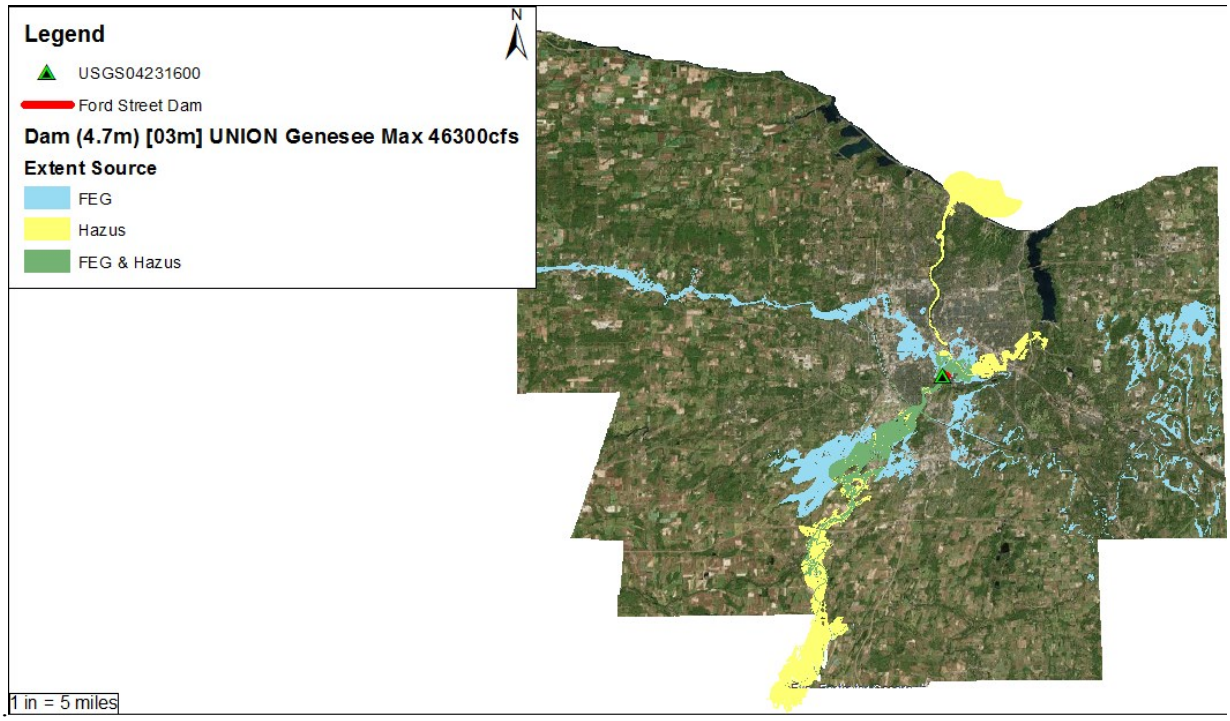

Figure 35 - FEG (4.7m) UNION Hazus Genesee (46300cfs). This figure demonstrates the flood extents generated for the Genesee River by both the FEG and Hazus. Areas of spatial agreement are green (28%), whereas FEG-only areas are blue, and Hazus-only areas are yellow.

When the immediate areas surrounding the Ford Street obstruction and USGS gauging station are investigated (Figure 36), the FEG and the Hazus data have high spatial agreement within a well-defined floodplain. In this area, Hazus seems more likely to predict flooding into the built areas and the FEG seems more likely to predict flooding immediately surrounding the waterways and river reach. This disparity between predictions is likely due to the more complex analyses involved in the Hazus model which take into account soil type among other variables (Meyer 2004), whereas the FEG is purely elevation-driven. Another possible factor is the data pre and post-processing done within Hazus which could have had a significant impact on the DEMs. Running the FEG with the Hazus-generated DEMs would help ascertain if the data pre and post-processing play a significant role in extent generation.

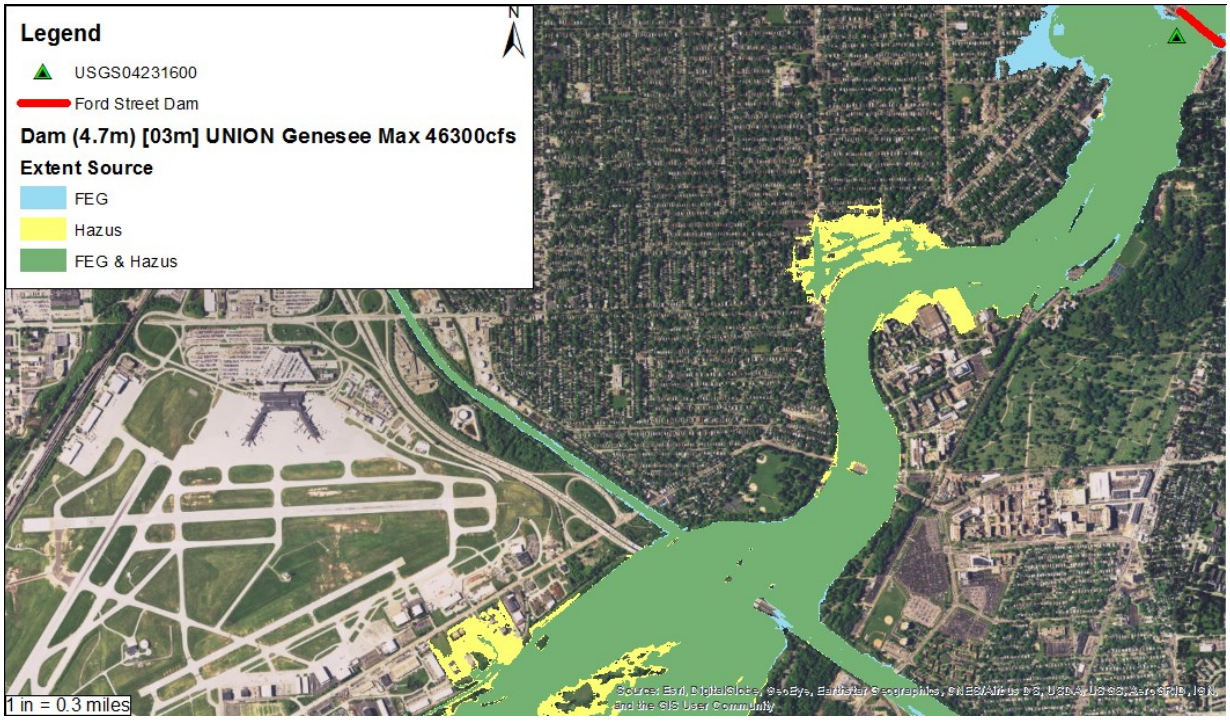

Figure 36 - FEG (4.7m) UNION Hazus Genesee (46300cfs): Ford Street. This figure shows the difference in coverage between the FEG and Hazus data near the Ford Street obstruction and around the University of Rochester campus.

Similar to the Ford Street view extent of Figure 36, the FEG and Hazus data have high agreement for the RIT campus, as seen in Figure 37. Referring back to the elevation visualized in Figure 28, the agreement between the FEG and Hazus data seems reasonable. The FEG extent goes beyond the Hazus extent, eclipsing most of the RIT campus east of the dormitories, whereas the Hazus data does not count that area as flooded. Given the low-lying terrain in that portion of the campus, it is not surprising that the FEG marked it as flooded, whereas the Hazus data determined that the flood extent would end just past the dormitories. It is possible that the unnatural cutoff of the Hazus extent could be due to constraints placed upon the floodplain during Hazus data pre-processing.

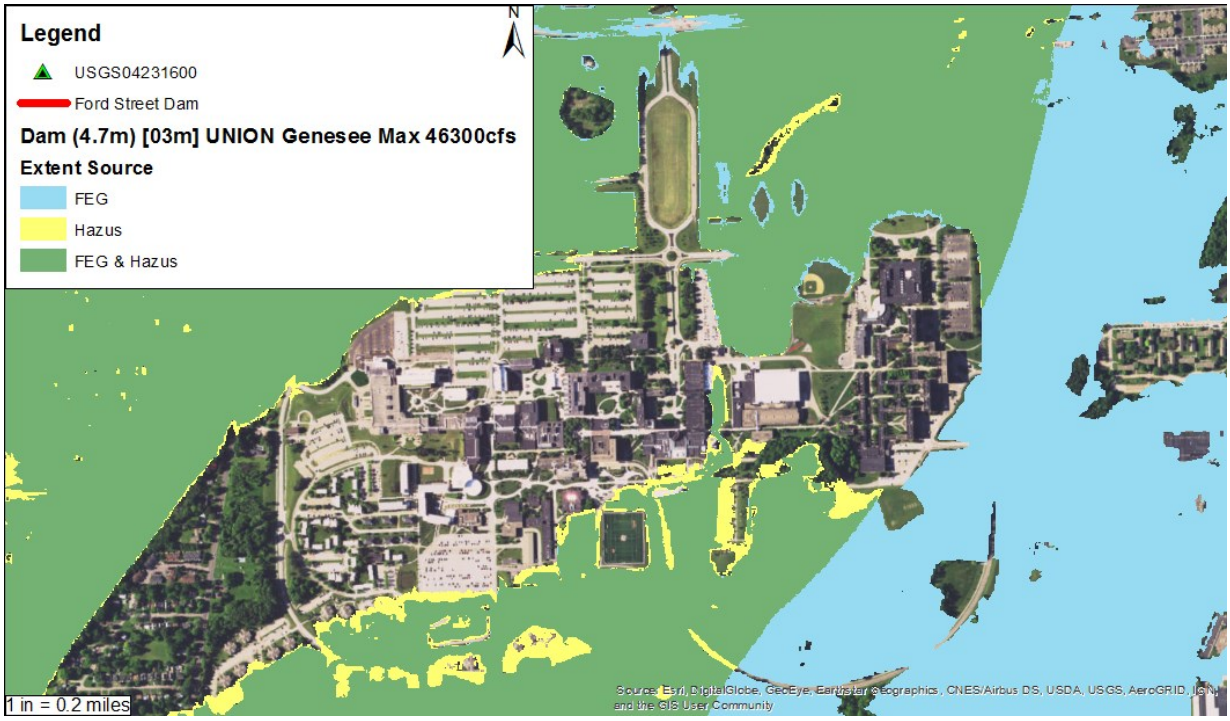

Figure 37 - FEG (4.7m) UNION Hazus Genesee (46300cfs): RIT Campus. This figure shows the difference in flood extents on and immediately around the RIT campus.

Results & Discussion (Risk Assessment Model):

The RAM generates results which seem to confirm that this piece of the model framework is usable, but somewhat limited by the availability of population data in appropriate spatial scales. Areas such as schools, elder care facilities, or major infrastructure are correctly identified as having high risk factors, based on the model. The variables also can be visualized in separate layers to investigate different questions than the risk factor answers (impact to the most people, costliest infrastructure damage, etc). If extents from the Hazus data are used instead of the FEG, the number of impacted parcels increases 5% with a 27% reduction in total impacted area, likely more closely approximating the realities of what the impacted areas would be in the event of a flood on the Genesee given Hazus' wide implantation and acceptance as a risk management tool (Table 20). Assuming the Hazus extents are correct for this study site, usage of the RAM workflow with the Hazus extents would better serve the purposes of risk assessment when compared to the usage of the RAM workflow with the FEG extents.

Table 20 - Impacted parcels and land area (FEG vs Hazus). This table provides the count of the impacted parcels and total affected land area for the FEG and Hazus, as well as the parcels both have identified as impacted in this scenario.

Impacted parcels and land area (FEG vs Hazus)		
	Parcel Count	Area
FEG	2148	359,458km^2
Hazus	2267	261,612km^2
FEG & Hazus	1690	172,922km^2

The current visualization of the Risk Factor is not as effective as initially envisioned. The summed numerical model is difficult to visualize in ArcGIS, as it is limited in how many variables can contribute to the symbolization, as well as to what types of visual variables can be used. For instance, if Monroe County valued the contribution of Human Impact more than Cost or Priority Rating, using transparency as a symbol level for Human Impact along with color for Risk Factor would help to show which parcels are of key interest much more effectively than overlaying another layer and drawing only the parcel locations with the highest Human Impact, as has currently been done.

The RAM also suffers from over-estimating the impact of the flood as the data for human impact, contributing to the Risk Factor are at the Census Block level, whereas the physical boundaries used are at the parcel level, causing multiple parcels to share the aggregate data contributing to Priority Rating, Human Impact, and Cost. If these data were available on the same scale as the parcel data, the model would more accurately represent the areas most in need of support in the event of a flood. A spatial normalization of the human impact variable would serve to mitigate the spatial resolution disparities in

this particular dataset, though the same issue may arise for the other variables in other datasets, requiring other means to normalize each variable across different spatial resolution data.

Figure 38 demonstrates the FEG's flood extent and the impacted parcels south of the Ford Street Dam obstruction by showing the Risk Factor for the impacted parcels. The parcels were selected using a select by location query and using the intersect selection method. Selection by intersect means that any parcel that touches the FEG flood extent will count as entirely at risk, grossly over-estimating the parcels at risk, and therefore the population and infrastructure at risk. When using intersect with the more restricted Hazus extent, the number of impacted parcels drops significantly (Figure 39). Using the centroid selection criteria, as in Figure 40 and Figure 41, yields a greatly reduced set of impacted parcels for both the FEG and Hazus extents. The centroid selection criteria works by only selecting a given parcel if the flood extent boundary crosses the centroid, which is the location that represents the geometric center of the parcel polygon. By using the centroid, the tendency to over-select by using intersect is reduced as having a flood extent reaching the centroid would mean that the flood extent has penetrated the boundary of the parcel by 50% or more.

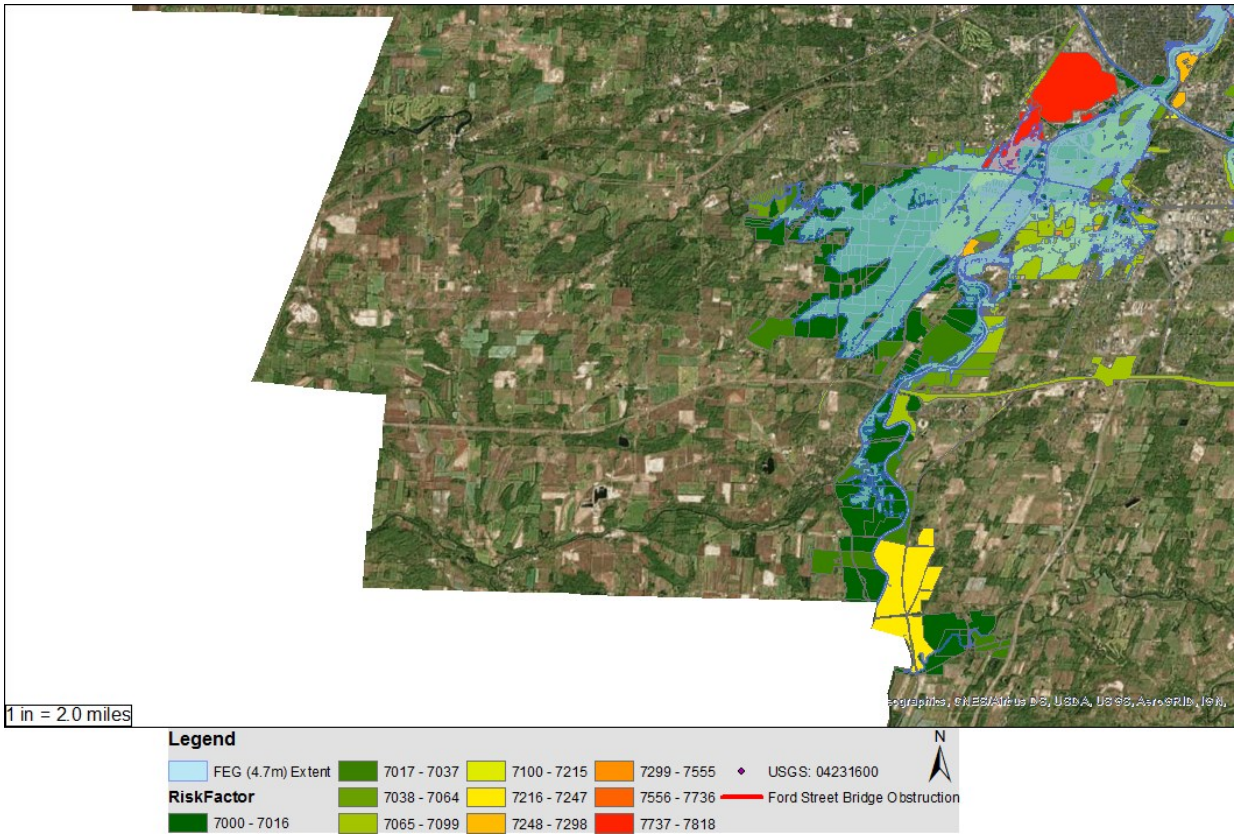

Figure 38 - FEG (4.7m) Extent INTERSECT RiskFactor. This image demonstrates the parcels counted as impacted when using the FEG extent and intersecting it against a parcel layer.

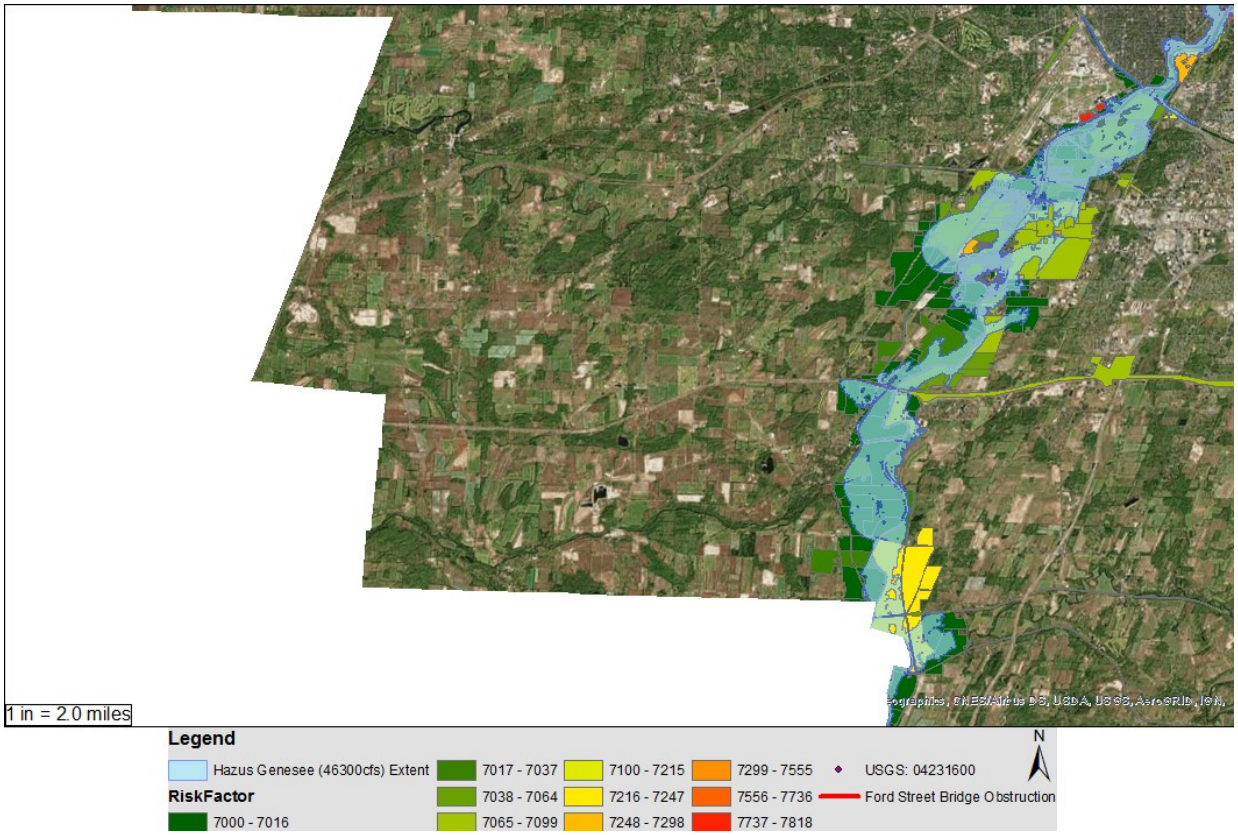

Figure 39 - Hazus (46300cfs) Extent INTERSECT RiskFactor. This image demonstrates the impacted parcels when using the Hazus flood extent.

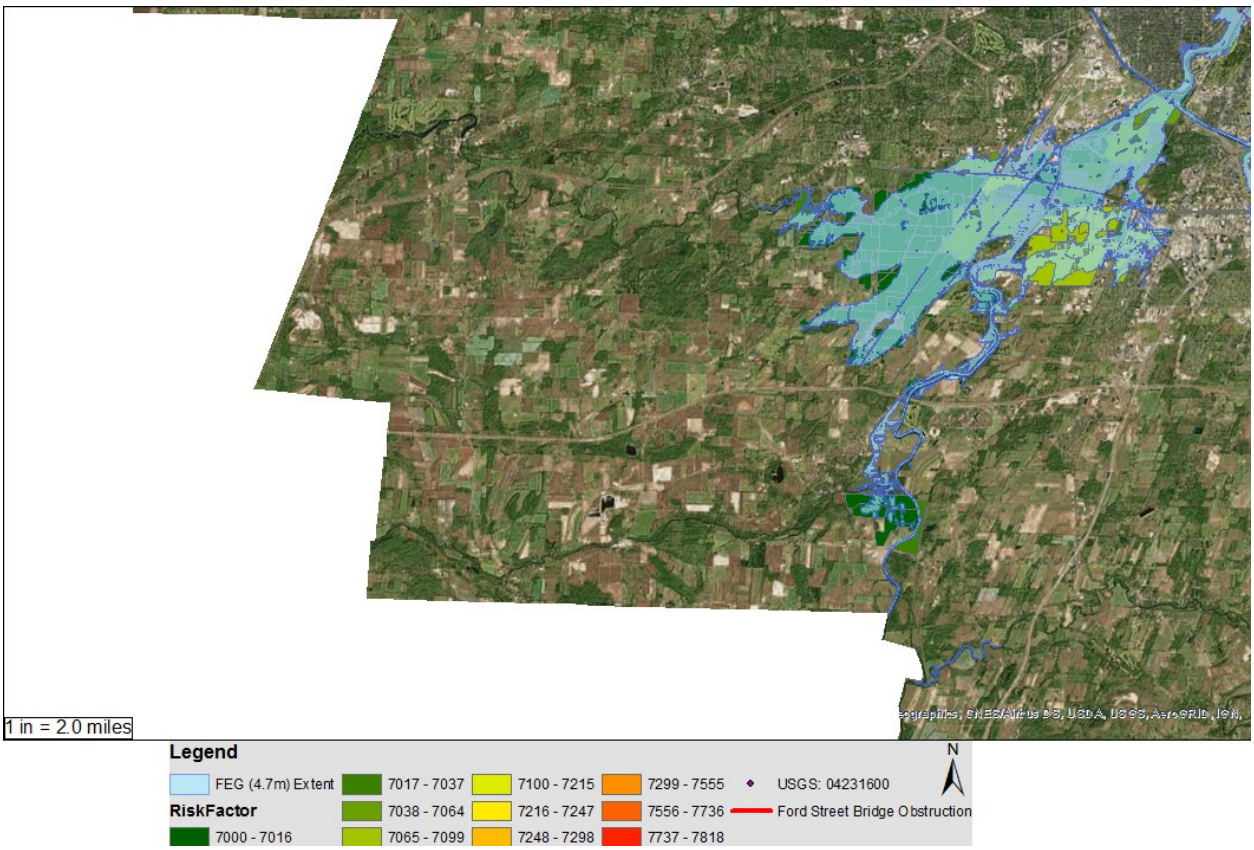

Figure 40 – FEG (4.7m) Extent CENTROID RiskFactor. This figure demonstrates how using the centroid selection criteria reduces the number of impacted parcels.

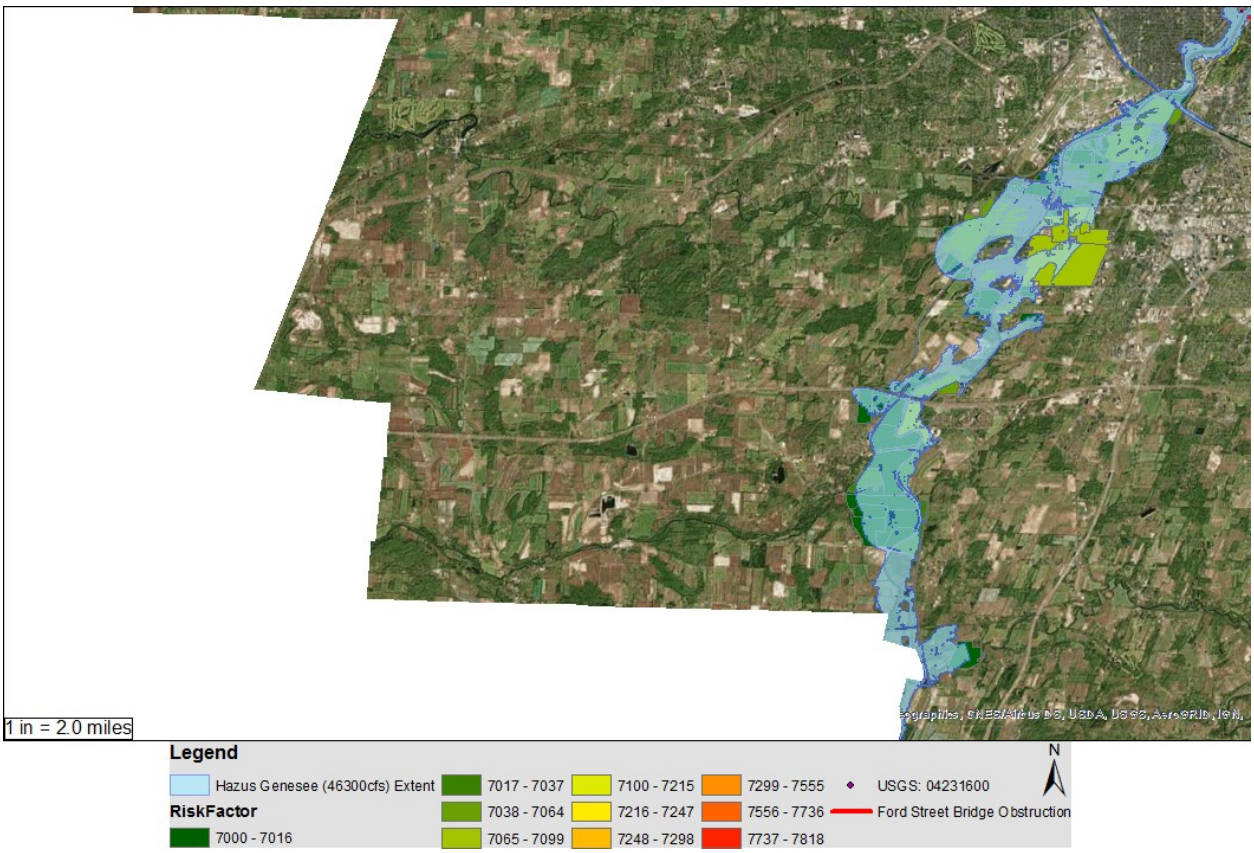

Figure 41 - Hazus (46300cfs) Extent CENTROID RiskFactor. This figure demonstrates how the centroid selection criteria can further refine the impacted parcels when used with the Hazus extent.

Conclusion:

The ODM may fill a niche role in planning and mitigation efforts in areas concerned with flooding, but it needs significant refinement and field verification at various river stages in order to verify that the manual classification bounds are widely applicable in different river reaches, and that they repeatedly detect riverine obstructions consistently. The Equal Interval, Geometric, Jenks, and Quantile classifications were found to be undesirable due to suboptimal groupings they created when used on the ODM data, requiring the usage of the Manual class definitions. By detecting and identifying potential flood risks in riverine areas, the ODM can be used to help guide flood planning activities. However, due to the changeable nature of river stages, the detection of riverine obstructions will be influenced by the river stage at the time of data collection, possibly resulting in under, or over, classification of features within the body of water. Using confirmed hits from the ODM as inputs into the RAM will also enable the decision makers to run various flood risk scenarios, which can help them prioritize which flood risk points are most important to manage first.

The RAM is closer to being suitable for use as a planning tool pending spatial differences between the model variables' data sources being addressed. By using the RAM to analyze what might happen in the event of a flood due to a given flood risk point, decision makers can assess the flood preparation and readiness of areas under their management. This is a key part of the planning phase of disaster management. By prioritizing mitigation to areas that are more vulnerable, or more costly in the event of a disaster, the likelihood of an expensive disaster decreases.

In general, the individual model components did work. The ODM highlighted objects within riverine areas, the FEG created flood extents based upon elevation alone, the TAM compared those extents to existing data, and the RAM used the FEG extents to visualize the impact of that scenario on study site. Taken as a whole, the framework and approach should, in theory, yield results that would be beneficial for use in first response situations, but given the limitations of the FEG and the RAM in terms of over-estimating the flood extents and therefore the impacted parcels, the utility of the framework is currently limited, and recommended only as an investigative tool or scenario generation tool. There was some minimal sensitivity analysis of the model components to resolution, with 10m data representing the best compromise between processing speed, file size, availability, and model output precision. The choice of interpolation method, as currently assessed, also proved to have little real impact on the ODM, and consequently the FEG results generated from the identified risk points of the ODM. Therefore, it is recommended that the interpolation method used be either IDW or NN, as both interpolate similarly and process rapidly.

Future Work:

The spectral analysis aspect of the ODM was deprecated for this version of the model. However, the use of spectral analysis could prove invaluable to the accuracy of the ODM in predicting actual flood risk points. By incorporating the spectral profile of areas identified as risky by the slope analysis, the ODM would be better able to determine the difference between a confirmed non-water hit (obviously an obstruction of some type) versus a potential hit (drastic change in water surface slope). The spectral profiling of the hits would also be beneficial in detecting obstructions that themselves are fairly flat, provided the free surface of the water has not risen above the object. The integration of the spectral data would require LiDAR and Orthophotography to be flown concurrently, limiting the usage of the spectral data to the planning and preparation phases of risk management, as it is unlikely that concurrently collected LiDAR and Orthophotos would be flown on-demand in an emergency event. The ODM's classes need to have a process-based method of derivation that will yield flood risk classes that are appropriate to all study sites and repeatable in nature, as opposed to the current manually derived classes.

The underlying mechanisms for the detection capability of the current class boundaries has not been determined for certain, though it is hypothesized, as stated earlier, that the deflection in the free surface of the water is a suitable proxy for direct detection of a possible flood obstruction. In order to determine if the current system is robust, multiple site-specific collections of concurrent LiDAR and orthophotograhy should be taken to detect and visually verify the presence of flood obstructions at various river stages. Furthermore, in-field verification of identified flood risk points needs to be performed to determine if the possible flood risk points identified by the ODM actually are present in-field. Finally, using the ODM to determine possible flood risk points and verifying that against historical flood data will help validate the current classes and the model itself.

The FEG needs to be improved in terms of model variables and data pre-processing to help increase its accuracy and agreement with other models, like Hazus. It is possible that the Hazus extents for this study site aren't completely accurate, but given Hazus' acceptance in the risk management field, it will serve as a good benchmark for FEG testing. Hazus constrains the flood extent analysis to the river reach and watersheds within the defined study site, whereas the FEG allows the flood extent analysis to run "globally" across the study site. If the FEG were to adopt the preprocessing step to constrain itself to the river reach in question, the results may change significantly. Unfortunately, adding input variables and data will add to model complexity and processing time, making the FEG potentially less attractive as a tool for first responder use. However, at the FEG's current accuracy and agreement levels, it is not recommended for usage in any capacity other than preliminary planning.

The TAM revealed that the FEG has significantly low agreement with Hazus data for the same flood event, though the lack of applicable in-situ field verification data limits the possibility to analyze where both the FEG and Hazus agreed, and why they agree in those specific locations. With more in-depth field verification of the FEG extents, it should be possible to determine what extra variables and data pre-processing would be beneficial to the FEG.

The RAM is limited by how many variables can be distinctly visualized at once without appearing too busy, or otherwise obfuscating visual analysis of the risk factor, as well as the other variables. In future iterations of the RAM, more visual variables (location, size, shape, orientation, hue, value, texture, saturation, arrangement, crispness, resolution, transparency) (Roth 2015) should be employed to help aid visual analysis of the RAM results, taking the current state of the RAM further. ArcGIS Pro, a recently released GIS suite (ESRI n.d.), has extended and enhanced visualization tools, allowing for the usage of more visual variables, as well as more robust and varied visualization of data.

Furthermore, the RAM needs a method to deal with data that do not share a common spatial scale, as evidenced in the data scale inconsistencies between the human impact and other variables. As noted earlier, a simple averaging of the population over the area of the parcel would be a reasonable first step towards mitigating this issue in data scale. Estimation of population in a given parcel can also be accomplished by using the number of bedrooms as a proxy for an occupancy value, assigning one person per bedroom. For properties that do not have bedrooms in the parcel data (hospitals, offices, etc), the max occupancy data (if available) would serve to estimate the population of that parcel. Other, more complex methods of normalizing the population data across data scales would go a long way towards mitigating the over-estimation of impacted populations by the RAM, along with using a better selection method to determine what parcels are actually considered impacted by the flood extent. Centroid provides a reasonable first approach, as half or more of the parcel must be overlapped by the flood extent for the parcel to count as impacted. Combining building footprints with centroid-based selection and population normalization would lead to the risk factor being more precise and more robust for usage in varied locations.

Another future prospect to explore is the generation of ArcToolbox tools for the ODM, FEG, TAM, and RAM, along with using the ArcPy scripting environment to generate GUI front-ends with contextual help that the user can employ to step through the various steps of the flood obstruction models. In this environment, the user would simply have to read the prompts and select their appropriate data. This workflow is greatly simplified from following a written text methodology. This streamlining fits the desired goal of simple/fast/light that is key for first responder usage. Along with the ArcToolbox tools,

QGIS plugins should be developed in tandem that have feature parity with the ArcToolbox extensions. By having the QGIS plugins, more people could use, study, improve upon, and iterate upon the flood extent models by virtue of QGIS' open-source and license-free model (QGIS 2017). Finally, once complete, the QGIS tools should be open-sourced and posted in a public repository like GitHub so that others can improve upon the work without restriction.

Works Cited

Banchini, Giovanni, L Feretti, G Lombardo, and L Surace. 2000. "Role of Digital Orthophotos in Environmental Disaster Management." *International Archives of Photogrammetry and Remote Sensing* 33 (B7): 106-112. Accessed May 23, 2012. http://www.isprs.org/proceedings/XXXIII/congress/part7/106_XXXIII-part7.pdf.

Bater, Christoper W, and Nicholas C Coops. 2009. "Evaluating Error Associated with Lidar-Derived DEM Interpolation." *Computers & Geosciences* 35: 289-300. doi:10.1016/j.cageo.2008.09.001.

Brooks, Maggie, and Frederick J Rion. n.d. "Monroe County Pre-Disaster Mitigation Plan." Accessed June 24, 2012. http://www2.monroecounty.gov/files/ps/oem/2010%20Pre-Disaster%20Mitigation%20Plan%20FEMA%20&%20MC%20approved.pdf.

Cole, Justin D. July 25, 2012. "Re: Field Data Procedure for Monroe County." E-mail message to Brett Edmond Carlock.

Department of Homeland Security FEMA. 2016. "Hazus Overview." *FEMA.gov.* November 09. Accessed January 12, 2017. https://www.fema.gov/hazus-mh-overview.

EagleView Pictometry. n.d. *June 2015 Calendar Image.* Accessed January 10, 2017. http://blog.eagleview.com/index.php/2015/06/june-2015-calendar-image/.

ESRI. n.d. "An overview of the Hydrology toolset." *Help | ArcGIS Desktop.* Accessed December 15, 2016. http://desktop.arcgis.com/en/arcmap/latest/tools/spatial-analyst-toolbox/an-overview-of-the-hydrology-tools.htm.

—. n.d. "Arc Hydro Overview." *ArcGIS Resources.* Accessed December 15, 2016. http://resources.arcgis.com/en/communities/hydro/01vn0000000s000000.htm.

—. n.d. *ArcGIS for Desktop.* Accessed December 05, 2016. http://www.esri.com/software/arcgis/arcgis-for-desktop.

—. n.d. *ArcGIS Pro.* Accessed January 20, 2017. https://pro.arcgis.com/en/pro-app/.

—. 2014. "Cell size and resampling in analysis." *ArcGIS Help 10.2.* March 7. http://resources.arcgis.com/en/help/main/10.2/index.html#//018700000006000000.

—. 2016. "Comparing interpolation methods." *Help | ArcGIS for Desktop.* Accessed January 09, 2017. http://pro.arcgis.com/en/pro-app/tool-reference/3d-analyst/comparing-interpolation-methods.htm.

—. 2016. *Data classification—Help | ArcGIS Desktop.* Accessed January 12, 2017. http://desktop.arcgis.com/en/arcmap/latest/extensions/geostatistical-analyst/data-classification.htm#GUID-BA9CFB7F-3838-4736-88B9-DAC27DFEFC66.

—. 2016. *FAQ: Does Esri support 64-bit processors with ArcGIS 10.0 products?* May 05. Accessed 12 13, 2016. http://support.esri.com/technical-article/000011074.

—. 2016. *FAQ: What is the Jenks optimization method?* May 5. Accessed January 12, 2017. http://support.esri.com/technical-article/000006743.

—. 2016. "How IDW works." *Help | ArcGIS for Desktop.* Accessed January 09, 2017. http://pro.arcgis.com/en/pro-app/tool-reference/3d-analyst/how-idw-works.htm.

—. 2016. "How Natural Neighbor works." *Help | ArcGIS for Desktop.* Accessed January 09, 2017. http://pro.arcgis.com/en/pro-app/tool-reference/3d-analyst/how-natural-neighbor-works.htm.

—. 2016. "How Spline works." *Help | ArcGIS for Desktop.* Accessed January 09, 2017. http://pro.arcgis.com/en/pro-app/tool-reference/3d-analyst/how-spline-works.htm.

—. n.d. "Search neighborhoods." *ArcGIS Pro | ArcGIS for Desktop.* Accessed January 10, 2017. http://pro.arcgis.com/en/pro-app/help/analysis/geostatistical-analyst/search-neighborhoods.htm.

Federal Geographic Data Committee. 2008. "Geographic Information Framework Data Content Standard Part 2: Digital Orthoimagery." 8.2.1 Spatial Resolution. Accessed August 10, 2012. http://www.fgdc.gov/standards/projects/FGD-standards-projects/framework-data-standard/GI_FrameworkDataStandard_Part2_DigitalOrthoimagery.pdf.

Gouldby, B P, P B Sayers, M C Panzeri, and J E Lanyon. 2010. "Development and Application of Efficient Method for the Forward Propagation of Epistemic Uncertainty and Sensitivity Analysis within Complex Broad-Scale Flood Risk System Models." *Canadian Journal of Civil Engineering* 37 (7): 955-967. Accessed November 10, 2010. doi:10.1139/L09-173.

Graumann, Axel. 2005. "Hurricane Katrine - A Climatological Perspective." Technical Report. Accessed December 2012. http://www.ncdc.noaa.gov/oa/reports/tech-report-200501z.pdf.

Gunes, A Ertug, and Jacob P Kovel. 2000. "Using GIS in Emergency Management Operations." *Journal of Urban Planning & Development* 126 (3): 136-149. Accessed August 2012. doi:10.1061/(ASCE)0733-9488(2000)126:3(136).

Hazards and Vulnerability Research Institute (HVRI). 2011. *Changes and Improvements in the SoVI® Formulation.* December 15. Accessed April 16, 2012. http://webra.cas.sc.edu/hvri/products/sovi_details.aspx.

Hudson-Smith, Andrew, Michael Batty, Andrew Crooks, and Richard Milton. 2009. "Mapping for the Masses: Accessing Web 2.0 Through Crowdsourcing." *Social Science Computer Review* 27 (4). doi:10.1177/0894439309332299.

Justin Cole, GISP. 2013. *Monroe County, NY, Hazus Models.* Rochester, NY: Monroe County GIS Department.

Li, Jin, and Andrew D Heap. 2011. "A Review of Comparative Studies of Spatial Interpolation Methods in Environmental Sciences: Performance and Impact Factors." *Ecological Informatics* 6 (3-4): 228-241. doi:10.1016/j.ecoinf.2010.12.003.

LIAS - RIT. 2008. "Wildfire Airborne Sensor Program (WASP)." *Laboratory for Imaging Algorithms and Systems.* Accessed August 14, 2012. http://lias.cis.rit.edu/projects/wasp.

Lu, Lin, Yu-Cheng Li, Bin Teng, and Bing Chen. 2008. "Numerical simulation of turbulent free surface flow over obstruction." *Journal of Hydrodynamics* B ser., 20 (4): 414-423. Accessed December 2012. doi:10.1016/S1001-6058(08)60075-X.

Maggino, Filomena, and Elena Ruviglioni. 2009. "Obtaining Weights: From Objective to Subjective Approaches in View of More Participative Methods in the Construction of Composite Indicators." *Eurostat NTTS-2009.* Accessed June 24, 2012. http://ec.europa.eu/eurostat/documents/1001617/4398464/POSTER-1A-OBTAINING-WEIGHTS-MAGGINO-RUVIGLIONI.pdf.

Matthews, Cara, and Joseph Spector. 2012. "New York will pick up local share of counties' flood costs." *The Ithaca Journal*, April 11. Accessed April 18, 2012. http://pqasb.pqarchiver.com/ithacajournal/doc/993542562.html.

Merrick & Company. 2017. *Mars LiDAR Software.* Accessed January 12, 2017. http://www.merrick.com/MARS.

Meyer, Jennifer Carol. 2004. *Comparative Analysis between Different Flood Assessment Technologies in Hazus-MH.* Shreveport, November 08. http://www.openthesis.org/documents/Comparative-Analysis-between-Different-Flood-526280.html.

Monroe County Department of Environmental Services. 2001. *Monroe County, NY, Centerlines.* Rochester, NY: Monroe County GIS Department.

—. 2011. *Monroe County, NY, Parcels.* Rochester, NY: Monroe County GIS Departement.

Monroe County Emergency Operations Center. 2012. *Critical Infrastructure and Key Resources (CIKR).* Rochester, NY: Monroe County Emergency Operations Center.

MonroeCounty.gov. 2012. *GIS Projects.* Accessed April 18, 2012. http://www2.monroecounty.gov/gis-projects.php.

NASA. 2005. "Project Status." *Shuttle Radar Topography Mission.* August 28. Accessed April 16, 2012. http://www2.jpl.nasa.gov/srtm/p_status.htm.

National Mapping Division. 1996. *Part 1: General, Standards for Digital Orthophotos.* National Mapping Program Technical Instructions, USGS. https://nationalmap.gov/standards/pdf/1DOQ1296.PDF.

Nayegandhi, Amar. 2007. "Lidar Technology Overview." *Airborne Lidar Technology and Applications Workshop.* Baton Rouge. Accessed October 2012. http://web.archive.org/web/20160305090327/http://lidar.cr.usgs.gov/downloadfile2.php?file=Nayegandhi_Lidar_Technology_Overview.pdf.

NOAA. 2011. "Flood Safety." *NOAA's National Weather Service Flood Safety Awareness Week.* July 5. http://web.archive.org/web/20130811055543/http://www.floodsafety.noaa.gov/floodsafe.shtml.

NYS GIS. 2015. *Monroe County, NY, Airborne 1 Corporation.* Albany, NY: NYS GIS Clearinghouse.

QGIS. 2017. *Welcome to the QGIS project!* January 12. Accessed January 12, 2017. http://qgis.org/en/site/.

Ramsey, Elijah, Dirk Werle, Zhong Lu, Amina Rangoonwala, and Yukihiro Suzuoki. 2009. "A Case of Timely Satellite Image Acquisitions in Support of Coastal Emergency Environmental Response Management." *Journal of Coastal Research* 25 (5): 1168-1172. Accessed November 10, 2010. doi:10.2112/JCOASTRES-D-09-00012.1.

rapidlasso GmbH. n.d. *LAStools | rapidlasso GmbH.* Accessed December 05, 2016. https://rapidlasso.com/lastools/.

Rayburg, S, M Thoms, and M Neave. 2009. "A Comparison of Digital Elevation Models Generated From Different Data Sources." *Geomorphology* 106 (3-4): 261-270. Accessed November 8, 2010. doi:10.1016/j.geomorph.2008.11.007.

Rion, Frederick J. Jr. August 13, 2013. "Rankings." E-mail message to Brett Edmond Carlock.

Robinson, Jerald B, William F Hazell, and Wendi S Young. 1998. *FS-036-98: What is a Recurrence Interval.* USGS Fact Sheet, Charlotte: USGS Publications Warehouse. Accessed June 11, 2012. https://pubs.usgs.gov/fs/FS-036-98/text/what.html.

Rochester Institute of Technology. 2011. *Cattaraugus Indian Reservation, Irving, NY, Leica ALS60.* Rochester, NY: Rochester Institute of Technology.

—. 2011. *Cattaraugus Indian Reservation, Irving, NY, WASP (RGB).* Rochester, NY: Rochester Institute of Technology DIRS.

—. 2011. *Cattaraugus Indian Reservation, Irving, NY. WASP (SWIR).* Rochester, NY: Rochester Institute of Technology DIRS.

Roth, Robert E. 2015. *Visual Variables.* http://www.geography.wisc.edu/faculty/roth/publications/Roth_2015_EG.pdf.

Satellite Imaging Corporation. n.d. *WorldView-2 Satellite Sensor Information and Specifications.* Accessed May 20, 2012. http://www.satimagingcorp.com/satellite-sensors/worldview-2.html.

Schueler, T R. 1994. "The Importance of Imperviousness." *Watershed Protection Techniques* 1 (3): 100-111. Accessed May 23, 2012. http://stormwatercenter.net/Practice/1-Importance%20of%20Imperviousness.pdf.

U.S. Department of Homeland Security FEMA. 2016. *Hazus.* November 9. Accessed December 15, 2016. https://www.fema.gov/hazus/.

USGS. 2011. *Cattaraugus Indian Reservation, Irving, NY, LandSat 5.* Reston, VA: USGS.

—. 2011. *Cattaraugus Indian Reservation, Irving, NY, National Hydrography Dataset.* Reston, VA: USGS.

—. 2012. "Floods: Recurrence intervals and 100-year floods (USGS)." *The USGS Water Science School.* March 9. Accessed June 11, 2012. http://water.usgs.gov/edu/100yearflood.html.

—. 2012. "Monthly Hydrologic Conditions for New York." *USGS NY Water Science Center (NYWSC): Hydologic Conditions data.* April 2. Accessed June 11, 2012. http://ny.water.usgs.gov/infodata/conditions.html.

USGS. n.d. *SRTM Topography.* USGS EROS Center. Accessed April 16, 2012. https://dds.cr.usgs.gov/srtm/version2_1/Documentation/SRTM_Topo.pdf.

—. 2012. "The National Map: Elevation." *USGS The National Map.* December 6. Accessed December 2012. https://nationalmap.gov/elevation.html#downloads.

Vaze, J, and J Teng. 2007. "Impact of DEM Resolution on Topographic Indices and Hydrological Modelling Results." *MODSIM07 Conference.* Christchurch: Modelling and Simulation Society of Australia and New Zealand Inc. (MSSANZ). Accessed May 23, 2012. http://www.mssanz.org.au/MODSIM07/papers/12_s27/.

Virtual University for the Small States of the Commonwealth (VUSSC). 2007. "Introduction to Disaster Management." Accessed April 16, 2012. http://oasis.col.org/bitstream/handle/11599/426/2007_VUSSC_Intro-Disaster-Management.pdf?sequence=5&isAllowed=y.

Wilson, Scott, and Chris Cretini. 2007. "Data Access and Dissemination for Emergency Response and Long-term Recovery Efforts Related to Hurricanes Katrina and Rita." *Science and the Storms-the USGS response to the hurricanes of 2005*, 71-74. https://pubs.usgs.gov/circ/1306/pdf/c1306_ch4_b.pdf.

Appendix:

Data Layers (Obstruction Detection Model):

This section gives detailed descriptions for each data layer used to create products in the ODM for ease of replication.

Base Rasters:

Landsat5 B50 SWIR

Landsat5 was chosen as the data source as at the time of import (2011), Landsat8 had not yet launched and Landsat7 had issues with its Scan Line Corrector (SLC). This layer was downloaded from the USGS EarthExplorer website and extracted using *7-Zip*. The single-band raster from Landsat5 (Band 5) [SWIR] was imported into the Seneca.gdb File GeoDatabase using *Raster to Geodatabase (multiple)* with no Configuration Keyword. Then, *Build Pyramids And Statistics* was used with Build Pyramids and Calculate Statistics enabled and Include Sub-Directories and Skip Existing disabled. Pyramid Levels were set to "-1" with "Cubic" for Resampling Technique and "DEFAULT" Pyramid Compression Type. The layer was clipped to the extent of the LiDAR data by using *Clip* with Output Extent as "LiDAR Extent (Clip Feature)" and Use Input Features for Clipping Geometry enabled. NoData Value and Maintain Clipping Extent were kept blank/disabled. This layer was tested for use with the ODM for visual analysis of the ODM output, but it was determined that the 30m data were too coarse to aid in visual analysis, and the layer was subsequently replaced by the RGB_CLIP and SWIR_CLIP data from the WASP sensor.

RGB_CLIP

The source of this layer was the RIT WASP sensor. This layer was hosted on Dr. Jan van Aardt's image server at RIT and downloaded locally to my machine for processing and use. *Clip* was run against the layer with Output Extent as "LiDAR Extent (Clip Feature)" and Use Input Features for Clipping Geometry enabled. NoData Value and Maintain Clipping Extent were kept blank/disabled.

SWIR_CLIP

This layer was hosted on Dr. Jan Van Aardt's image server at RIT and downloaded locally to my machine for processing and use. *Clip* was run against the layer with Output Extent as "LiDAR Extent (Clip Feature)" and Use Input Features for Clipping Geometry enabled. NoData Value and Maintain Clipping Extent were kept blank/disabled. The layer was set to Display with a Transparency value of 50%.

Multipoint Data:

Ground (Full Site)

The LiDAR imagery was processed by Dr. Jan Van Aardt in Merrick MARS® Explorer into first, ground, and all/classified sets. Only the first return LAS file was imported into ArcGIS. Using the LAS to Multipoint tool in ArcGIS, the LiDAR data were converted into a multipoint file. The data were checked to make sure the import process functioned properly and were then used in the *Point to Raster* tool with default values of Cell Assignment: MOST_FREQUENT, Priority Field: None, Cellsize: 1.619524, and Z (return height) specified for the "Value Field", creating the layer "ground_new". The layer was clipped to the extent of the study site using "Site Extent (Clip Feature)".

Ground New (Full Site)

This layer was re-imported/processed into multipoint data using ArcGIS v10.3 which resulted in a different automatic evaluation of the point density, yielding a calculated point spacing of 1.621846. All other values were kept consistent with "Ground (Full Site)".

Hydrography (Clipped)

This layer was created by running *Clip* against the "Ground (Full Site)" multipoint dataset with the "Hydrological Features" layer to subset the multipoint data to only the riverine areas in order to generate the Hydrography Rasters.

Point Spacing Summary:

Seneca LiDAR Classified: Ground

This layer was created by running *Point File Information* against the original "All_TMcorrected_Seneca_classified_ground_returns.las" file which was used to generate the "Ground (Full Site)" layer. This layer stores metadata about the LAS dataset including Point Count, Point Spacing, Z Min, and Z Max.

Seneca LiDAR Classified: Ground (New)

This layer was created by running *Point File Information* against the "All_TMcorrected_Seneca_classified_ground_new.las" file which was a copy of the original LAS dataset. The *Point File Information* tool was run against this dataset in ArcGIS v10.3 which yielded a different point spacing estimate than the original file did when imported under ArcGIS v10.1.

Clip Features:

Hydrological Features

This layer was created by hand-digitizing the approximate riverine areas of interest in the study site. The purpose of this layer is to be used to subset the "Ground (Full Site)" / "Ground New (Full Site)" multipoint data to speed up processing and to focus the results on the relevant test data (water's surface).

Site Extent (Clip Feature)

This layer was created to go beyond the boundaries of the "LiDAR Extent (Clip Feature)" to set the view for the Full Extent command, as well as to form the Clip Boundaries to limit the data displayed from WMS (basemaps, USGS NHD, etc).

LiDAR Extent (Clip Feature)

This layer was hand-digitized to the outer boundaries of the "Ground (Full Site)" in order to set processing extents and to clip and subset other datasets such as the original "LandSAT B50 SWIR", "WASP RGB", and "WASP SWIR" datasets into their current CLIP states.

Ground Rasters:

Each of the datasets in the Ground Rasters group is comprised of a set of rasters not interpolated (Raw), interpolated using Inverse Distance Weighting (IDW), Natural Neighbors (NN), and Spline with Barriers (SPLB). Each of the resultant interpolated rasters were clipped using the "Hydrological Features" clip layer to subset the data to the riverine areas of interest.

Raw (1.62)

This dataset is comprised of groups of layers generated by different interpolation methods used against the Ground (Full Site) multipoint data. Each layer was converted into rasters using: Value Field: Shape.Z, Cell Assignment Type: Most Frequent, Priority Field: None, Cellsize: 1.619524 as the parameters for *Point to Raster*.

Ground (Raw)

This layer was created by running *Point to Raster* against "Ground (Full Site)" with the above parameters. It was not interpolated, so the dataset has holes/NULL cells.

IDW (1.62)

This layer was created by running *IDW* against "Ground (Full Site)" with the above parameters. This layer was interpolated using Inverse Distance Weighting to fill any holes in the site.

IDW Clip (1.62)

This layer was created by running *Clip (Data Management)* against "IDW (1.62)" with "LiDAR Extent (Clip Feature)" as the Output Extent. "Use Input Features for Clipping Geometry" was enabled.

NN (1.62)

This layer was created by running *Natural Neighbor* against "Ground (Full Site)" with the above parameters, and all other options as default.

NN Clip (1.62)

This layer was created by running *Clip (Data Management)* against "NN (1.62)" with "LiDAR Extent (Clip Feature)" as the Output Extent. "Use Input Features for Clipping Geometry" was enabled.

SPLB (1.62)

This layer was created by running *Spline with Barriers* against "Ground (Full Site)" with the above parameters, and all other options as default.

SPLB Clip (1.62)

This layer was created by running *Clip (Data Management)* against "SPLB (1.62)" with "LiDAR Extent (Clip Feature)" as the Output Extent. "Use Input Features for Clipping Geometry" was enabled.

3.00m

This dataset is comprised of groups of layers generated by different interpolation methods used against the Ground (Full Site) multipoint data. Each layer was converted into rasters using: Value Field: Shape.Z, Cell Assignment Type: Most Frequent, Priority Field: None, Cellsize: 3.00 as the parameters for *Point to Raster*.

As in the "Raw (1.62)" dataset, it contains rasters for Raw, IDW, NN, and SPLB with Clip variants.

5.00m

This dataset is comprised of groups of layers generated by different interpolation methods used against the Ground (Full Site) multipoint data. Each layer was converted into rasters using: Value Field: Shape.Z, Cell Assignment Type: Most Frequent, Priority Field: None, Cellsize: 5.00 as the parameters for *Point to Raster*.

As in the "Raw (1.62)" dataset, it contains rasters for Raw, IDW, NN, and SPLB with Clip variants.

10.00m

This dataset is comprised of groups of layers generated by different interpolation methods used against the Ground (Full Site) multipoint data. Each layer was converted into rasters using: Value Field: Shape.Z, Cell Assignment Type: Most Frequent, Priority Field: None, Cellsize: 10.00 as the parameters for *Point to Raster*.

As in the "Raw (1.62)" dataset, it contains rasters for Raw, IDW, NN, and SPLB with Clip variants.

30.00m

This dataset is comprised of groups of layers generated by different interpolation methods used against the Ground (Full Site) multipoint data. Each layer was converted into rasters using: Value Field: Shape.Z, Cell Assignment Type: Most Frequent, Priority Field: None, Cellsize: 3.00 as the parameters for *Point to Raster*.

As in the "Raw (1.62)" dataset, it contains rasters for Raw, IDW, NN, and SPLB with Clip variants.

Hydrography Rasters:
This dataset is comprised of groups of layers for Raw, IDW, NN, and SPLB. These layer groups were created by running *Clip (Data Management)* against the various layers from "Ground Rasters" with "Hydrological Features" as the clipping extent. Each interpolation set also contains rasters in 1.62, 3.00, 5.00, 10.00, and 30.00 meter resolutions as per the previous sets.

Slopes:
Each of the datasets in the Slopes group is comprised of a set of rasters not interpolated (Raw), interpolated using Inverse Distance Weighting (IDW), Natural Neighbors (NN), and Spline with Barriers (SPLB). Each group is comprised of rasters in 1.62, 3.00, 5.00, 10.00, and 30.00 meter resolutions as per the previous sets. Each raster was created by running *Slope (Spatial Analyst)* against the layers from "Hydrography Rasters". *Slope (Spatial Analyst)* was run with defaults, being Output Measurement: DEGREE and Z-Factor: 1.

Interpolation Differences:
This dataset is comprised of layers generated by running *Raster Calculator (Spatial Analyst)* with an expression of "Layer 1" – "Layer 2" to visualize the difference between the various interpolation methods when compared to the Raw (1.62m) source data. The various interpolation methods were also subtracted from one another to visualize the difference between the various interpolation methods themselves.

Random Point Samples:
This dataset is comprised of layers generated by using *Extract Values to Points (Spatial Analyst)* to create feature-class layers which will contain the Z-Field (Height in m) of the various layers. The sampled layers all were run with "Random Sample" as the Input Point Features layer and one of the Hydrography Rasters as the Input Raster, with all other fields/options at their default values.

Random Sample
Create Random Points (Data Management) was run with the Minimum Allowed Distance set to the spatial resolution of the Raw data (1.619524m) and the Number Of Points set to 1528334 (a value derived from *Sample (Spatial Analyst)* done against the "Raw Hydro (1.62)" layer), with a Constraining Feature

of “Hydrological Features” and all other options to their defaults. The resultant layer was used as the Input Point Features layer to generate the Random Point Sample layers.

Reclassed:

This dataset is comprised of layers generated using *Reclassify (Spatial Analyst)* with different settings against the various interpolations and raster resolutions from previous datasets. The 5-class reclassification schemas used were the manual classification derived from visual inspection of the “Raw Hydro (1.62)” layer with manual random sampling. The other reclassification schemas were derived from the ArcGIS Symbology Classifications and include Equal Interval, Quantile, Natural Breaks (Jenks), and Geometrical Interval.

Manual 5-Class Reclassification Schema

Class 1: 0 – 1.1

Class 2: 1.1 – 1.5

Class 3: 1.5 – 3.0

Class 4: 3.0 – 10.0

Class 5: 10.0 – 89.9

Data Layers (Flood Extent Generator):

This section gives detailed descriptions for each data layer used to create products in the FEG for ease of replication.

LiDAR Base Layers:

LiDAR (Monroe County) [02m]

This layer was created from the Monroe County 2 Meter DEM tiles downloaded from the NYS GIS Clearinghouse’s County 2-Meter DEM dataset. The individual tiles were batch-downloaded using the *DownThemAll* extension for *Mozilla Firefox*. They were then extracted using *7-zip* into a common directory so that the individual IMG files could be mosaicked into a contiguous raster DEM using *Mosaic To New Raster.* The new mosaicked raster was created with Spatial Reference: NAD 1983 UTM Zone 18N, Pixel Type: 32_BIT_FLOAT, Cellsize: 2, Number of Bands: 1, Mosaic Operator: Blend, Mosaic Colormap Mode: Match. The resultant raster was then clipped to the extent of the “Monroe County (Clip Boundary)” layer.

LiDAR (Monroe County) [03m]

This layer was created from the "LiDAR (Monroe County) [02m]" dataset by running *Resample* with X: 3, Y: 3, and Resampling Technique: Cubic. The resultant raster was saved as a new raster within the lidar_02m_monroe File Geodatabase.

LiDAR (Monroe County) [05m]

This layer was created from the "LiDAR (Monroe County) [02m]" dataset by running *Resample* with X: 5, Y: 5, and Resampling Technique: Cubic. The resultant raster was saved as a new raster within the lidar_02m_monroe File Geodatabase.

LiDAR (Monroe County) [10m]

This layer was created from the "LiDAR (Monroe County) [02m]" dataset by running *Resample* with X: 10, Y: 10, and Resampling Technique: Cubic. The resultant raster was saved as a new raster within the lidar_02m_monroe File Geodatabase.

LiDAR (Monroe County) [30m]

This layer was created from the "LiDAR (Monroe County) [02m]" dataset by running *Resample* with X: 30, Y: 30, and Resampling Technique: Cubic. The resultant raster was saved as a new raster within the lidar_02m_monroe File Geodatabase.

Ford Street Obstruction:

Ford Street Bridge (07m Depth Test)

This vector layer was created by hand-digitzing a line from one edge of the Ford Street Bridge across the Genesee River. This vector file would represent the location of a flood obstruction which would be used to generate a flood scenario to be evaluated by the Risk Assessment Model.

Ford Street Obstruction (Raster) [02m]

This layer was generated by running *Feature To Raster* against "Ford Street Bridge (07m Depth Test)" with Output Cell Size: 2. This layer was then reclassified using *Reclassify* so that it was a binary raster consisting of NoData = 0 and 1 = 7.

Ford Street Obstruction (Raster) [03m]

This layer was generated by running *Feature To Raster* against "Ford Street Bridge (07m Depth Test)" with Output Cell Size: 3. This layer was then reclassified using *Reclassify* so that it was a binary raster consisting of NoData = 0 and 1 = 7.

Ford Street Obstruction (Raster) [05m]

This layer was generated by running *Feature To Raster* against "Ford Street Bridge (07m Depth Test)" with Output Cell Size: 5. This layer was then reclassified using *Reclassify* so that it was a binary raster consisting of NoData = 0 and 1 = 7.

Ford Street Obstruction (Raster) [10m]

This layer was generated by running *Feature To Raster* against "Ford Street Bridge (07m Depth Test)" with Output Cell Size: 10. This layer was then reclassified using *Reclassify* so that it was a binary raster consisting of NoData = 0 and 1 = 7.

Ford Street Obstruction (Raster) [30m]

This layer was generated by running *Feature To Raster* against "Ford Street Bridge (07m Depth Test)" with Output Cell Size: 30. This layer was then reclassified using *Reclassify* so that it was a binary raster consisting of NoData = 0 and 1 = 7.

Ford Street Road Dam [Raw]

Dam [02m]

This layer was generated by running *Raster Calculator* with a formula of: "Ford Street Obstruction (Raster) [02m] + LiDAR (Monroe County) [02m]".

Dam [03m]

This layer was generated by running *Raster Calculator* with a formula of: "Ford Street Obstruction (Raster) [03m] + LiDAR (Monroe County) [03m]".

Dam [05m]

This layer was generated by running *Raster Calculator* with a formula of: "Ford Street Obstruction (Raster) [05m] + LiDAR (Monroe County) [05m]".

Dam [10m]

This layer was generated by running *Raster Calculator* with a formula of: "Ford Street Obstruction (Raster) [10m] + LiDAR (Monroe County) [10m]".

Dam [30m]

This layer was generated by running *Raster Calculator* with a formula of: "Ford Street Obstruction (Raster) [30m] + LiDAR (Monroe County) [30m]".

Ford Street Dam [Fill]

Dam (Fill) [02m]

This layer was generated by running *Fill* with an Input Surface Raster of "Dam [02m]" and Z-Limit left blank (to fill all).

Dam (Fill) [03m]
This layer was generated by running *Fill* with an Input Surface Raster of "Dam [03m]" and Z-Limit left blank (to fill all).

Dam (Fill) [05m]
This layer was generated by running *Fill* with an Input Surface Raster of "Dam [05m]" and Z-Limit left blank (to fill all).

Dam (Fill) [10m]
This layer was generated by running *Fill* with an Input Surface Raster of "Dam [10m]" and Z-Limit left blank (to fill all).

Dam (Fill) [30m]
This layer was generated by running *Fill* with an Input Surface Raster of "Dam [30m]" and Z-Limit left blank (to fill all).

Ford Street Dam [Flood Depth]

Flood Depth [02m]
This layer was generated by running *Raster Calculator* with a formula of: "Dam [02m] – LiDAR (Monroe County) [02m]".

Flood Depth [03m]
This layer was generated by running *Raster Calculator* with a formula of: "Dam [03m] – LiDAR (Monroe County) [03m]".

Flood Depth [05m]
This layer was generated by running *Raster Calculator* with a formula of: "Dam [05m] – LiDAR (Monroe County) [05m]".

Flood Depth [10m]
This layer was generated by running *Raster Calculator* with a formula of: "Dam [10m] – LiDAR (Monroe County) [10m]".

Flood Depth [30m]

This layer was generated by running *Raster Calculator* with a formula of: "Dam [30m] – LiDAR (Monroe County) [30m]".

Flood Extent

Flood Extent (7m Depth) [02m Cell]

This layer was generated by running a *Reclassify (Spatial Analyst)* against "Dam Fill [02m]" with Reclass Field: Value, Reclassification as in

Table 8 - Flood Level Reclassification Values (≈4.7m scenarios) for the Ford Street Bridge., and Change Missing Values To NoData checked.

Flood Extent (7m Depth) [03m Cell]

This layer was generated by running a *Reclassify (Spatial Analyst)* against "Dam Fill [03m]" with Reclass Field: Value, Reclassification as the above table, and Change Missing Values To NoData checked.

Flood Extent (7m Depth) [05m Cell]

This layer was generated by running a *Reclassify (Spatial Analyst)* against "Dam Fill [05m]" with Reclass Field: Value, Reclassification as the above table, and Change Missing Values To NoData checked.

Flood Extent (7m Depth) [10m Cell]

This layer was generated by running a *Reclassify (Spatial Analyst)* against "Dam Fill [10m]" with Reclass Field: Value, Reclassification as the above table, and Change Missing Values To NoData checked.

Flood Extent (7m Depth) [30m Cell]

This layer was generated by running a *Reclassify (Spatial Analyst)* against "Dam Fill [03m]" with Reclass Field: Value, Reclassification as the above table, and Change Missing Values To NoData checked.

Data Layers (Truth Assessment Model):

This section gives detailed descriptions for each data layer used to create products in the TAM for ease of replication.

Flood Survey

Flood Stage Survey May 17

This vector was provided by Justin Cole and represents the field-collected ground truth points for the edge of the flood extent on Black Creek.

Flood Scenario Rasters (Hazus)

GENESEEMAJORFLD55000CFS

This raster was provided by Justin Cole and represents a flood of the Genesee River at 55,000cfs.

GENESEEMAX46300CFS

This raster was provided by Justin Cole and represents a flood of the Genesee River at 46,300cfs.

HAZUS_BLACK_CREEK_MAX4880CFS

This raster was provided by Justin Cole and represents a flood of Black Creek at 4,880cfs.

IRONDEQUOITCREEK3300CFS

This raster was provided by Justin Cole and represents a flood of Irondequoit Creek at 3,300cfs.

Flood Scenario Rasters (FEG)

Dam (Fill) [02m]

This layer was generated by running *Fill* with an Input Surface Raster of "Dam [02m]" and Z-Limit left blank (to fill all).

Dam (Fill) [03m]

This layer was generated by running *Fill* with an Input Surface Raster of "Dam [03m]" and Z-Limit left blank (to fill all).

Dam (Fill) [05m]

This layer was generated by running *Fill* with an Input Surface Raster of "Dam [05m]" and Z-Limit left blank (to fill all).

Dam (Fill) [10m]

This layer was generated by running *Fill* with an Input Surface Raster of "Dam [10m]" and Z-Limit left blank (to fill all).

Dam (Fill) [30m]

This layer was generated by running *Fill* with an Input Surface Raster of "Dam [30m]" and Z-Limit left blank (to fill all).

Flood Scenario Vectors

Dam Fill Vector (7m scenario) [03m]

This vector was created by running *Reclassify* against "Dam [03m]" with Old Values: 155.1 - 162.46 as 1 and all others as No Data. The resultant layer was turned into a Polygon using *Raster To Polygon* with Simplify enabled. The resultant layer was then dissolved using *Dissolve* with Create Multipart Features enabled.

Dam Fill Vector (4.7m scenario) [03m]

This vector was created by running *Reclassify* against "Dam [03m]" with Old Values: 155.1 - 159.76 as 1 and all others as No Data. The resultant layer was turned into a Polygon using *Raster To Polygon* with Simplify enabled. The resultant layer was then dissolved using *Dissolve* with Create Multipart Features enabled.

Genesee Major 55000cfs Vector

This vector was created by running *Reclassify* against "GENESEEMAJORFLD55000CFS" with all values as 1 and all NoData as No Data. The resultant layer was turned into a Polygon using *Raster To Polygon* with Simplify enabled. The resultant layer was then dissolved using *Dissolve* with Create Multipart Features enabled.

Genesee Max 46300cfs Vector

This vector was created by running *Reclassify* against "GENESEEMAX46300CFS" with all values as 1 and all NoData as No Data. The resultant layer was turned into a Polygon using *Raster To Polygon* with Simplify enabled. The resultant layer was then dissolved using *Dissolve* with Create Multipart Features enabled.

Black Creek Max 4880cfs Vector

This vector was created by running *Reclassify* against "HAZUS_BLACK_CREEK_MAX4880CFS" with all values as 1 and all NoData as No Data. The resultant layer was turned into a Polygon using *Raster To Polygon* with Simplify enabled. The resultant layer was then dissolved using *Dissolve* with Create Multipart Features enabled.

Irondequoit 3300cfs Vector

This vector was created by running *Reclassify* against "IRONDEQUOITCREEK3300CFS" with all values as 1 and all NoData as No Data. The resultant layer was turned into a Polygon using *Raster To Polygon* with Simplify enabled. The resultant layer was then dissolved using *Dissolve* with Create Multipart Features enabled.

HAZUS Flood Extents Merge

This vector was created by running *Merge* against "Genesee Major 55000cfs Vector", "Black Creek Max 4880cfs Vector", and "Irondequoit 3300cfs Vector" to create an aggregate vector layer that contained all the river reaches that "Dam Fill Vector [03m]" encompassed.

Dam Fill [03m] Union Hazus Flood Extents

This vector was created by running *Union* against "Dam Fill Vector [03m]" and "HAZUS Flood Extents Merge", to create a layer that contains the areas of agreement between the various HAZUS boundaries and the flood boundary created by the FEG.

Dam Fill [03m] Union Genesee Major 463000cfs

This vector was created by running *Union* against "Dam Fill Vector [03m]" and "Genesee Max 46300cfs Vector" to create a layer that contains the areas of agreement between the Hazus Genesee Major flood event boundary and the flood boundary created by the FEG.

Parcel Data

Road Centerlines (Monroe County)

This layer was downloaded from the US Census TIGER/Line FTP server, extracted using 7-zip, and imported into ArcGIS.

Data Layers (Risk Assessment Model):

This section gives detailed descriptions for each data layer used to create products in the RAM for ease of replication.

Monroe County Vectors

Road Centerlines (Monroe County)

This layer was downloaded from the US Census TIGER/Line FTP server, extracted using 7-zip, and imported into ArcGIS.

Parcels (Monroe County)

This layer was provided by Justin Cole of Monroe County and imported into ArcGIS.

CIKR (Critical Infrastructure & Key Resources)

CIKR Points (Monroe County)

This layer was provided by Justin Cole of Monroe County and imported into ArcGIS.

CIKR Parcels (Monroe County)

This layer was provided by Justin Cole of Monroe County and imported into ArcGIS.

Block Data (Monroe County)

Census 2010 Block (Monroe County)

This layer was downloaded from the US Census TIGER/Line FTP server, extracted using 7-zip, and imported into ArcGIS.

Parcel & CIKR Spatial Join

Parcels (Monroe County) & CIKR Parcels (Monroe County)

This layer was created by running a join of "Parcels (Monroe County)" with "CIKR Parcels (Monroe County)", with the option: Each polygon will be given the attributes of the polygon it falls completely inside of in the layer being joined.

Parcel, Block, & CIKR Spatial Join

Parcels (Monroe County) & CIKR Parcels (Monroe County) + Census 2010 Block (Monroe County)

This layer was created by running a join of "Parcels (Monroe County) & CIKR Parcels (Monroe County)" with "Census 2010 Block (Monroe County)", with the option: Each polygon will be given a summary of the numeric attributes of the polygons in the layer being joined that intersect it, and a count field showing how many polygons intersect it.

RAM Variables

RAM Parcels

This layer was created by performing a series of Edit/Field calculations on "Parcels (Monroe County) & CIKR Parcels (Monroe County) + Census 2010 Block (Monroe County)".

The fields FloodStage, PriorityRating, HumanImpact, Cost, and RiskFactor were added to the "RAM Parcels" layer.

FloodStage was set using Field Calculator as 7000 for ALL records in the table to indicate a Historic Flood Percentile Scenario.

PriorityRating was set using Field Calculator as 0 for all records with a CIKR_TYPE = Null. Records with a CIKR_TYPE were set in accordance with Table 12.

HumanImpact was set using Field Calculator with groupings determined through ArcGIS's Symbology Natural Breaks (Jenks) Classification with 10 classes. The Value field was Sum_POP10. This resulted in the following Classes shown in Table 16:

Cost was set using Field Calculator with groupings determined through ArcGIS's Symbology Geometric Classification with 10 classes. The Value Field was TOTAL_AV. This resulted in the following Classes shown in Table 17:

Risk Factor was calculated using the Field Calculator with a formula of:

RiskFactor = [FloodStage] + [PriorityRating] + [HumanImpact] + [Cost].

RAM Impact Visualized

Risk Factor

This layer is a copy of the "RAM Parcels" layer with the Symbology set to Quantiles – Graduated Colors with a Value Field of RiskFactor and a Natural Breaks (Jenks) Classificiation with 10 classes.

Priority Rating

This layer is a copy of the "RAM Parcels" layer with the Symbology set to Quantiles – Proportional Symbols with a Value Field of PriortyRating and Data Exclude Query: PriorityRating < 800 to show the highest PriortyRating ranked parcels.

Human Impact

This layer is a copy of the "RAM Parcels" layer with the Symbology set to Quantiles – Proportional Symbols with a Value Field of HumanImpact and Data Exclude Query: HumanImpact < 90 to show the highest HumanImpact ranked parcels.

Cost

This layer is a copy of the "RAM Parcels" layer with the Symbology set to Quantiles – Proportional Symbols with a Value Field of Cost and Data Exclude Query: Cost < 90 to show the highest Cost ranked parcels.

Priority Rating Versions:

This section contains early iterations of the Priority Rating classes, an unused remapping of NLCD classes to the final Priority Ratings, and a remapping of Property Class codes (Monroe County, NY) to Priority Rating.

Version 1- Based upon Anderson Level 1. (Brett Carlock)

Table 21 - Priority Ratings V1.
This table illustrates a preliminary version of the Priority Ratings classification.

0	Undeveloped		5	School and Care
1	Rural Unoccupied		6	Hospital and Med.
2	Rural Developed		7	Electrical Infrastructure
3	Suburban		8	Fossil Fuel Power
4	Urban/Populated		9	Nuclear Power

Version 2 – Based upon CIKR classes. (Brett Carlock, Justin Cole)

Table 22 - Priority Ratings V2.
This table illustrates another preliminary version of the Priority ratings classification based upon input by Justin Cole.

0	Business		5	Power
1	Telecommunications		6	Government
2	Agriculture & Food		7	First Responders
3	Transport		8	Care Facilities
4	Schools		9	Chemical & Haz-Mat

NLCD Land Cover Classification to Priority Rating:

Table 23 - NLCD Land Cover to Priority Rating.
This table shows the preliminary mapping of NLCD Classes to Priority Rating established by Mr. Fred Rion of Monroe County, NY.

NLCD Class	NLCD Description	Priority Rating
11	Open Water	3
12	Perennial Ice/Snow	NoData
21	Developed, Open Space	6
22	Developed, Low Intensity	7
23	Developed, Medium Intensity	8
24	Developed, High Intensity	9
31	Barren Land (Rock/Sand/Clay)	0
41	Deciduous Forest	4
42	Evergreen Forest	4
43	Mixed Forest	4
51	Dwarf Scrub	NoData
52	Shrub/Scrub	1
71	Grassland/Herbaceous	1
72	Sedge/Herbaceous	2
73	Lichens	NoData
74	Moss	NoData
81	Pasture/Hay	5
82	Cultivated Crops	5
90	Woody Wetlands	4
95	Emergent Herbaceous Wetlands	4

Monroe County Property Class to Priority Rating:

Table 24 - Monroe County Property Class to Priority Rating Mapping.
This table shows the preliminary mapping of Monroe County Property Classes to Priority Rating as established by Mr. Fred Rion of Monroe County, NY.

Property Class	Priority Rating
100 – 199	5
200 – 299	0
300 – 399	0
400 – 499	0
500 – 532	0
533	5
534 – 569	0
570	8
571 – 599	0
600 – 620	2
621 – 639	2
630 – 649	6
650 – 661	7
662	4
670	7
680 – 690	7
692	8
694	7
695	0
710 – 749	3
800 – 829	9
830 – 839	1
840 – 849	8
847 – 853	3
860 – 889	9
910, 912, 920, 932	5
960 – 963	7
970 – 972	5